MASTER'S THESIS

Active Vibration Isolation with an Active Stage

ROY KELDER

Faculty of Engineering Technology
Precision Engineering

Examination committee:

Prof. Dr. Ir. D.M. Brouwer PDEng
Dr. Ir. W.B.J. Hakvoort
Ir. S.T. Spanjer
Dr. Ir. W. Roozing

UNIVERSITY OF TWENTE.

MASTER'S THESIS

Active Vibration Isolation with an Active Stage

ROY KELDER
Born on the 23th of Octobre 1994 in Hardenberg, The Netherlands

Faculty of Engineering Technology
Department of Mechanics of Solids, Surfaces and Systems
Chair of Precision Engineering

Examination committee:

Prof. Dr. Ir. D.M. Brouwer PDEng
Dr. Ir. W.B.J. Hakvoort
Ir. S.T. Spanjer
Dr. Ir. W. Roozing

UNIVERSITY OF TWENTE.

Preface

Before you lies the master's thesis entitled 'Active Vibration Isolation with an Active Stage'. It is the basis of scientific research on actively attenuate vibrations with adaptive control for precision machines conducted by me. I was engaged in researching and writing this thesis for the last 9 months.

It has been a long road to get to this point of almost successfully finishing a master's in Mechanical Engineering at the University of Twente. For the last 10 years, I studied in Almelo, Hengelo, and Enschede. At both the level of MBO and HBO. I remember well that during my MBO years the fascination for mechanics increased significantly. It was fun to design, manufacture and realise mechanisms out of solid blocks of aluminum and steel. Also, in those years it became apparent that it was frustrating that I could not understand all the physics behind it. That's why I applied for Saxion, the University of Applied Sciences, and subsequently for the University of Twente. It was not until my first year of the master that my passion for control engineering began to grow. In particular the combination of designing mechanics and accurately realise movements with controllers up to the nanometer scale.

That's why I choose this assignment. It had both the design aspect of a precision mechanism and controller. I have to admit that the assignment gave a bunch of stress at the beginning of the research due to a lack of controller knowledge. Nevertheless, after a full four months of research things became to fall in place. I designed, constructed, and implemented a flexure mechanism on top of a vibration isolation system. Subsequently, I conducted experiments with different controllers in the laboratory at the Horst for a total of two (maybe three) months. Finally, in the last three months, I worked on writing all obtained knowledge in a systematic and concise matter in this thesis. I am satisfied with the result and I hope it contributes to construct and control more precise machines in the future.

I would like to thank several people for their support throughout the graduation period. In particular my supervisors Wouter Hakvoort and Sil Spanjer. I can imagine that the tons of questions of me every now and then were a bit irritating. However, both of you were always helping me out, by giving me a certain direction to further research or a direct answer that speeded up my research progress. The biweekly meetings were interesting and I did learn a lot about the theoretical and practical aspects of controllers. The atmosphere of openly discussing the findings of simulations and experiments was good! I would also like to thank Leo Tiemersma for helping me realise the mechanism. I am very grateful that you have spent hours of your time helping me finetune the technical drawings and manufacture all parts. Also, for all the times you fixed a snapped component in less than an hour when I was doing experiments.

Special thanks to my girlfriend for all the support and for correcting all my grammar errors. I found it very relaxing to spend a few days with you in Ameland just a few weeks before my deadline. It gave me new energy to finish the thesis. Finally, thanks to all my friends in Enschede my second home, and to all the friends and family in Mariënberg my first home!

I hope you enjoy your reading.

Roy Kelder,

Mariënberg, June 11, 2021

Summary

Vibrations in high-precision machines can cause a loss of accuracy in moving part(s) and sensitive equipment. One of the limiting factors is the internal deformation between the moving part(s) and sensitive equipment. This deformation is caused by indirect and direct disturbances, where indirect disturbances act on the base of the machine, and direct disturbances directly on the sensitive payload. Especially indirect disturbances due to seismic activity and direct disturbances generated by the moving part(s) induce a major part of vibrations.

Active vibration isolation systems can be used to attenuate the effect of these disturbances by using controllers which utilize measurements of the isolated base with the interconnected sensitive payload and the source of the disturbances as control inputs. The first tries to dampen the suspension modes of the vibration isolation system and attenuate vibrations with feedback control. With the use of absolute sensors in combination with the controller so-called virtual mass, skyhook stiffness, and skyhook damping can be added. This would ideally create an artificial suspension with respect to an imaginary hook in the sky, unaffected by indirect disturbances and less susceptible to direct disturbances. The second tries to generate forces with feedforward control which cancels the forces induced by the sum of all disturbances on the isolated base.

In the case of only a vibration isolation system it is common to quantify the performance with the transmissibility of indirect disturbances and compliance for the direct disturbances. However, with an active stage with moving part(s) and sensitive equipment, the performance also depends on the tracking characteristics of the moving part(s) and the amount of internal deformation. So far, none considers an active stage in combination with a vibration isolation system. Therefore, in this research, a multi-objective control strategy is proposed for an active stage with a vibration isolation system wherein the goal is to have accurate tracking properties and minimal internal deformation. To achieve this, a theoretical framework is set up in which all important characteristics for are incorporated. According to this framework, all performance objectives are easily linked to the control strategies.

Based on the theoretical framework, a control strategy is designed for both the active stage as well as the vibration isolation system. It utilizes both the measured indirect base vibrations and the reference profile of the moving part in the case of the vibration isolation system feedforward controller. A self-tuning IIR-filter with fixed poles is implemented in which physics-based parameters are contained that are estimated with a Filtered-Error Least Mean Square (FeLMS) algorithm. The algorithm tries to find a global minimum using the measured vibrations of the isolated base and respective disturbances. The signals are pre-filtered with a noise shaping filter to choose the frequency range of interest and to suppress frequencies that otherwise cause instability due to parasitic modes. This self-tuning filter can handle time-varying parameters, lacks the need for extensive system identification, and automatically takes into account the effect of noise.

Although feedforward control can improve the performance significantly, the use of measured machine base vibrations as control input for discretized controllers is inherently too late and insufficient to cancel the forces induced by the continuous disturbance. Besides that, the moving part states differ from the reference components used as a control input for the direct disturbance feedforward control due to a tracking error. The difference in moving part states and used direct disturbance control input causes the feedforward control, even with parameters estimated exactly, to generate a force which not cancels the force generated by the moving part completely. This causality and mismatch in states deteriorate the system's performance. Therefore, also feedback control is used with aid of absolute sensors located on the isolated base which further attenuates residual vibrations. Tuning is accomplished by considering the power spectral densities of all measured disturbances and noises in which it is aimed to minimize the measured vibrations of the isolated base.

The control system for the moving part consists of an adaptive feedforward controller whose parameters are estimated with a Kalman filter. This is appended with a PID controller which is tuned such that the influence of all disturbances and noises on the tracking error is balanced. For this, sensitivity and complementary sensitivity are considered.

The controller's feasibility is experimentally demonstrated on a benchmark system that consists out of an active stage mounted on top of a Stewart Gough vibration isolation system. The active stage is designed in this research. It has a single degree of freedom flexure-based translational moving part and intentional frame compliance in which a sensor is placed that measures the internal deformation perpendicular to the part movements.

The proposed controllers show promising experimental results. With a total of 66 estimated parameters for the vibration isolation system, the vibrations are attenuated with 24 dB in comparison to the passive vibration isolation system. Due to this, the internal deformation reduces with a ratio of five and tracking error with a ratio of three. Furthermore, the moving part is able to track a reference, that has acceleration components up to 50 $\mathrm{m/s^2}$, with a tracking error of 1 μm.

Contents

1. Introduction

1.1. Background

There is an increasing demand for precision machines with high throughput and accuracy. This often implies a minimal tracking error of the moving part(s) and the ability to accurately examine moving part(s) by means of measurements or other processes with sensitive equipment fastened in the framework of a machine. The performance of a machine depends primarily on the dynamic behavior of the mechanical structure, used control strategies, and the noise characteristics of sensors and actuators.

The mechanical structure is fundamentally limited with a finite stiffness that inevitably causes internal flexibility. However, it only results in a negative effect on the system's accuracy when vibrations from indirect or direct disturbances are transmitted on the machine. The indirect disturbances affect the respective moving part(s) and equipment due to vibrations transmitted through the machine suspension. While the other type of disturbances induces vibrations directly on the moving part(s) and equipment. Examples of indirect disturbances are seismic activity and other machines operating in the surroundings. For direct disturbances, these are reaction forces induced by the actuators to track a reference with moving part(s), forces due to cables that are fixated to the moving part(s), and acoustics. Of all disturbances, seismic activity and forces due to moving part(s) cause a major part of vibrations.

To decrease the influence of disturbances on the machine, often a vibration isolation system is used. Such a vibration isolation system tries to attenuate vibrations passively with physical springs and dampers. In addition, a vibration isolation system can be equipped with actuators that actively attenuate the influence of disturbances with aid of sensors and controllers. A vibration isolation system is commonly quantified with the transmissibility and compliance curve which defines the transfer from vibrations induced by indirect and direct disturbances on the sensitive payload.

Implementation of vibration isolation systems in precision machines can roughly be realised in two ways as shown in figure 1. In the first, the system is constructed such that the metrology and positioning framework are separated from each other [1]. In this, the metrology frame is connected to a vibration isolation system that is fixated on the floor, and the framework that provides guidance for the moving part(s) directly on the floor. In the second configuration [2], the metrology and positioning are integrated into one framework, the so-called active stage. These active stages are often quantified considering settling time and tracking error of the moving part(s) in combination with the amount of internal deformation between the sensitive equipment and moving part(s). The interconnection of the active stage to the floor is provided by the vibration isolation system. A drawback with this configuration is the increased susceptibility for direct disturbances that are mainly generated by reaction forces, in order to track a reference with the moving part(s). However, this configuration is much more modular, as the isolating and positioning system can be designed separately. Moreover, with separate frameworks, the controller complexity significantly increases because it needs to track a reference with the moving part(s) and simultaneously requires leveling of the metrology framework with respect to the positioning framework.

The guidance of moving part(s) in an active stage is in most applications realised with bearings that have a medium of rollers, air, or magnetics [3]. Although a medium of air or magnetics shows promising results in terms of compliance and deterministic behavior, it is quite complex and in most cases expensive to implement. In the case of roller bearings, play and friction are present that cause hysteresis. An alternative is the use of flexure-based guidance [4, 5]. These create freedom of movement from elastic elements rather than kinematic joints. Although most flexure-based guidance types have a limited stroke and support stiffness. They behave much more deterministic compared to roller bearings and in most cases are more simple to implement in practice than a bearing with a medium of air or magnetics.

1.2. Control of active stages

In this research, the focus is put on control strategies for the second category of precision machines. These strategies relate to motion and vibration control [6]. The goal of motion control is to generate forces to track the desired motion with the moving part(s) of the active stage such that high throughput is achieved with minimal settling time and accurate reference tracking. In general, a control strategy is constructed out of a feedback and a feedforward controller [7]. The feedback controller provides disturbance rejection and a part of the tracking performance. The fundamental limitation of feedback controllers is the bode sensitivity integral that quantifies the maximum achievable performance with noise and disturbances present [7]. For an increase in tracking performance, a feedforward controller is used in most application [8, 9]. In the case of non-repetitive motion profiles, model-based controllers are proposed that try to mimic the inverse of the dynamics of the moving part. The effectiveness of these controllers primarily depends on the accuracy of the inverse model.

1.3. Control of vibration isolation systems

The goal of vibration isolation control is to attenuate the effect of both indirect and direct disturbances that otherwise cause vibrations and internal deformation between the sensitive equipment and moving part(s). When a passive vibration isolation system is used a clear trade-off exists between the attenuation of vibrations due to indirect and direct disturbances [10]. The addition of active control can improve performance by means of damping the suspension frequencies of the vibration isolation system and minimizing the influence of disturbances acting on the system [11]. In this, it is aimed to control the actuators such that a force is created that cancels the force caused by the sum all disturbances. With relative sensors, that measure between the floor and isolated base, vibrations due to direct disturbances can be attenuated. However, a drawback is that the influence of indirect disturbances increases. This fundamental limitation of both a passive configuration and relative sensors can be circumvented with the use of absolute sensors. As a result, maximum achievable performance is primarily dependent on the noise characteristics of sensor and actuator noise.

A number of feedback controllers are proposed that uses absolute measurements of sensors that are located on the isolated base [12, 13]. These controllers add so-called virtual mass, skyhook damping, and skyhook stiffness, which can improve the dampening of suspension frequencies and attenuation of vibrations due to disturbances. Although feedback controllers can improve performance, they are bounded to the stability of the closed-loop that is dependent on the physics of the system. Besides that, they use measured vibrations that are filtered by the mechanical system that can cause a poor signal-to-noise ratio. Also, most sensors exhibit noise in low-frequent regions which induces drift.

With the use of feedforward controllers, the drawbacks of feedback can be circumvented. It uses the absolute sensor measurements of indirect and direct disturbances, as a control input [14]. Subsequently, the controller is designed in such a way that, compared to the forces induced by indirect and direct disturbance forces, an opposite phase force is created by the actuators. Although these controllers improve the attenuation of vibration significantly, still performance is limited by causality (in the case of indirect disturbances) and noise characteristics of sensors and actuators.

1.4. Adaptive control

The effectiveness of feedforward controllers for active vibration isolation primarily depends on the accuracy of parameter estimation for the model [15]. In the case of an active stage with an vibration isolation system, this requires a proper estimate of the transfer path from the moving part(s) of the active stage through the guide dynamics on the isolated base, and the transfer path from the floor through the vibration isolation system suspension on the isolated base. The latter requires complex offline identification techniques because it is extremely difficult to sufficiently excite an industrial floor. An alternative is using online identification techniques (self-tuning filters) in the format of finite or infinite impulse response filters [16, 17]. Finite impulse response filters require many parameters for slightly damped vibration isolation system suspension resonance frequencies [15], whereas infinite impulse response filters exhibit in most cases instability and difficulty to guarantee that the filter in combination with an algorithm finds a global minimum [18]. A more suited self-tuning filter is an infinite impulse response with fixed poled, also called generalized finite impulse response filter [19].

Filters are in most applications adapted with Least Mean Square (LMS) algorithms. In this, a choice needs to be made which signal to use as a regressor and as an error to be minimized. Commonly used are Filtered-reference LMS (FxLMS) [20] which filters the floor signal(s) and Filtered-error LMS (FeLMS) [21] that filters the isolated base signal(s) such that the regressor and error are correctly aligned [22]. In the case of a multiple-input-multiple-output system, the FeLMS outperforms the FxLMS. The reason is that FxLMS uses a Kronecker product which requires a significant amount of computational power. However, stability and convergence properties are similar.

A further advantage of self-tuning filters is that they automatically account for the influence of sensor and actuator noise. Due to this, it converges to a minimum of measured vibrations on the isolated base.

1.5. Research challenges

The knowledge of using controllers for active stages to minimize the tracking error and settling time is well-known. However, there is to the best of the author's knowledge no research on the influence of active stages on the vibration isolation system and vice versa. Also, there is a lack of knowledge for a multi-objective control strategy that is simultaneously operational for the active stage and vibration isolation system. Besides that, a theoretical framework is not present for a vibration isolation system that uses both indirect and direct disturbances as control input for a model-based feedforward controller in combination with a feedback controller with the aim of minimal internal deformation and maximal tracking accuracy. Therefore, in this research, the goals are to set up a theoretical framework in which the important transfer paths and performance limiters are present, design a multi-objective control strategy for both the active stage and vibration isolation system, and conducting experiments to validate the proposed control strategies.

For this, the focus is put on a benchmark system that consists out of an active stage mounted on top of a Stewart Gough vibration isolation system. The active stage has a translational single degree of freedom for the moving part with flexure-based guidance. Moreover, it has intentional frame compliance in which a sensor is fastened that measures the internal deformation perpendicular to the guided part movements. The active stage is designed and verified in this research. Next to that, all dominant transfer paths are experimentally identified and characterised for the benchmark system such that a proper theoretical framework can be designed.

1.6. Outline of the thesis

This thesis consists out of three self-contained chapters and additional appendices. In chapter 2 the theoretical framework that describes all relevant transfer paths, and con-

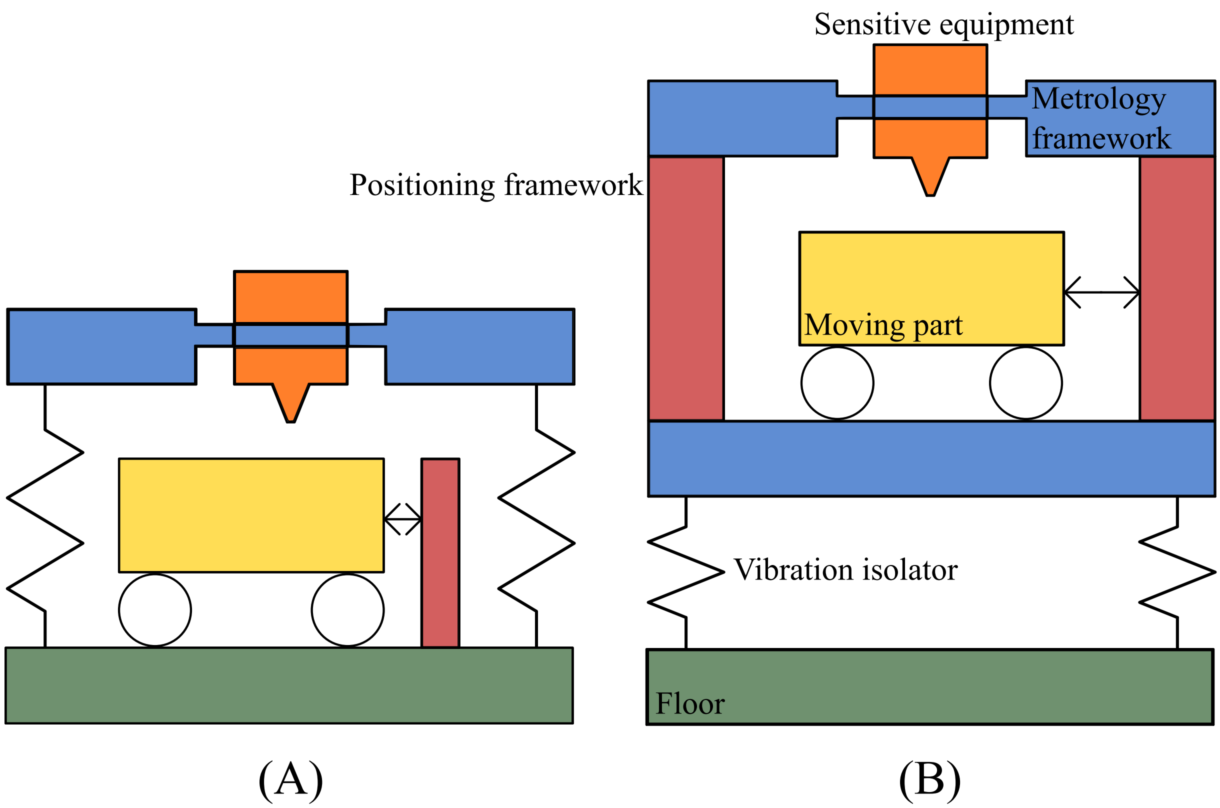

Figure 1: Precision machines configurations: (*A*) Seperated metrology and positioning framework and (*B*) integrated frameworks.

trol strategies for both the active stage and vibration isolation system are presented. Furthermore, control strategies are proposed and validated with simulations and experiments for a single degree of freedom translation flexure-based active stage mounted on top of a Stewart Gough vibration isolation system. The active stage feedback is tuned such that the influence of all disturbances and noises on the error is balanced. For this, the parameters of a PID controller are determined according to the sensitivity and complementary sensitivity. This is appended with a feedforward controller whose parameters are estimated with a Kalman filter. In addition, the vibration isolation system makes use of a feedback controller that is tuned according to the power spectral densities of the measured vibration of the isolated base, that take into account the known disturbances and noises of sensors and actuators. Finally, an indirect and direct disturbance feedforward controller is applied in which a self-tuning filter is implemented that aims to minimize the measured vibrations of the isolated base. All this is written in a paper format.

Chapter 3 describes the design and verification of an active stage. The active stage is constructed out of a translational single degree of freedom flexure-based mechanism for the moving part and intentional frame compliance in which a sensor is fastened that measures perpendicular to the part movements the internal deformation. The active stage is constructed for conducting experiments that are explained in the paper of Chapter 2.

Chapter 4 describes the implementation of the active stage on the vibration isolation system and analyses the dominant transfer paths that are needed to set up a theoretical framework and a multi-objective control strategy, which is explained in the paper of Chapter 2.

Overall conclusion and recommendations are provided in Chapter 5. Extended results, block diagram manipulations and modal analysis of the active stage are given in the Appendices.

2. Paper: Control design for a vibration isolation system with an active stage

Control design for a vibration isolation system with an active stage

Roy Kelder[a] (Student)

[a]*Paulus Potterstraat 95, 7545 DV Enschede, The Netherlands*

ARTICLE INFO

Keywords:
reference tracking
settling time
active vibration isolation
internal deformation
adaptive control
disturbance attenuation

ABSTRACT

This paper proposes a multi-objective control strategy for a vibration isolation system with an active stage to improve tracking of a reference profile, attenuate vibrations of the isolated base and minimize internal deformations. As a basis for designing the controllers is set up a theoretical framework taking into account the dynamics, sensors, actuators, disturbances, and noises. A PID controller in combination with a model-based adaptive feedforward controller is designed for the active stage. The feedforward control parameters are estimated online with a Kalman filter. The active vibration isolation system is implemented with a feedback controller tuned such that the power spectral density relating to the measured vibrations of the isolated base is minimal. Furthermore, a self-tuning feedforward controller with a Filtered-error Least Mean Square (FeLMS) algorithm is proposed that uses both measured indirect disturbances and generated direct disturbances as control inputs. The feasibility of the control strategies is demonstrated on a multi-degree of freedom flexure-based benchmark system. Experiments show promising results. The vibrations of the isolated base are attenuated with 24 dB compared to the passive configuration. Due to this, the internal deformation reduces with a ratio of five and tracking error with a ratio of three. The active stage is able to track a reference, that has acceleration components up to 50 $\mathrm{m/s^2}$, with a maximum tracking error of 1 μm only. After each reference step, with all controllers operational, the moving part settles in 0.048 s and internal deformation in 0.128 s with an error of 0.01 μm.

1. Introduction

The demand for accurate reference tracking is ever-increasing [23]. This is often combined with a requirement for minimal internal deformation between the moving part(s) and sensitive equipment. Examples for which these requirements hold are wafer steppers and electron-microscopes [23]. The performance of these systems is limited by vibrations caused by indirect and direct disturbances, where in particular indirect disturbances are induced through seismic activity and direct disturbances from forces generated by the moving part(s). The indirect disturbances act through the machine's suspension and direct disturbances directly on the isolated base of the system.

A passive vibration isolation system can be used to isolate the base with moving part(s) and sensitive equipment from the indirect disturbances [24]. For these passive systems, a clear trade-off exists between the sensitivity for indirect and direct disturbances. Relative low suspension modes are required to have good properties in terms of transmissibility and high suspension modes are needed to have a good compliance [25]. Active vibration isolation systems can be used to mitigate the trade-off between sensitivity to indirect and direct disturbances.

A numerous amount of feedback controllers already show an increase in performance with aid of absolute acceleration and/or velocity measurements [26], force feedback [27] and sensor fusion with state observer [28]. Tuning approaches are for example based on LQG [28], H_∞ norms [29], MRAC [30, 31] and optimal parameter tuning taking into account the influence of all individual noises and disturbances in terms of power spectral densities [32].

roy_kelder@hotmail.com (R. Kelder)

Another essential category for active vibration is feedforward control. Herein the aim is to mimic the transfer paths that are in between disturbances and isolated base, such that a force is created that cancels the force induced by the sum of all disturbances on the isolated base [33, 34]. In this, the effectiveness is determined mostly by the accuracy of parameter estimation [33]. One way to minimize uncertainty is by performing extensive identification experiments. However, this cannot take time-varying uncertainties into account. A solution is using self-tuning filters that make use of minimizing a quadratic cost function by a gradient descent method which are known as Least Mean Square (LMS) algorithms. These algorithms automatically include the influence of sensor and actuator noise because it tries to minimize the error of the system, which in this case are the vibrations of the isolated base [33]. To deal with plant dynamics a Filter-error Least-Mean-Square (FeLMS) algorithm [21, 35] in combination with a generalized FIR filter can be used. This correctly aligns the signals [22], make the filter inherently stable, and requires few parameters to accurately estimate the dynamic response.

The objective of all mentioned controllers is to minimize vibrations of the isolated base, however, none considers an active stage with moving part(s) and sensitive equipment in combination with a vibration isolation system. Furthermore, most focus only on transmissibility and compliance as performance indicators without considering the tracking error and internal deformation.

Therefore, this paper presents a multi-objective control strategy for an active stage with a vibration isolation system that is designed, taking into account the tracking error and internal deformation. For this, both types of disturbances are used as control inputs.

To achieve this, the first contribution of this paper is a model-based theoretical framework in which all important characteristics for are incorporated. Based on this theoretical framework, performance requirements can easily be linked to the control strategies. The interaction of the active stage to the vibration isolation system and vice versa thereby explicitly taken into account.

For reference tracking of the moving part in the active stage, a controller is designed. It comprises a PID controller [36] to ensure stability and accurate tracking. Herein the parameters are tuned taking into account the sensitivity and complementary sensitivity. This is combined with a model-based feedforward controller for a more refined tracking, wherein the parameters are estimated with a Kalman filter [37, 38].

The second contribution is a control strategy for the vibration isolation system. For this, a feedback controller is chosen in which the parameters are manually tuned to minimize the power spectral densities that relate to the vibrations of the isolated base [32]. In addition, a generalized self-tuning FIR filter with FeLMS is implemented as a feedforward controller that takes both the indirect and direct disturbances as control inputs [33].

The control strategies of the active stage and vibration isolation system are evaluated by means of simulations and experiments for which a flexure-based benchmark system is used [39]. Herewith it is shown that the proposed control strategies show promising results for accurate reference tracking and minimal internal deformation. The benchmark system is used throughout the paper for visualization and reference to clarify the theoretical framework and proposed control strategies.

The remainder of this paper is organized as follows. In Section 2 an overview of the benchmark system is given. The problem formulation with the theoretical framework is presented in Section 3. The controller design is given in Section 4 and verified with simulations in Section 5 and experiments in Section 6. The conclusions and main findings of the research are given in Section 7.

2. System description

The benchmark system shown in figure 1 and with a schematic section view in figure 2 is representative of high-end precision machines and is modular in the sense that the active stage and vibration isolation system are designed separately and can be detached from each other. The modularity allows the active vibration isolation control system to be tested for other types of active stages and passive payloads.

In total, the system has 10 actuated Degrees Of Freedom (DOFs) and a single intentional frame compliance to mimic internal deformation between the equipment of interest. The vibration isolation system has all six DOFs and resembles a Stewart Gough platform. On top of the vibration isolation system, an active stage is mounted. This active stage consists out of a framework with an intentional frame compliance mode and a single translational DOF moving part guided by folded leaf springs. A three DOF floor assembly enables

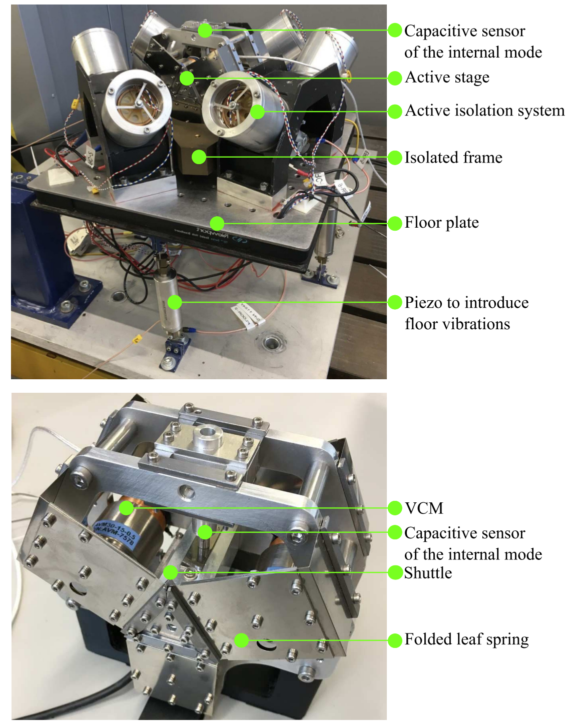

Figure 1: Photos of the total benchmark system and active stage only.

the introduction of floor vibrations in three out-of-plane directions. The functionalities of the benchmark system can roughly be described by four categories(①-④); ① mimic an industrial floor spectrum, ② attenuate vibrations with the vibration isolation system, ③ tracking of a reference with the moving part and ④ measuring internal deformation.

In the remainder of this section, the schematic shown in figure 2 is used to further explain the important components. At the bottom is positioned a three-DOF $(z_f, \theta_{xf}, \theta_{yf})$ floor base actuated with three piezo's (Piezomechanik PSt 150/5/40) that induce an industrial floor spectrum ①. The indirect disturbances (floor vibrations) are measured in local coordinates $\ddot{\boldsymbol{q}}_f(t) \in \mathbb{R}^6$ with six accelerometers (Endevco 7703A-1000). Connected to this is a vibration isolation system that consists of an axisymmetric isolated base connected by wire springs to the active suspension systems [39]. The active attenuation ② is realised with six Voice Coil Motors (VCMs, Geeplus VM4032-250) with parallel flexure-based straight guides with one side fixed to the wire springs and the other to the floor frame. Another set of six accelerometers (Endevco 7703A-1000) are placed in line with wire springs to be able to measure all six-DOF of the isolated base, in local coordinates $\ddot{\boldsymbol{q}}_i(t) \in \mathbb{R}^6$. The voltage controlled VCMs $\boldsymbol{f}_i(t) \in \mathbb{R}^6$ serve as output of the feedback and disturbance feedforward controller.

The moving part of the active stage is denoted as the shuttle and on both sides, a VCM (AVM 30-15) is positioned for tracking of the desired reference profile ③. Both VCMs are current-controlled and their currents are balanced such that the VCMs can be considered as a single control output

$F_a(t) \in \mathbb{R}$. The shuttle guided by means of six folded leaf springs with a resonance frequency of around 9.5 Hz in the nominal DOF. The folded leaf springs are designed such that a stroke of ±5 mm can be achieved. Each folded leaf spring is equipped with a sandwich-based reinforcement that prevents buckling and increases the first parasitic frequency to around 650 Hz. On the shuttle's lower side a linear scale (Renishaw, RGSZ20) is glued as a reference for an optical incremental encoder. The encoder (Renishaw, T1000-15A) itself is mounted to the active stage framework and measures the relative displacement $\triangle x_a = x_a - x_i \in \mathbb{R}$. Above the shuttle and inside the active stage framework a capacitive sensor (Lion Precision, C5R) is located that measures the internal deformation $\delta z_c = z_c - z_i \in \mathbb{R}$ ④. A combination of leaf springs is used to fasten the sensor and to introduce an intentional frame compliance. As a result, a parasitic mode is present around 390 Hz. The shuttle top plane is equipped with a block for reference of the capacitive sensor that measures perpendicular to the shuttle driving direction the internal deformation.

All signals are processed and the control strategies are implemented on a a real-time dSpace processor board (DS-1005) at a sample rate of 6.4 kHz. Correct read-out of the accelerometers requires signal conditioners (Bruël Kjaer nexus 2692-0S4) and Analog-to-Digital Converters (dSpace, ADC DS-2004). The analog incremental encoder makes use of another dSpace sub-module (dSpace, DS-3002). Furthermore, the capacitive sensor is read-out with a lion precision device and passed on to the ADC sub-module.

The analog outputs of the system are filtered by anti-imaging filters (Frequency devices, 424 Series) to remove sampling artifacts, and amplified with actuator drivers (Trust Automation, TA-105). The active stage VCMs are only amplified by the actuator drivers. Independently of both control strategies, the piezos are excited. Actuation is realised with the help of reconstruction filters and respective amplifiers (piezomechanic, SVR 150-3-bip).

2.1. Modeling

The complete system is designed such that the vibration isolation system's DOFs and active stage shuttle DOF is actuated [40]. Furthermore, all parasitic modes of the mechanical structure (except for the intentional frame compliance) lie above 500 Hz. This justifies the use of a rigid-body representation of the complete system that describes the most important dynamics accurately for frequencies below 500 Hz.

In order to fit all important dynamics in a compact notation. All local accelerometer signals $\ddot{\boldsymbol{q}}_f(t)$, $\ddot{\boldsymbol{q}}_i(t)$ and actuator forces $\boldsymbol{f}_i(t)$ of the vibration isolation system are mapped to the elastic center with transformation matrices $\boldsymbol{R}_f, \boldsymbol{B}_J \in \mathbb{R}^{6x6}$ [39],

$$\begin{aligned}\ddot{\boldsymbol{x}}_f(t) &= \boldsymbol{R}_f \ddot{\boldsymbol{q}}_f(t),\ \ddot{\boldsymbol{x}}_i(t) = \boldsymbol{B}_J^{-T} \ddot{\boldsymbol{q}}_i(t),\\ \boldsymbol{F}_i(t) &= \boldsymbol{B}_J \boldsymbol{f}_i(t).\end{aligned} \tag{1}$$

With this, the equations of motion of the benchmark system can be written as

$$\boldsymbol{M}\ddot{x}(t) + \boldsymbol{C}\dot{x}(t) + \boldsymbol{K}x(t) = \boldsymbol{B}\boldsymbol{F}(t) + \boldsymbol{D}\boldsymbol{d}(t). \tag{2}$$

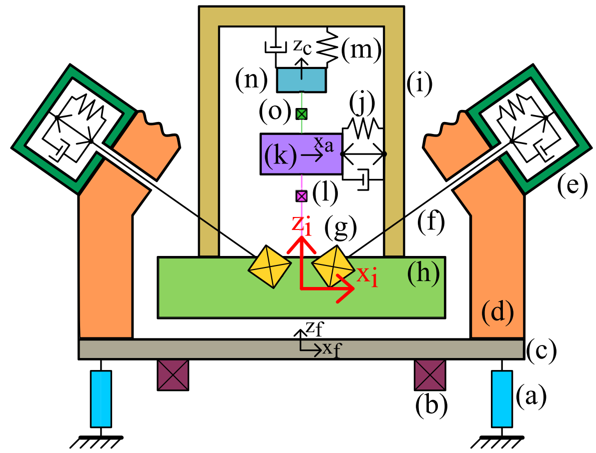

Figure 2: Schematic section view of the benchmark system: (a) piezo for floor excitation, (b) accelerometer floor, (c) floor base frame, (d) floor frame, (e) active vibration isolation system with VCMs and circular leaf springs, (f) wire springs, (g) accelerometer isolated base, (h) isolated base, (i) active stage frame, (j) active stage VCMs and guidance by means of folded leaf springs, (k) shuttle, (l) incremental encoder, (m) intentional frame compliance, (n) capacitive sensor assembly and (o) capacitive sensor. The global coordinate system is denoted with red-arrows and the DOF of the active stage with $x_a(t)$ and parasitic deformation with $z_c(t)$.

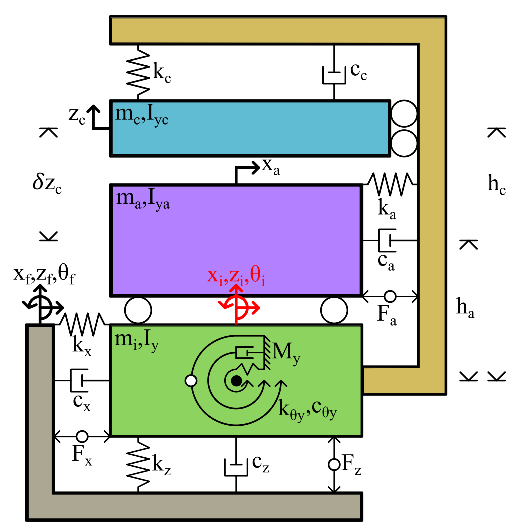

Figure 3: Conceptual 2D-representation of the floor, vibration isolation system, active stage and capacitive sensor assembly with intentional frame compliance. All rigid body dynamics parameters are denoted with: force F or moment M, mass m, inertia I, damping c, stiffness k and height h.

The displacements $\boldsymbol{x}(t) = \left\{\boldsymbol{x}_i(t) \quad x_a(t) \quad x_c(t)\right\}^T \in \mathbb{R}^8$ are written in the elastic center [39]. The $\boldsymbol{M}, \boldsymbol{C}, \boldsymbol{K} \in \mathbb{R}^{8x8}$ terms represent the global system mass, damping and stiffness matrices. The respective forces $\boldsymbol{F}(t) \in \mathbb{R}^8$ are transformed by the matrix $\boldsymbol{B} \in \mathbb{R}^{8x7}$. Furthermore, the floor is considered rheonomic [34] and therefore written as a disturbance source denoted by $\boldsymbol{d}(t) \in \mathbb{R}^6$ where $\boldsymbol{D} \in \mathbb{R}^{8x6}$ is used as a transformation matrix. The schematic of figure 2 is further simplified to a conceptual drawing as shown in figure 3, which represents the benchmark system in the plane of motion. Herein the elastic center is denoted by red arrows and is named the global coordinate system. Note, however, that the vibration isolation system also has dynamics in three additional out-of-plane directions. Expanding the equations of motion in a more detailed form, gives

$$
\begin{aligned}
&\underbrace{\left[\begin{bmatrix} \boldsymbol{M_i} & \boldsymbol{0} & \boldsymbol{0} \\ \boldsymbol{0} & m_a & \boldsymbol{0} \\ \boldsymbol{0} & \boldsymbol{0} & m_c \end{bmatrix} + \boldsymbol{M_{i,o}}\right]}_{\mathrm{M}} \begin{Bmatrix} \ddot{\boldsymbol{x}}_i(t) \\ \ddot{x}_a(t) \\ \ddot{z}_c(t) \end{Bmatrix} \\
&+ \underbrace{\left[\begin{bmatrix} \boldsymbol{C_f} & \boldsymbol{0} \\ \boldsymbol{0} & \boldsymbol{0} \end{bmatrix} + \begin{bmatrix} \boldsymbol{C_i} & \boldsymbol{C_{ia}} & \boldsymbol{0} \\ \boldsymbol{C_{ai}} & c_a & 0 \\ \boldsymbol{0} & 0 & 0 \end{bmatrix} + \boldsymbol{C_c}\right]}_{\mathrm{C}} \begin{Bmatrix} \dot{\boldsymbol{x}}_i(t) \\ \dot{x}_a(t) \\ \dot{z}_c(t) \end{Bmatrix} \\
&+ \underbrace{\left[\begin{bmatrix} \boldsymbol{K_f} & \boldsymbol{0} \\ \boldsymbol{0} & \boldsymbol{0} \end{bmatrix} + \begin{bmatrix} \boldsymbol{K_i} & \boldsymbol{K_{ia}} & \boldsymbol{0} \\ \boldsymbol{K_{ai}} & k_a & 0 \\ \boldsymbol{0} & 0 & 0 \end{bmatrix} + \boldsymbol{K_c}\right]}_{\mathrm{K}} \begin{Bmatrix} \boldsymbol{x}_i(t) \\ x_a(t) \\ z_c(t) \end{Bmatrix} = \\
&\underbrace{\begin{bmatrix} \boldsymbol{B_i} & \boldsymbol{B_{ia}} \\ \boldsymbol{0} & 1 \\ \boldsymbol{0} & \boldsymbol{0} \end{bmatrix}}_{\mathrm{B}} \begin{Bmatrix} \boldsymbol{F}_i(t) \\ F_a(t) \end{Bmatrix} + \underbrace{\begin{bmatrix} \boldsymbol{C_f} & \boldsymbol{K_f} \\ \boldsymbol{0} & 0 \end{bmatrix}}_{\mathrm{D}} \begin{Bmatrix} \boldsymbol{v}_f(t) \\ \boldsymbol{x}_f(t) \end{Bmatrix}.
\end{aligned}
\tag{3}
$$

Note that the equations of motion are complemented with zeros for correct matrix sizes. The associated numerical values for the simulations are given in Appendix A.

The displacements of the isolated base are expressed with $\boldsymbol{x_i}(t) \in \mathbb{R}^6$ and correspond to the ideal mass, damping, and stiffness matrices, $\boldsymbol{M_i}, \boldsymbol{C_f}, \boldsymbol{K_f} \in \mathbb{R}^{6x6}$. The damping and stiffness matrix also relate to the rheonomic floor velocities and displacements, $\boldsymbol{v_f}(t), \boldsymbol{x_f}(t) \in \mathbb{R}^3$. Additional dynamics due to the active stage for the vibration isolation system are accounted for by matrices $\boldsymbol{C_i}, \boldsymbol{K_i} \in \mathbb{R}^{6x6}$. The dynamics of the capacitive sensor assembly and springs of the intentional frame compliance are described with parameter $m_c \in \mathbb{R}$ and matrices $\boldsymbol{C_c}, \boldsymbol{K_c} \in \mathbb{R}^{8x8}$. These dynamics relate to the displacements $\boldsymbol{x_i}(t)$ but also $z_c(t) \in \mathbb{R}$ of the capacitive sensor which is unactuated, intentional parasitic deformation. The influence of shuttle displacements $x_a(t) \in \mathbb{R}$ on the vibration isolation system and vice versa is accounted for with vectors $\boldsymbol{C_{ia}}, \boldsymbol{K_{ia}} \in \mathbb{R}^{6x1}$ and $\boldsymbol{C_{ai}}, \boldsymbol{K_{ai}} \in \mathbb{R}^{1x6}$. Matrix $\boldsymbol{B_i} \in \mathbb{R}^{6x6}$ describes the relation between vibration isolation system actuator forces $\boldsymbol{F_i} \in \mathbb{R}^6$ and displacements $\boldsymbol{x_i}(t)$, whereas the relations between active stage actuator force $F_a \in \mathbb{R}$ to displacements $\boldsymbol{x_i}(t)$ are described by vector $\boldsymbol{B_{ia}} \in \mathbb{R}^{6x1}$. The shuttle and guidance dynamics are described by parameters $m_a, c_a, k_a \in \mathbb{R}$. In practice, an extra matrix $\boldsymbol{M_{io}} \in \mathbb{R}^{8x8}$ with off-diagonal terms is needed that accounts for an out of alignment center of mass with respect to the elastic center.

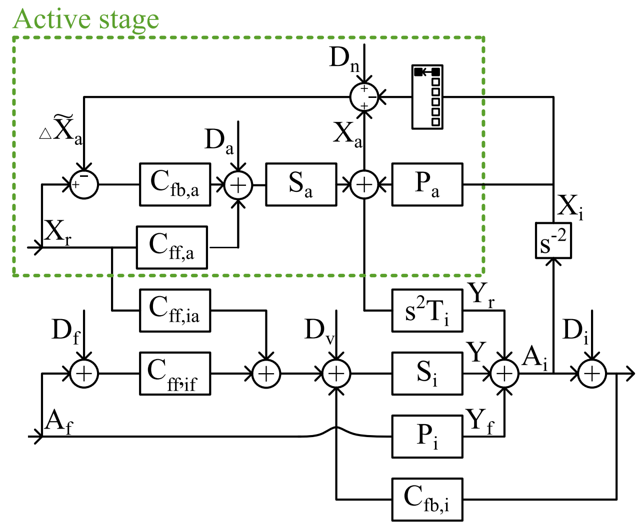

Figure 4: Schematics of mixed feedback and non-adaptive feedforward control strategies for both the vibration isolation system and active stage with respective noise sources.

3. Problem formulation

3.1. System characteristics

The characteristics of the benchmark system are necessary to identify the influence of physical parameters and control strategies on the performance objectives, which are: 1 accurate reference tracking and settling time of shuttle displacement $x_a(t)$, 2 attenuation of vibrations in the isolated base $\ddot{\boldsymbol{x}}_{\boldsymbol{i}}(t)$, and 3 minimal internal deformation and settling time which is denoted by $\delta z_c(t)$.

These influences are quantified by the transfer paths obtained by converting the equations of motion to the Laplace domain. A schematic of all relevant transfer paths is shown in figure 4. It is chosen to exclude the effect of internal deformation from the scheme because the performance objectives of 3 are dependent from objective 2.

3.1.1. Active stage characteristics

The encircled active stage in figure 4 includes a primary path $\boldsymbol{P}_a(s)$ which describes the transfer from displacements of the isolated base $\boldsymbol{X_i}(s)$ through the guidance dynamics on the shuttle displacement $X_a(s)$, and a secondary transfer path $S_a(s)$ between control output $F_a(s)$ and displacement $X_a(s)$. Both transfer paths can be described with the variables of the equation of motion as

$$
\begin{aligned}
S_a(s) &= (m_a s^2 + c_a + k_a)^{-1}, \\
\boldsymbol{P_a}(s) &= (\boldsymbol{C_{ai}} s + \boldsymbol{K_{ai}}) S_a(s).
\end{aligned}
\tag{4}
$$

The active stage is controlled in terms of a feedback $C_{fb,a}(s)$ and a feedforward $C_{ff,a}(s)$ controller. Reference $X_r(s)$ is used as control input for the feedforward controller and both the reference and relative position $\triangle X_a(s) = X_a(s) - X_i(s)$ in case of feedback control. The relative position results from the measurement head being attached to the isolated base with translational coordinate $X_i(s)$ and scale to the shuttle $X_a(s)$. Furthermore, noise of sensor and actuator are taken into account by the terms $D_n(s)$ and $D_a(s)$.

In order to quantify the performance objectives of $\boxed{1}$, reference tracking error $E(s) = (X_r(s) - \triangle X_a(s))$, is written in terms of the signal sources mentioned above,

$$\begin{aligned} E(s) = &\underbrace{\mathbb{S}_a(s)\left(1 - C_{ff,a}(s)S_a(s)\right)}_{t_1} X_r(s) - \mathbb{S}_a(s)X_i(s) \\ &+ \underbrace{\mathbb{S}_a(s)\boldsymbol{P_a}(s)}_{t_2} \boldsymbol{X_i}(s) - \underbrace{\mathbb{S}_a(s)S_a}_{t_3} D_a(s) \\ &+ \mathbb{T}_a(s)D_n(s), \end{aligned} \tag{5}$$

with sensitivity and complementary sensitivity

$$\begin{aligned} \mathbb{S}_a(s) &= \left(1 + C_{fb,a}(s)S_a(s)\right)^{-1}, \\ \mathbb{T}_a(s) &= \mathbb{S}_a(s)\left(C_{fb,a}(s)S_a(s)\right). \end{aligned} \tag{6}$$

This shows that the influence of the reference, disturbances, and noises on the error $E(s)$ depends on the following transfer paths:

- The terms in t_1 where the shuttle guidance dynamics $S_a(s)$, feedback $C_{fb,a}(s)$ controller and feedforward $C_{ff,a}(s)$ controller determines the influence of the reference $X_r(s)$.
- The sensitivity $\mathbb{S}_a(s)$ only, in the case of the isolated base frame translational displacement $X_i(s)$, which causes an error because a relative incremental encoder is used.
- The terms in t_2 that describes the transfer paths from displacements of the isolated base $\boldsymbol{X_i}(s)$ through the guidance dynamics $\boldsymbol{P_a}(s)$ and sensitivity $\mathbb{S}_a(s)$.
- The sensitivity $\mathbb{S}_a(s)$ which determines the influence of actuator noise $D_a(s)$.
- The complementary sensitivity $\mathbb{T}_a(s)$ which determines the influence of incremental encoder noise $D_n(s)$.

With specified dynamics, noises, and disturbances, the active stage control problem can now be formulated as follows. Find a feedback $C_{fb,a}(s)$ and a feedforward $C_{ff,a}(s)$ controller which minimizes the tracking error and settling time. More specifically, find a feedforward controller $C_{ff,a}(s)$ that cancels the terms of t_1, and find a feedback controller $C_{fb,a}(s)$ considering both the sensitivity and complementary sensitivity function with the respective spectra of noises and disturbances.

3.1.2. Vibration isolation system characteristics

The influence of isolated base displacements $\boldsymbol{X_i}(s)$ on the error $E(s)$, also depends on the vibration isolation system control strategy, since isolated base displacements can be actively attenuated with the vibration isolation system.

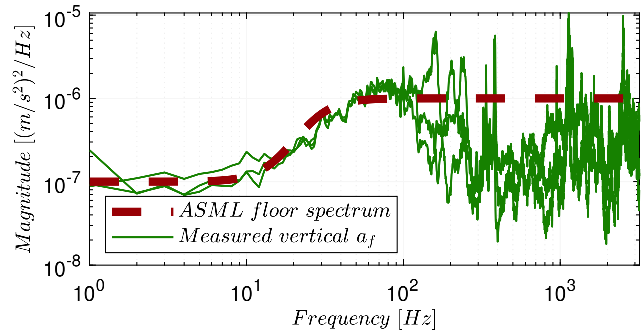

Figure 5: Power spectral density of the ASML floor spectrum and measured vertical floor accelerometers spectra.

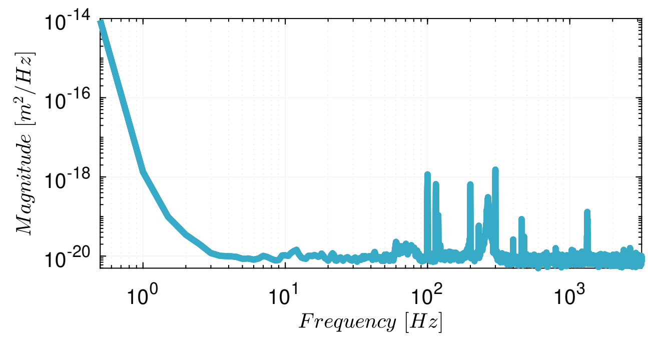

Figure 6: Power spectral density of incremental encoder noise.

For this, consider the transfer paths of the vibration isolation system as shown in figure 4. It consists out of primary path $\boldsymbol{P_i}(s)$ which describes the transfer from measured floor vibrations $\boldsymbol{A_f}(s)$ through the suspension dynamics on the measured vibrations of the isolated base $\boldsymbol{A_i}(s) = s^2\boldsymbol{X_i}(s)$, secondary transfer path $\boldsymbol{S_i}(s)$ from control output $\boldsymbol{F_i}(s)$ to $\boldsymbol{A_i}(s)$, and tertiary path $\boldsymbol{T_i}(s)$ from shuttle displacement $X_a(s)$ to $\boldsymbol{A_i}(s)$. The vibration isolation system is controlled with a feedback controller $\boldsymbol{C_{fb,i}}(s)$ which utilizes the measured vibrations of the isolated base $\boldsymbol{A_i}(s)$ and a feedforward controller $\boldsymbol{C_{ff,i}}(s) = \left\{\boldsymbol{C_{ff,if}}(s) \quad \boldsymbol{C_{ff,ia}}(s)\right\}$ that uses measured indirect floor vibrations $\boldsymbol{A_f}(s)$ and the reference component $A_r(s) = s^2X_r(s)$ as control inputs. The latter is linked to the direct disturbance caused by shuttle movements. It will be shown in Section 4 that $X_r(s) \approx X_a(s)$ if certain conditions are met.

The input-output relations that quantify the performance objective $\boxed{2}$ and indirectly influences the error $E(s)$ of the active stage can be described as

$$\boldsymbol{A_i}(s) = \boldsymbol{P_i}(s)\boldsymbol{A_f}(s) + \boldsymbol{S_i}(s)\boldsymbol{F_i}(s) - \boldsymbol{T_i}(s)s^2X_a(s). \tag{7}$$

The performance objectives of $\boxed{3}$ are directly related to this, since (with the rigid body dynamics up to 500 Hz) the intentional frame compliance $\delta Z_c(s)$ is only excited when the isolated base vibrates.

Elaborating the transfer functions of the input-output relations in terms of the variables in the equations of motion gives

$$
\begin{aligned}
&\boldsymbol{P_i}(s) = \boldsymbol{G^{-1}}(s)\left(\boldsymbol{C_f} s + \boldsymbol{K_f}\right), \\
&\boldsymbol{S_i}(s) = s^2 \boldsymbol{G^{-1}}(s)\boldsymbol{B_i}, \\
&\boldsymbol{T_i}(s) = s^2 \boldsymbol{G^{-1}(s)} \boldsymbol{B_{ia}} m_a,
\end{aligned}
\tag{8}
$$

with common terms

$$
\boldsymbol{G}(s) = (\boldsymbol{M_i} + \boldsymbol{M_{i,0}})s^2 + \boldsymbol{C_f} s + \boldsymbol{K_f}. \tag{9}
$$

Further elaborating equation (7) by including the effect of control disturbances and noise sources gives

$$
\begin{aligned}
\tilde{\boldsymbol{A}}_{\boldsymbol{i}}(s) = {} & \mathbb{R}(s)[\mathbb{T}(s)\boldsymbol{A_f}(s) + \mathbb{C}_r(s)A_r(s) \\
& + \mathbb{N}_v(s)\boldsymbol{D}_v(s) + \mathbb{N}_f(s)\boldsymbol{D}_f(s) \\
& + \mathbb{N}_a(s)D_a(s) - \mathbb{N}_n(s)D_n(s)] \\
& + \mathbb{N}_i(s)\boldsymbol{D}_i(s),
\end{aligned}
\tag{10}
$$

with a so-called return difference

$$
\mathbb{R}(s) = [\boldsymbol{1} + \left(\mathbb{T}_a(s)\boldsymbol{Q}(s)\right)\mathbb{S}_{\boldsymbol{fb}}(s)]^{-1}, \tag{11}
$$

and

$$
\begin{aligned}
\mathbb{T}(s) &= \mathbb{S}_{\boldsymbol{fb}}(s)\left(\boldsymbol{P_i}(s) + \boldsymbol{C_{ff,if}}(s)\boldsymbol{S_i}(s)\right), \\
\mathbb{C}_r(s) &= \mathbb{S}_{\boldsymbol{fb}}(s) \\
&\quad [\left(\boldsymbol{C}_{ff,a}(s) + \boldsymbol{C}_{fb,a}(s)\right) S_a(s)\boldsymbol{Q}(s)\mathbb{S}_a(s) \\
&\quad + \boldsymbol{C_{ff,ia}}(s)\boldsymbol{S_i}(s)], \\
\mathbb{N}_v(s) &= \mathbb{S}_{\boldsymbol{fb}}(s)\boldsymbol{S_i}(s), \\
\mathbb{N}_f(s) &= \mathbb{S}_{\boldsymbol{fb}}(s)\boldsymbol{C_{ff,if}}(s)\boldsymbol{S_i}(s), \\
\mathbb{N}_i(s) &= \mathbb{S}_{\boldsymbol{fb}}(s)\boldsymbol{C_{fb,i}}(s)\boldsymbol{S_i}(s), \\
\mathbb{N}_a(s) &= \mathbb{S}_{\boldsymbol{fb}}(s)\boldsymbol{Q}(s)[s^2 S_a(s)\mathbb{S}_a(s)], \\
\mathbb{N}_n(s) &= \mathbb{S}_{\boldsymbol{fb}}(s)\boldsymbol{Q}(s)[s^2 C_{fb,a}(s)S_a(s)\mathbb{S}_a(s)],
\end{aligned}
\tag{12}
$$

where the feedback sensitivity of the vibration isolation system is

$$
\mathbb{S}_{\boldsymbol{fb}}(s) = \left(\boldsymbol{1} - \boldsymbol{C_{fb,i}}(s)\boldsymbol{S_i}(s)\right)^{-1}, \tag{13}
$$

with common terms in $\mathbb{R}(s)$, $\mathbb{C}_r(s)$, $\mathbb{N}_a(s)$ and $\mathbb{N}_n(s)$ given by

$$
\boldsymbol{Q}(s) = \boldsymbol{T_i}(s)(1 - \boldsymbol{P_a}(s)\boldsymbol{T_i}(s))^{-1}. \tag{14}
$$

In equation (10), all terms can be interpreted as follows: the return difference $\mathbb{R}(s)$ is the result of a relative position encoder that influences all terms except for the isolated base accelerometer noise terms $\mathbb{N}_i(s)\boldsymbol{D}_i(s)$. The terms in $\boldsymbol{Q}(s)$ describes a feedback loop from vibrations of the isolated base through the shuttle with guidance dynamics and the transfer paths from shuttle displacements on the isolated base. Furthermore, transmissibility $\mathbb{T}(s)$ and compliance reference $\mathbb{C}_r(s)$ characterizes the transfer from floor vibrations $\boldsymbol{A_f}(s)$ and acceleration reference component $A_r(s)$ to the vibrations of the isolated base $\boldsymbol{A_i}(s)$. Next to that, noise sources of vibration isolation system actuators, accelerometers floor, actuators active stage, incremental encoder and accelerometers isolated base are described by noise sensitivities; $\mathbb{N}_v(s)$, $\mathbb{N}_f(s)$, $\mathbb{N}_a(s)$, $\mathbb{N}_n(s)$ and $\mathbb{N}_i(s)$.

With all disturbances and noises characterised the vibration isolation system controller problem can be formulated as follows. Find a feedback $\boldsymbol{C_{fb,i}}(s)$ and a feedforward $\boldsymbol{C_{ff,i}}(s)$ controller such that vibrations of the isolated base $\boldsymbol{A_i}(s)$ are minimized. In the absence of feedback controllers $\boldsymbol{C_{fb,i}}(s)$ and $C_{fb,a}(s)$, neglected noise contributions and a shuttle state $A_a(s)$ that equals the reference component $A_r(s)$. The objective simplifies to finding a feedforward controller $\boldsymbol{C_{ff,i}}(s)$ which mimics the respective transfer paths such that a force is generated that cancels the force caused by all measured indirect floor disturbances $\boldsymbol{A_f}(s)$ and direct generated active stage reference component disturbance $A_r(s)$. However, due to discretization perfect cancellation is not possible as both types of disturbances are continuous, and in the case of indirect disturbances, the control force is inherently too late. Besides that, the direct disturbance control input $A_r(s)$ slightly differs from the real direct disturbance source $A_a(s)$ due to a tracking error. Therefore, a feedback controller $\boldsymbol{C_{fb,i}}(s)$ is needed in which the objective is to find a controller where a balanced trade-off is made between all spectra of noises and disturbances such that the influence of it on the vibrations of the isolated base are minimal in a certain frequency range.

3.2. Reference profile

The shuttle of the active stage is required to track a third-order reference with a stroke of $x_r(t) = \pm 5$ mm and maximum acceleration $a_r(t) = 50$ m/s^2 [36]. The difference of this reference and measured position $\triangle x_a(t)$ quantifies the performance objectives of ▯.

3.3. Floor vibrations

The floor vibrations of industrial high-tech sites are often characterised by standardized Power Spectral Density (PSD) curves. In this research the piezos are controlled such that the vertical floor accelerometers $\ddot{\boldsymbol{q}}_{\boldsymbol{f}}(t)$ measure an approximated ASML-spectrum [41]. The respective ASML floor spectrum and measured vertical accelerometer signals are shown in figure 5. For the simulations, the floor spectrum is mimicked by feeding a white noise through a shaping filter of the ASML spectrum.

3.4. Noises

The non-white noise spectra of the accelerometers $\bar{S}_{D_f}(s) = \bar{S}_{D_i}(s)$ and actuators $\bar{S}_{D_a}(s) \approx \bar{S}_{D_v}(s)$ are adopted from earlier research [32]. The noise of the incremental encoder $\bar{S}_{D_n}(s)$ is determined by firmly locking the shuttle and subsequently measuring the output. The respective power spectral density is shown in figure 6.

4. Control design

This section presents the controller design for both the active stage and vibration isolation system. First, a PID controller is presented for which equation (5) and the shuttle and guidance dynamics of the active stage are considered. Second, an adaptive feedforward for the active stage is presented wherein the terms in t_1 of equation (5) are taken into account. Third, a high-gain feedback controller is presented where the suspension modes of the vibration isolation system and all known noises and disturbances are considered. Finally, a feedforward controller is presented that consists out of a self-tuning filter with a FeLMS algorithm wherein measured indirect floor disturbances, generated direct shuttle disturbances, respective actuator noises and floor accelerometer noises are considered.

4.1. Active stage control

The proposed PID-feedback controller [36] is based on tuning only the cross-over frequency of the open-loop

$$L(s) = C_{fb,a}(s) S_{\triangle a}(s). \tag{15}$$

Herein the augmented secondary path $S_{\triangle a}(s)$ can be approximated by

$$\begin{aligned} &S_{\triangle a}(s) \approx \\ &\frac{\triangle X_a(s)}{F_a(s)} = \frac{w_2^2(s^2+w_3^2)(s^2+w_{ar}^2)}{m_a w_{ar}^2 (s^2+w_1^2)(s^2+w_2^2)(s^2+w_3^2)}, \\ &\omega_1 = \sqrt{\frac{k_a}{m_a}},\ \omega_2 = \sqrt{\frac{k_i}{m_i+m_c}},\ \omega_3 = \sqrt{\frac{k_\theta}{I_{tot}}}, \\ &\omega_{ar} = \sqrt{\frac{k_i}{m_i+m_a}}. \end{aligned} \tag{16}$$

This shows the main resonance frequency of the active stage guide at ω_1. The influence of the vibration isolation system is reflected with the resonance frequencies ω_2 and ω_3, whereas the anti-resonance frequency with ω_{ar}. These latter terms can be interpreted as follows: ω_2 is the suspension frequency in the x_i-direction, ω_3 in θ_{yi}-rotation and ω_{ar} is the mode in which the shuttle and isolated base move in phase with equal amplitude.

The influence of the vibration isolation system dynamics is negligible if the suspension frequencies are damped appropriately and $m_a << (m_i + m_c)$ (figure 13). As a result of this, the open-loop can be simplified to

$$L(s) \approx C_{fb,a}(s) S_a(s). \tag{17}$$

The influence of all components, except for the incremental encoder noise, on the error $E(s)$ as described with the input-output relations of equation (5) decreases with a large open-loop gain because it makes the sensitivity smaller and the complementary sensitivity larger. This signifies that a balanced trade-off needs to be made such that the influence of incremental encoder noise in comparison with the sum of all other components on the error is approximately equal. In practice, parasitic modes are present above 500 Hz. Therefore, the cross-over frequency is chosen, taking into account stability and the influence of all components on the error.

For the feedforward controller design, the terms in t_1 of equation (5) are considered, therefore the error is written as

$$E(s) = \mathbb{S}_a(s)\left(1 - C_{ff,a}(s) S_a(s)\right) X_r(s). \tag{18}$$

From this, it can seen that $E(s) = 0$ when

$$C_{ff,a}(s) = S_a^{-1}(s). \tag{19}$$

In order to accurately find the parameters of $S_a^{-1}(s)$, a Kalman filter [37] is used that estimates the parameters online. It requires the inverse secondary path to be rewritten such that the parameters are linear in those parameters. However, not all states of the system are measured and therefore it is necessary to include differentiators. The gain of the differentiator increases linearly with frequency and thereby amplifies noise content at higher frequencies. To account for this both $F_a(s)$ and $\tilde{\theta}$ are filtered with a low pass filter $F(s)$. The rewritten form with the inclusion of the filter, parameter vector $\tilde{\theta}$ and a so-called linear regressor is given by

$$\underbrace{F(s)F_a(s)}_{\text{y(s)}} = \underbrace{F(s)\left\{s^2 \quad s \quad 1\right\} X_a(s)}_{\text{H(s)}}\,\tilde{\theta}, \tag{20}$$

with

$$\tilde{\theta} = \{m_a\ c_a\ k_a\}^T. \tag{21}$$

The Kalman filter noise variances are determined according to the actuator and incremental encoder noise spectra. The initial parameter vector and covariance matrix are chosen from the identified transfer path $S_a(s)$ for tuning the feedback controller $C_{fb,a}(s)$.

4.2. Vibration isolation system control

The proposed feedback controller is based on minimizing the power spectral density of the measured vibrations of the isolated base $\ddot{\boldsymbol{x}}_{\boldsymbol{i}}\boldsymbol{(t)}$ [32]. With this, the feedback controller can be manually tuned by taking into account all disturbances and noises. The feedback format is a combination of virtual mass m_s, skyhook damping c_s and skyhook stiffness k_s. The feedback utilizes the accelerometer signals $\ddot{x}_i$, $\ddot{z}_i$ and $\ddot{\theta}_i$ and respective velocity and position integral as control input. To cope with noise in the low-frequency region, integration is done with so-called weak integrators [33] that act as high-pass filters

$$H(s) = \left(1 - \left(\frac{\alpha}{s+\alpha}\right)^n\right) s^{-1}. \tag{22}$$

The feedback format complemented with the weak integrators gives

$$\begin{aligned} &C_{fb,i}(s) = -\left\{1 \quad H(s) \quad H^2(s)\right\}\phi, \\ &\quad \text{with } \phi = \{m_s\ c_s\ k_s\}^T. \end{aligned} \tag{23}$$

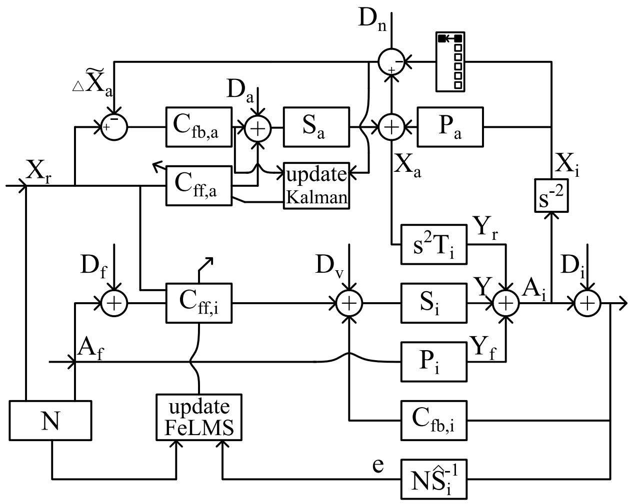

Figure 7: Schematics of mixed feedback and adaptive feedforward control strategies for both the vibration isolation system and active stage with respective noise sources.

Tuning of those parameters is done by writing equation (10) as power spectral densities

$$\begin{aligned} S_{\tilde{A}_i}(s) &= |\mathbb{R}(s)\mathbb{T}(s)|^2 \cdot |\bar{S}_{A_f}(s)| \\ &+ \left|\mathbb{R}(s)\mathbb{C}_r(s)\right|^2 \cdot |\bar{S}_{A_r}(s)| + \left|\mathbb{R}(s)\mathbb{N}_v(s)\right|^2 \cdot |\bar{S}_{D_v}(s)| \\ &+ \left|\mathbb{R}(s)\mathbb{N}_f(s)\right|^2 \cdot |\bar{S}_{D_f}(s)| \\ &+ \left|\mathbb{R}(s)\mathbb{N}_a(s)\right|^2 \cdot |\bar{S}_{D_a}(s)| \\ &+ \left|\mathbb{R}(s)\mathbb{N}_n(s)\right|^2 \cdot |\bar{S}_{D_n}(s)| \\ &+ \left|\mathbb{N}_i(s)\right|^2 \cdot |\bar{S}_{D_i}(s)|. \end{aligned} \tag{24}$$

The feedforward controller uses the measured indirect floor disturbances and generated direct shuttle reference disturbance for control inputs such as explained in Section 3.1. In the case of feedback controllers and associated noises omitted, and not considering the influence of vibrations due to the isolated base through the primary transfer path $\boldsymbol{P_a}(s)$ (which is valid if the following feedforward controllers are implemented correctly). Then equation (10) can be written as

$$\begin{aligned} \tilde{\boldsymbol{A}}_{\boldsymbol{i}}(s) =& \mathbb{T}(s)\boldsymbol{A_f}(s) + \mathbb{C}_r(s)A_r(s) \\ &+ \mathbb{N}_v(s)\boldsymbol{D}_v(s) + \mathbb{N}_f(s)\boldsymbol{D}_f(s). \end{aligned} \tag{25}$$

Expanding gives

$$\begin{aligned} \tilde{\boldsymbol{A}}_{\boldsymbol{i}}(s) &= \left(\boldsymbol{P_i}(s) + \boldsymbol{C_{ff,if}}(s)\boldsymbol{S_i}(s)\right)\boldsymbol{A_f}(s) \\ &+ \left(\boldsymbol{C}_{ff,a}(s)\boldsymbol{S}_a(s)\boldsymbol{T_i}(s) + \boldsymbol{C_{ff,ia}}(s)\boldsymbol{S_i}(s)\right)A_r(s) \\ &+ \boldsymbol{S_i}(s)\boldsymbol{D}_v(s) + \boldsymbol{C_{ff,if}}(s)\boldsymbol{S_i}(s)\boldsymbol{D}_f(s). \end{aligned} \tag{26}$$

If the proposed active stage feedforward controller given in equation (19) is implemented correctly and noise sources are not considered. Then an ideal indirect disturbance feedforward controller equals

$$\begin{aligned} \boldsymbol{C_{ff,if}}(s) &= -\boldsymbol{S_i}^{-1}(s)\boldsymbol{P_i}(s) = \\ &(\boldsymbol{1} + \boldsymbol{A}s)\left(\boldsymbol{C_f}s^{-1} + \boldsymbol{K_f}s^{-2}\right), \end{aligned} \tag{27}$$

and for the direct disturbance feedforward controller

$$\boldsymbol{C_{ff,ia}}(s) = -\boldsymbol{S_i}^{-1}(s)\boldsymbol{T_i}(s) = (\boldsymbol{1} + \boldsymbol{A}s)\,\boldsymbol{m_a}. \tag{28}$$

With $\boldsymbol{m_a} \in \mathbb{R}^{3x1}$ and $\boldsymbol{A}, \boldsymbol{C_i}, \boldsymbol{K_i} \in \mathbb{R}^{3x3}$. Expanding the respective feedforward terms gives

$$\begin{aligned} &\boldsymbol{C_{ff,if}}(s)(\mathrm{j},\mathrm{j}) = -V(s)(c_{\mathrm{j}}s^{-1} + k_{\mathrm{j}}s^{-2}), \\ &\qquad\qquad \text{for } \mathrm{j} = x, z, \theta \\ &\boldsymbol{C_{ff,ia}}(s)(1,1) = V(s)m_a, \\ &\boldsymbol{C_{ff,ia}}(s)(3,1) = V(s)h_a m_a, \\ &\qquad \text{with } V(s) = K_{M_i}^{-1}\left(L_i s + R_i\right). \end{aligned} \tag{29}$$

Note that $V(s)$ represents the voltage-controlled VCM properties, with motor constant K_{M_i}, inductance L_i and resistance R_i. In matrix format, this is represented with an actuator pole on the diagonal entries of matrix $\boldsymbol{A}$.

It can be seen that the indirect disturbance feedforward terms depend on damping and stiffness components related to the vibration isolation system suspension [33]. In the case of the active stage, only components related to acceleration affect the vibration isolation system. The forces related to velocity and position are compensated internally. It can be stated that if both terms are estimated ideal in the continuous domain and noises are not considered, the controller creates a force that cancels the force induced by both types of disturbances.

In order to obtain effective feedforward controllers, all associated parameters need to be accurately estimated. For this, a self-tuning filter is chosen. The reason is that with such a filter time-varying parameters can be estimated. Besides that, it also automatically includes the effect of actuator and sensor noise, since it aims to minimize the measured vibrations of the isolated base.

For this a FeLMS algorithm with residual noise shaping [42] is used. This algorithm has attractive convergence properties and is easy to implement as it only needs an estimation of the secondary path [35]. The structure presented in this section is primarily adopted from [43]. The difference is that in this research a passive payload and not an active stage is considered. As a consequence, the so-called generalized FIR-structure [44] and derivation of update law changes. The FIR structure makes it possible to separate the poles and zeros from each other. In this, the zeros can be adaptively identified and the poles are fixed to make the controller inherently stable [45]. In the remainder of this section, the derivation of both FIR-structure format and update law for the vibration isolation system control strategy are given.

The control output of the self-tuning filter can be written in matrix-vector notation as

$$\begin{aligned} &\boldsymbol{u_{ff,i}}(s) = (\boldsymbol{1} + \boldsymbol{A}s) \\ &\qquad \left[\boldsymbol{m_a} \quad \left(\boldsymbol{C_f}s^{-1} + \boldsymbol{K_f}s^{-2}\right)\right]\begin{Bmatrix} A_r(s) \\ \boldsymbol{A_f}(s) \end{Bmatrix}. \end{aligned} \tag{30}$$

Merging all dynamics properties and separation of all poles and zeros gives

$$\begin{aligned}\boldsymbol{u}_{\boldsymbol{ff},\boldsymbol{i}}(s) = &\begin{bmatrix}\boldsymbol{A}\boldsymbol{m}_{\boldsymbol{a}} & \boldsymbol{m}_{\boldsymbol{a}} & \boldsymbol{A}\boldsymbol{C}_{\boldsymbol{f}} & \boldsymbol{C}_{\boldsymbol{f}} + \boldsymbol{A}\boldsymbol{K}_{\boldsymbol{f}} & \boldsymbol{K}_{\boldsymbol{f}}\end{bmatrix} \\ &\left\{\boldsymbol{J}_r(s) \quad A_r(s) \quad \boldsymbol{A}_{\boldsymbol{f}}(s) \quad \boldsymbol{V}_{\boldsymbol{f}}(s) \quad \boldsymbol{X}_{\boldsymbol{f}}(s)\right\}^T.\end{aligned} \tag{31}$$

A newly introduced term herein is the jerk reference component $\boldsymbol{J}_r(s)$. Furthermore, the weak integrators replace the velocity and position terms of the floor. Next to that, the terms β_{1-3} are used for normalisation such that convergence is improved [43]. With weight matrix $\boldsymbol{W}(k) \in \mathbb{R}^{3x11}$ and regression vector $\boldsymbol{\psi}(k) \in \mathbb{R}^{11}$ one can write in discrete time,

$$\begin{aligned}&\boldsymbol{u}_{\boldsymbol{ff},\boldsymbol{i}}(k) = \\ &\underbrace{\left[\tfrac{1}{\beta_1}\boldsymbol{A}\boldsymbol{m}_{\boldsymbol{a}}\ \tfrac{1}{\beta_2}\boldsymbol{m}_{\boldsymbol{a}}\ \boldsymbol{A}\boldsymbol{C}_{\boldsymbol{f}}\ \tfrac{1}{\beta_3}(\boldsymbol{C}_{\boldsymbol{f}} + \boldsymbol{A}\boldsymbol{K}_{\boldsymbol{f}})\ \tfrac{1}{\beta_3^2}\boldsymbol{K}_{\boldsymbol{f}}\right]}_{\boldsymbol{W}(k)} \\ &\underbrace{\left\{\beta_1 j_r \quad \beta_2 a_r\ \tilde{\boldsymbol{a}}_{\boldsymbol{f}}\ \beta_3 H(q)\tilde{\boldsymbol{a}}_{\boldsymbol{f}}\ \beta_3^2 H(q)^2\tilde{\boldsymbol{a}}_{\boldsymbol{f}}\right\}^T}_{\boldsymbol{\psi}^T(k)}.\end{aligned} \tag{32}$$

For use in the update law, the matrix is rewritten as a single column vector $\boldsymbol{w}(k)^T \in \mathbb{R}^{33}$ and regression parameters in matrix format $\boldsymbol{\Psi}(k) \in \mathbb{R}^{3x33}$,

$$\boldsymbol{u}_{\boldsymbol{ff},\boldsymbol{i}}(k) = \underbrace{\begin{bmatrix}\boldsymbol{\psi}(k)^T & \dots & 0 \\ \vdots & \ddots & \vdots \\ 0 & \dots & \boldsymbol{\psi}(k)^T\end{bmatrix}}_{\boldsymbol{\Psi}(k)}\underbrace{\begin{bmatrix}\boldsymbol{W}_{(1,:)}(k)^T \\ \vdots \\ \boldsymbol{W}_{(3,:)}(k)^T\end{bmatrix}}_{\boldsymbol{w}(k)}. \tag{33}$$

The FeLMS algorithm with residual noise shaping in which the derivation is based on the steepest descent method and minimizes a quadratic cost function

$$\boldsymbol{J}(k) = \boldsymbol{e}^T(k)\boldsymbol{e}(k). \tag{34}$$

In this the error (see figure 7) is

$$\begin{aligned}\boldsymbol{e}(k) \approx\ &\boldsymbol{N}(k)\hat{\boldsymbol{S}}_{\boldsymbol{i}}^{-1}(q)(\boldsymbol{y}_{\boldsymbol{f}}(k) \\ &+ \boldsymbol{y}_{\boldsymbol{r}}(k) + \boldsymbol{d}_{\boldsymbol{i}}(k)) + \left[\boldsymbol{N}(k)\hat{\boldsymbol{S}}_{\boldsymbol{i}}^{-1}(q)\boldsymbol{S}_{\boldsymbol{i}}(q)\boldsymbol{\Psi}(k)\right]\boldsymbol{w}(k),\end{aligned} \tag{35}$$

with $\boldsymbol{N}(k)$ used as residual noise shaping to define the frequency band and filter to cope with parasitic modes or disturbances. As a result of using a FeLMS algorithm, $\tilde{A}_i(s)$ needs to be filtered with the inverse of the secondary path. In this case the secondary path consists out of

$$\hat{\boldsymbol{S}}_{\boldsymbol{i}}(s) = \mathbb{S}_{\boldsymbol{fb}}(s)\boldsymbol{S}_{\boldsymbol{i}}(s). \tag{36}$$

The weights are updated according the gradient-based update law

$$\boldsymbol{w}(k+1) = \boldsymbol{w}(k) - \frac{\mu(k)}{2}\left(\frac{\partial \boldsymbol{J}(k)}{\partial \boldsymbol{w}}\right)^T. \tag{37}$$

In which the gradient of the quadratic cost function is given by

$$\left(\frac{\partial \boldsymbol{J}(k)}{\partial \boldsymbol{w}}\right)^T \approx 2\left[\boldsymbol{N}(k)\boldsymbol{\Psi}(k)\right]^T \boldsymbol{e}(k). \tag{38}$$

The adaptation rate equation for $\mu(k)$ is adopted from [43].

5. Simulations in 2D

The proposed control strategy is validated in simulations according to the schematic as shown in figure 7 with a sample rate of 6400 Hz. The numerical values for transfer paths: $\boldsymbol{P}_{\boldsymbol{a}}$, S_a, $\boldsymbol{P}_{\boldsymbol{i}}$, $\boldsymbol{S}_{\boldsymbol{i}}$ and $\boldsymbol{T}_{\boldsymbol{i}}$ can be derived from the matrices in Appendix A. All noise spectra are explained in Section 3.2, 3.3 and 3.4.

Inspection of the incremental encoder power spectral density reveals that the noise spectra are significantly lower than the sum of all noise spectra influencing the tracking error. Therefore, a cross-over frequency can be chosen such that the sensitivity $\mathbb{S}_a$ is pushed towards zero and complementary sensitivity $\mathbb{T}_a$ to one. However, in practice, the cross-over frequency is limited due to the presence of parasitic modes as shown in figure 13. Therefore, a cross-over frequency of $\omega_c = 200$ Hz with $\beta = 2$ and $\alpha = 0.1$ [36] is chosen such that with experiments equal settings can be used.

The feedforward controller $\boldsymbol{C}_{\boldsymbol{ff},a}$ is simulated with a process noise covariance of 10^{-8} and initial covariance matrix as a diagonal matrix with entries 0.1. The low-pass filter F is designed as a 2$^{\text{nd}}$ order with cutt-off frequency at 500 Hz. To investigate robustness an initial $\tilde{\theta}(0)$ is chosen with 40 % mismatch to the 'real' parameters.

The vibration isolation system feedback controller $\boldsymbol{C}_{\boldsymbol{fb},\boldsymbol{i}}$ is tuned with the assumption that the FeLMS algorithm identify all parameters with a mismatch of 5 % and that performance limiters are discretization, disturbances, noises, weak integrators and a 5 % mismatch between $A_r(s)$ and $A_a(s)$. In order to use equation (24) for minimization of $\boldsymbol{S}_{\tilde{A}_i}$, the power spectral density of the floor is specified as the ASML spectrum $|\bar{S}_{A_f}|$ [23], accelerometer $|\bar{S}_{D_i}|$ $(= |\bar{S}_{D_i}|)$ and actuator noise $|\bar{S}_{D_v}|$ $(= |\bar{S}_{D_a}|)$ according adopted data [32]. For $|\bar{S}_{A_r}|$ the acceleration $a_r(t)$ is decomposed to the frequency domain with aid of Fourier transform and subsequently the absolute squared. Experimental data of $\boldsymbol{D}_n$ is used to determine $|\bar{S}_{D_n}|$ as shown in figure 6. Visual inspection of all individual contributions ($S_{\tilde{A}_i,A_r}$, $S_{\tilde{A}_i,A_f}$, etc.) to $S_{\tilde{A}_i}$ reveals that the major part defining $\boldsymbol{S}_{\tilde{A}_i}$ are due to measured indirect floor disturbances and generated forces due to shuttle movements. Therefore, it is chosen to tune the artificial parameters with S_{A_r} and S_{A_f} as performance indicator. The result is shown in figure 8. The corresponding parameters obtained with loop shaping are: $m_s = 0.4$, $c_s = 350$, $k_s = 100$, weak integrator order $n = 5$ and cutt-off frequency $\alpha = 1$ Hz. The parameter gains are constrained such that with experiments approximately equal settings can be used. The reason is that higher gains in combination with parasitic modes otherwise cause instability.

The self-tuning filter $\boldsymbol{C}_{\boldsymbol{ff},\boldsymbol{i}}$ is simulated with $\epsilon = 10^{-7}$, $\mu = 10^{-3}$ and parameters β_{1-3} such that the components are normalised [33]. The inverse of the secondary path is obtained from the secondary path with the identified paths (given in Appendix B) and taking into account the feedback controller as denoted in equation (36). The noise shaping

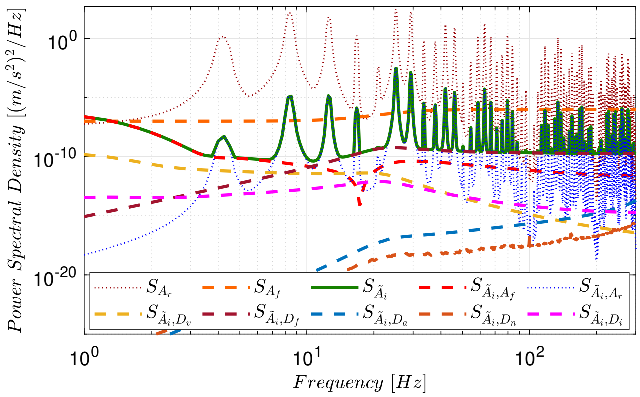

Figure 8: Power spectral densities in the x_i-direction of reference acceleration S_{A_r}, floor S_{A_f}, performance objective $S_{\tilde{A}_i}$ and all individual contributions to the performance objective.

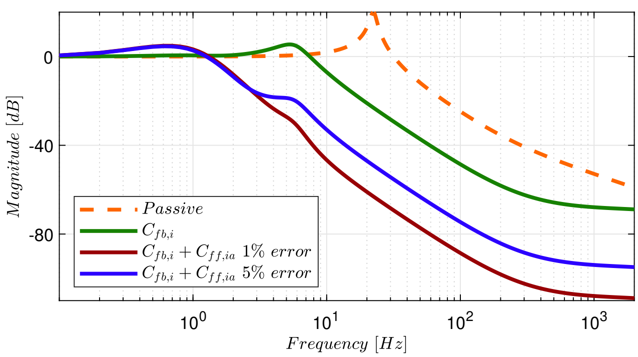

Figure 9: Magnitude frequency reponse of transmissiblity $\mathbb{T}(s)$ in x_i-direction, in case of passive system (dashed-orange), the feedback controlled system (green) and mixed feedback and ideal feedforward controlled system using a parameter mismatch of 1 % (reddish) and 5 % (blue).

filter $N(s)$ consists out of a 4$^{\text{th}}$ order bandpass filter in the range of $10 - 300$ Hz.

In the proceeding section, results are shown related to measurements in x_i-direction. To illustrate the behavior of the vibration isolation control strategy, both the transmissibility and compliance reference as denoted in equation (25) are plotted without noise. In this, the effect of only using a feedback controller and a mismatch in parameter estimation for feedforward control are shown with respect to the passive configuration. From the transmissibility (figure 9) it is observed that in the low-frequency region the weak integrators limit the attenuation. Moreover, feedback attenuates the resonance peak and already gives 40 dB attenuation for $\omega > 10$ Hz. Besides that, it shows that a mismatch in parameter estimation dramatically influences the effectiveness of the controller. For the compliance reference as shown in figure 10, it can be clearly seen that the performance is only subject to the actuator pole and not the weak integrator.

The inspection of simulation results reveals that both the active stage and vibration isolation system feedforward al-

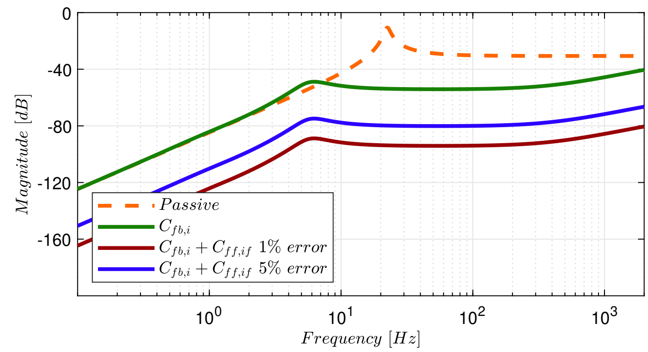

Figure 10: Magnitude of the compliance reference $\mathbb{C}_r(s)$ in x_i-direction, in case of the passive system (dashed-orange), the feedback controlled system (green) and mixed feedback and feedforward controlled system using a parameter mismatch of 1 % (reddish) and 5 % (blue).

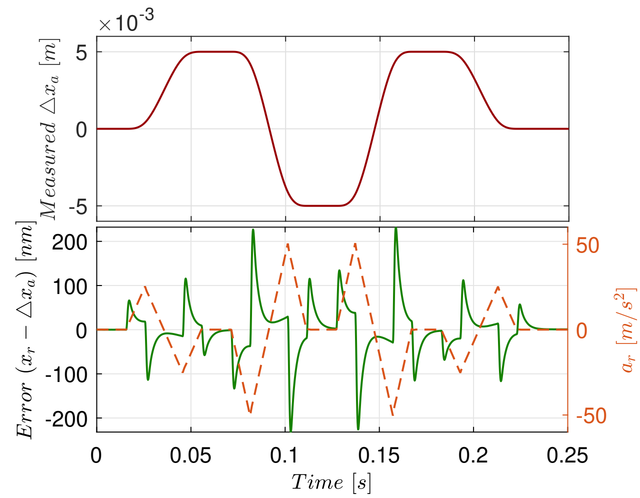

Figure 11: Simulated result of the measured reference (reddish), reference acceleration component (dashed-orange) and tracking error (green).

gorithms converge in about 10 s. In total 33 weights are estimated for the vibration isolation system and three for the active stage feedforward control. Those weights converge in about 10 s. Figure 11 shows the measured reference and tracking error with the reference acceleration component. From the figure, it can be clearly seen that a change in acceleration (and jerk) is directly linked to the reference tracking error made. Which is expected, because the major part that defines movement of the shuttle is due acceleration component $a_{r,max} m_a \approx 10$ N ($v_{r,max} c_a = 1.5$ N and $x_{r,max} k_a = 3.25$ N). Besides that, performance limiters are a mismatch in parameter estimation of the feedforward controllers, noises, and discretization. The result is a maximum tracking error of approximately 220 nm and in about 0.042 s the feedback+feedforward settles in between an error band of 2 % with respect to the required final value.

Figure 12 shows the measured internal deformation with both the passive and active configuration. The internal defor-

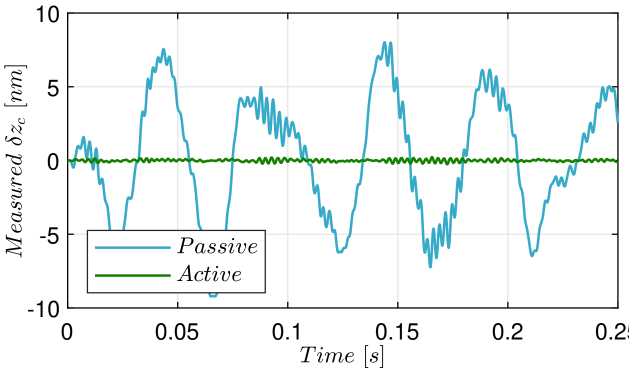

Figure 12: Simulated results of internal deformation in case of a passive (violet) and active (orange) vibration isolation system.

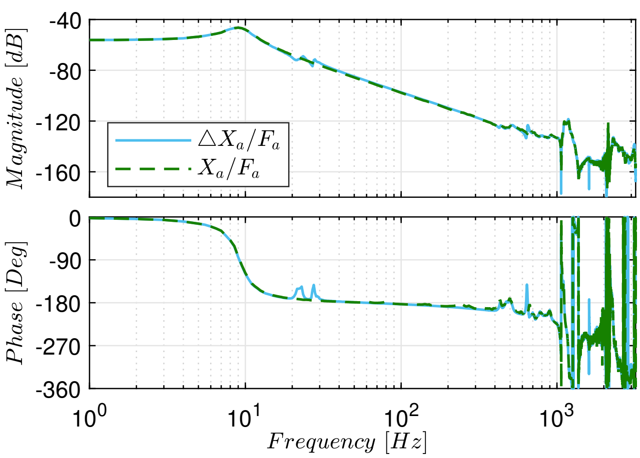

Figure 13: Augmented secondary path $S_{\triangle_a}$ and secondary path S_a measurements of the active stage. Obtained with a passive and an active vibration isolation system.

mation is, for the rigid body approach, completely dependent on floor disturbances and the respective noises. Therefore, similar performance is achieved compared to the attenuation of the vibrations measured on the isolated base.

6. Experimental results

This section presents the results of four experiments. In the first experiment, both feedback controllers are activated and subsequently, parameters are estimated for the feedforward controllers. In the second experiment, the tracking error of the active stage is examined with non-adaptive feedforward controllers in which the found parameters are adopted. In the third experiment, the feedforward controllers are stepwise activated and the measured vibrations of the isolated base are examined. In the last experiment, the influence of the vibration isolation system controller on the tracking error and settle time is examined. Besides that, also is examined the measured internal deformation.

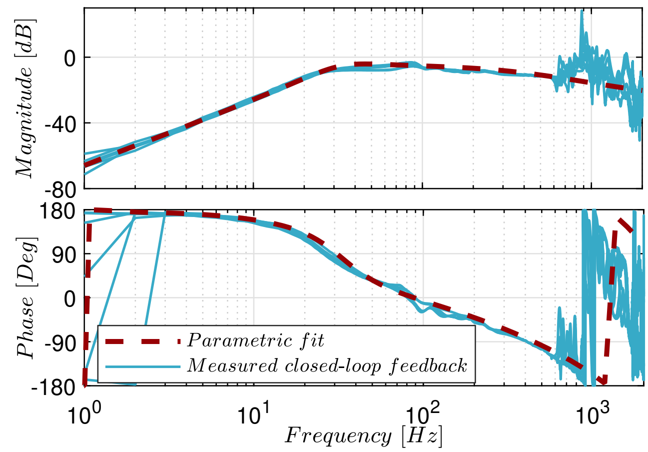

Figure 14: Secondary path $\hat{S}_i$ (closed-loop feedback) measurements in local coordinates of the vibration isolation system and the related parametric fit obtained from equation (36).

The active stage feedback controller is similar to the controller used in simulations. The only difference is that two notch filters are placed at 1090 Hz and 1186 Hz to cope with parasitic modes that cause instability (figure 13). The settings for the Kalman filter are $\tilde{\theta}(0) = \mathbf{0}$, noise variances of 10^{-12} and diagonal covariance matrix with entries 0.1.

The feedback and feedforward control of the vibration isolation system are implemented in local coordinates with feedback parameters: $m_s = 0.4$, $c_s = 400$ and $k_s = 100$. Furthermore, weak integrators are designed 5$^{\text{nd}}$ order with a cutoff frequency of 1 Hz. The result is an open-loop phase margin of 5 ° and gain margin of 5. For each feedback, notch filters are added to cope with parasitic modes that otherwise cause stability issues. The FeLMS algorithm is implemented with a parametric fit of the secondary path in local coordinates. This fit is obtained with equation (36) and visually inspected with measurements of the closed-loop feedback shown in figure 14. The noise shaping filter consists out of a 5$^{\text{nd}}$ order bandpass filter in the range of $3 - 300$ Hz. With this, both the reference and floor vibrations are filtered. The measured vibration of the isolated base are filtered with the secondary path inverse and noise shaping filter to obtain the filtered error.

In the first experiment, the parameter estimations of the vibration isolation system and the active stage are examined. For this, the feedback controllers are activated and subsequently both feedforward controllers. Controller $\boldsymbol{C_{ff,if}}$ estimates a total of 54 weights that correspond to the primary path and the actuator pole. These weights are estimated with three vertical floor accelerometers, respective velocity and position integrals, and the six isolated base accelerometers. The other controller $\boldsymbol{C_{ff,ia}}$ estimates 12 weights that correspond to the tertiary path and actuator pole. These weights are estimated with the six isolated base accelerometers, jerk reference, and acceleration reference components. In figure 18 the convergence of a representative part of the weights is displayed. It can be seen that the algorithm converges af-

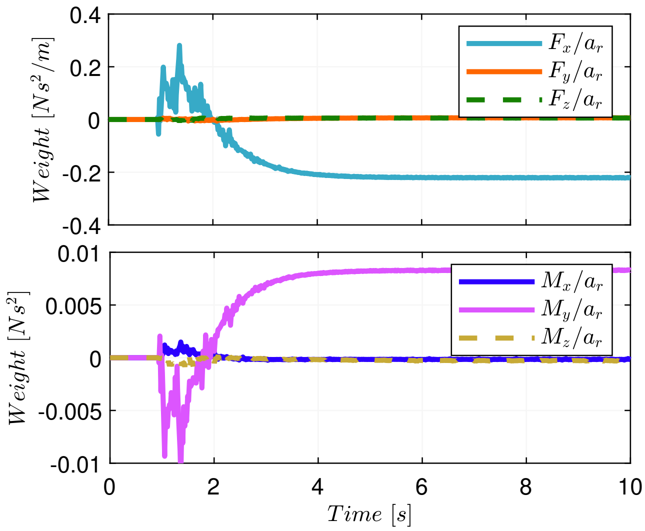

Figure 15: Measured convergence of the acceleration components related to feedforward $C_{ff,ia}$. The weights are estimated in local coordinate frames and transformed to the global coordinate system for visualization.

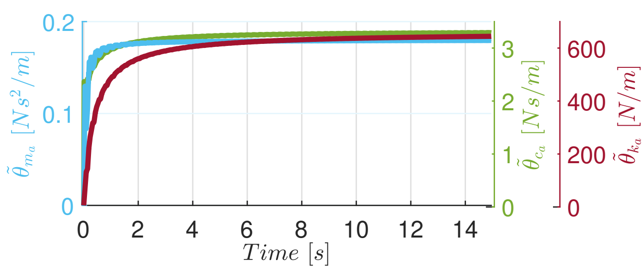

Figure 16: Measured convergence of the weights related to active stage feedforward control $C_{ff,a}$.

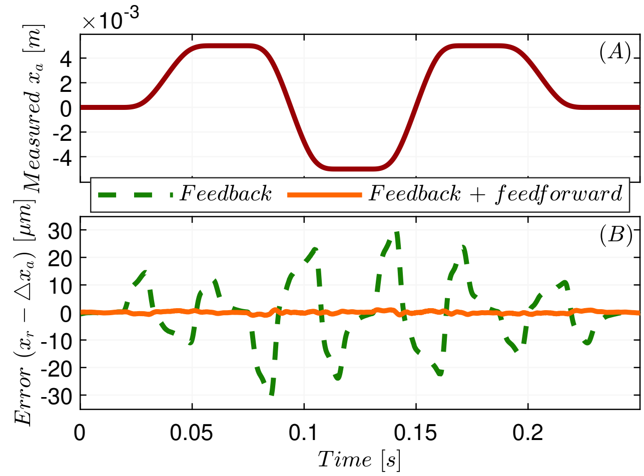

Figure 17: Measured (A) incremental encoder position $\triangle x_a$ and (B) error $x_r - \triangle x_a)$. Visualized for feedback $C_{fb,a}$ and feedback + feedforward $C_{ff,a}$.

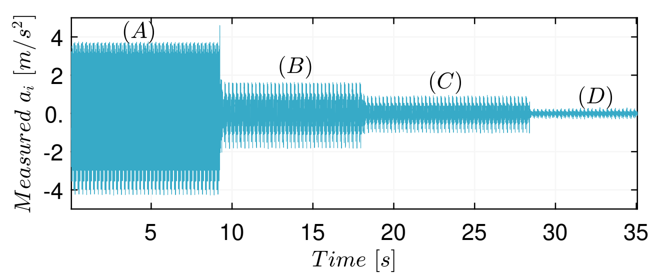

Figure 18: Measured acceleration of a single accelerometer in local coordinate system of the isolated base for different configurations: (A) Passive with both disturbances from floor as active stage + (B) feedback $C_{fb,i}$ and feedforward $C_{ff,if}$, + (C) feedforward $C_{ff,ia}$ in x_i-direction + (D) feedforward $C_{ff,ia}$ in θ_{yi}-direction. All feedforward parameters are initially estimated online and used in a non-adaptive controller for visualizing the influence of each controller.

ter 5 s. The feedforward terms related to translation in x_i and rotation θ_{yi} show most compensation of reference disturbance. As expected because movements of shuttle are in the x_a-direction at a certain height above the global coordinate system. This causes a force in the x_i-direction and moment around θ_{yi} on the isolated base.

The convergence of weights corresponding to $C_{ff,a}$ are shown in figure 16. It can be seen that all weights converge after 10 s.

In the second experiment, the influence of the active stage feedback and feedforward controller on the tracking error is examined. The experiment is conducted with the vibration isolation system activated. For this, the found parameters are adopted in a non-adaptive feedforward controller.

Figure 17 shows the measured position and the resulting tracking error. It can be seen that the maximum tracking error with both controllers active is approximately 1 μm. The tracking error characteristics correspond with simulations. However, the error is a ratio of around five higher. This is primarily due to the vibration isolation system feedforward controller which does not cancel all displacements of the isolated base caused by direct disturbances. The reason is that the reference components used as control input for the direct disturbance feedforward controller differ from the 'real' direct disturbances, i.e. the states of the shuttle.

In the third experiment, the vibrations of the isolated base are examined. The same settings were used for this as in experiment two. The difference is that the feedforward controller responsible for attenuation of active stage disturbances is step-wise activated.

Figure 18 shows that vibrations are attenuated with 24 dB when all controllers are activated. The effect of $C_{ff,if}$ is minimal and therefore not independently shown. The lack of performance improvement from $C_{ff,if}$ is due to direct disturbances that are a few orders higher in energy. The controller $C_{ff,ia}$ is not able to completely attenuate these direct disturbances such that the effect of $C_{ff,if}$ is minimal. Besides that, it is found is that actuators of the vibration isolation system influence the floor assembly. As a result, these actuators try to attenuate indirect and direct disturbances but at the same time generates indirect disturbances through the floor assembly on the isolated base.

In the last experiment, the reference is complemented with longer breaks between the position steps such that the characteristics can be examined in more detail. The position measurement and internal deformation are inspected with a passive, feedback, and feedback + feedforward configuration. The adjusted reference, incremental encoder, and capacitive sensor signal are shown in figure 19. The passive configuration shows poor damping with a maximum overshoot of around 4.2 µm. For the feedback and feedback+feedforward rise time is almost equal. The difference is that the feedforward drastically improves the settling time and damping. In about 0.048 s the feedback+feedforward settles in between an error band of 2 % with respect to the required final value. After another 0.075 s the error is around 0.01 µm.

Figure 19 (C) shows that active control reduces the internal deformation with a ratio of around five. The addition of a feedforward controller is minimal compared to only using feedback. At the moment the active stage settles it takes another 0.08 s before the capacitive sensor settles to an error of around 0.01 µm. The residual internal deformation is primarily caused for the same reason as the residual tracking error. The difference with simulations is that in practice the shuttle movements are coupled with the internal deformation. There are several reasons that can explain this observation. The active stage framework is finite in stiffness, the guidance is not exactly linear such that also force components other than in the required direction are present, and the vibration isolation system is not an exact decoupled system.

7. Conclusions

In this paper, a theoretical framework is presented for active vibration isolation systems with an active stage for the design of control strategies. A multi-objective control strategy is derived that depends on the mechanical and electrical properties of respective suspension, guidance, and actuators. All to achieve accurate reference tracking, attenuation of vibrations, and minimal internal deformation. First, an active stage feedback controller is tuned according to the open-loop cross-over frequency, taking into consideration the sensitivity and complementary sensitivity. Then, an adaptive feedforward controller is implemented whose parameters are estimated with a Kalman filter. Next, a vibration isolation system feedback controller is tuned such that the power spectral densities of the vibrations measured on the isolated base are minimized. After that, a self-tuning generalized FIR filter with a FeLMS algorithm is implemented which estimates a total of 66 parameters to generate forces that cancel the forces induced by indirect and direct disturbances. Finally, all controllers are validated with aid of simulations and experiments on a benchmark system. The results show that such an approach is promising. The internal deformation reduces with a ratio of five and tracking error with a ratio of three compared to the passive vibration isolation system. With shuttle accelerations up to 50 m/s^2 a tracking error of around 1 µm is measured.

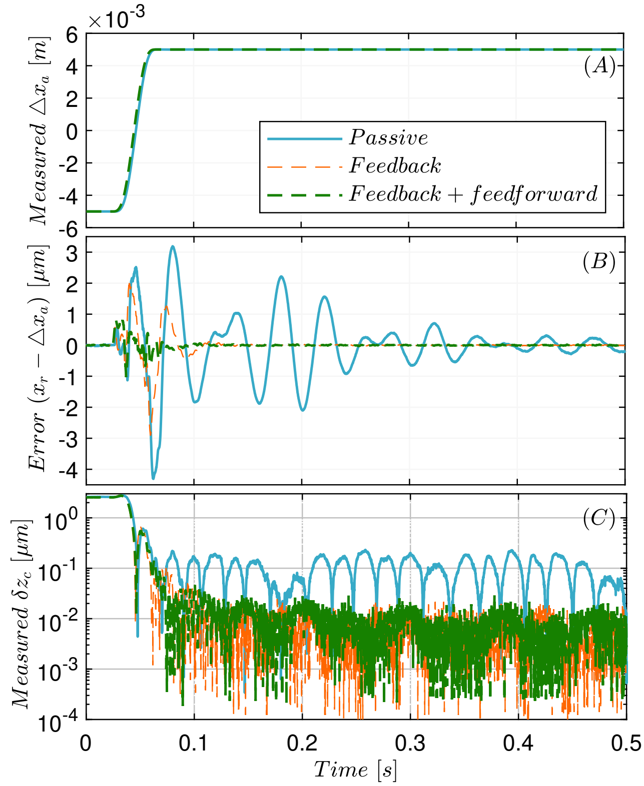

Figure 19: Measured (A) incremental encoder position $\triangle x_a$, (B) error $(x_r - \triangle x_a)$ and (C) internal deformation δz_c. Visualized for the passive, feedback $C_{fb,i}$ and feedback + feedforward $C_{ff,i}$ configuration.

A. Numerical values

Mass matrix;

$$\boldsymbol{M}\begin{Bmatrix}\ddot{\boldsymbol{x}}_i\\ \ddot{x}_a\\ \ddot{z}_c\end{Bmatrix} = \begin{bmatrix} 5.7600 & 0 & 0 & 0 & 0.0005 & 0 & 0 & 0\\ 0 & 5.9293 & 0 & 0.0090 & 0 & 0 & 0 & 0\\ 0 & 0 & 5.9193 & 0 & 0 & 0 & 0 & 0\\ 0 & 0.0090 & 0 & 0.0230 & 0 & 0 & 0 & 0\\ 0.0005 & 0 & 0 & 0 & 0.0225 & 0 & 0 & 0\\ 0 & 0 & 0 & 0 & 0 & 0.0425 & 0 & 0\\ 0 & 0 & 0 & 0 & 0 & 0 & 0.1693 & 0\\ 0 & 0 & 0 & 0 & 0 & 0 & 0 & 0.0100 \end{bmatrix}\begin{Bmatrix}\ddot{x}_i\\ \ddot{y}_i\\ \ddot{z}_i\\ \ddot{\theta}_{xi}\\ \ddot{\theta}_{yi}\\ \ddot{\theta}_{zi}\\ \ddot{x}_a\\ \dot{z}_c\end{Bmatrix} \tag{A.1}$$

Damping matrix;

$$\boldsymbol{C}\begin{Bmatrix}\dot{\boldsymbol{x}}_i\\ \dot{x}_a\\ \dot{z}_c\end{Bmatrix} = \begin{bmatrix} 105 & 0 & 0 & 0 & 0.25 & 0 & -5 & 0\\ 0 & 75 & 0 & 0 & 0 & 0 & 0 & 0\\ 0 & 0 & 102 & 0 & 0 & 0 & 0 & -2\\ 0 & 0 & 0 & 0.28 & 0 & 0 & 0 & 0\\ 0.25 & 0 & 0 & 0 & 0.2625 & 0 & -0.25 & 0\\ 0 & 0 & 0 & 0 & 0 & 0.6 & 0 & 0\\ -5 & 0 & 0 & 0 & -0.25 & 0 & 5 & 0\\ 0 & 0 & -2 & 0 & 0 & 0 & 0 & 2 \end{bmatrix}\begin{Bmatrix}\dot{x}_i\\ \dot{y}_i\\ \dot{z}_i\\ \dot{\theta}_{xi}\\ \dot{\theta}_{yi}\\ \dot{\theta}_{zi}\\ \dot{x}_a\\ \dot{z}_c\end{Bmatrix} \tag{A.2}$$

Stiffness matrix;

$$\boldsymbol{K}\begin{Bmatrix}\boldsymbol{x}_i\\ x_a\\ z_c\end{Bmatrix} = \begin{bmatrix} 114830 & 0 & 0 & 0 & 30 & 0 & -650 & 0\\ 0 & 104440 & 0 & 0 & 0 & 0 & 0 & 0\\ 0 & 0 & 159240 & 0 & 0 & 0 & 0 & -50000\\ 0 & 0 & 0 & 680 & 0 & 0 & 0 & 0\\ 30 & 0 & 0 & 0 & 680 & 0 & -30 & 0\\ 0 & 0 & 0 & 0 & 0 & 2780 & 0 & 0\\ -650 & 0 & 0 & 0 & -30 & 0 & 650 & 0\\ 0 & 0 & -50000 & 0 & 0 & 0 & 0 & 50000 \end{bmatrix}\begin{Bmatrix}x_i\\ y_i\\ z_i\\ \theta_{xi}\\ \theta_{yi}\\ \theta_{zi}\\ x_a\\ z_c\end{Bmatrix} \tag{A.3}$$

Force matrix;

$$
\boldsymbol{B}\begin{Bmatrix}\boldsymbol{F_i}\\ F_a\end{Bmatrix}=\begin{bmatrix}1&0&0&0&0&0&-1\\0&1&0&0&0&0&0\\0&0&1&0&0&0&0\\0&0&0&1&0&0&0\\0&0&0&0&1&0&-1/20\\0&0&0&0&0&1&0\\0&0&0&0&0&0&1\\0&0&0&0&0&0&0\end{bmatrix}\begin{Bmatrix}F_x\\F_y\\F_z\\M_x\\M_y\\M_z\\F_a\end{Bmatrix} \tag{A.4}
$$

Disturbance matrix;

$$
\boldsymbol{D}\begin{Bmatrix}\boldsymbol{v_f}\\ x_f\end{Bmatrix}=\begin{bmatrix}0&0&0&0&0&0\\0&0&0&0&0&0\\100&0&0&109240&0&0\\0&0.28&0&0&682&0\\0&0&0.25&0&0&682\\0&0&0&0&0&0\\0&0&0&0&0&0\\0&0&0&0&0&0\end{bmatrix}\begin{Bmatrix}\dot{z}_f\\ \dot{\theta}_{xf}\\ \dot{\theta}_{yf}\\ z_f\\ \theta_{xf}\\ \theta_{yf}\end{Bmatrix} \tag{A.5}
$$

B. Measured and modeled global secondary paths

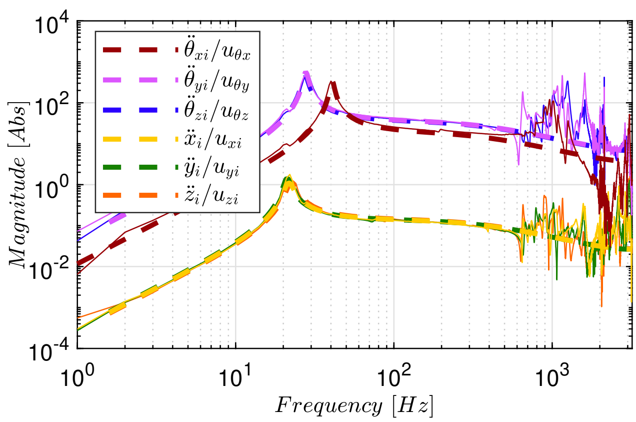

Figure A.1: Global measured (solid) and modeled (dashed) secondary paths $S_i(s)$.

References

[21] E.A. Wan. "Adjoint LMS: an efficient alternative to the filtered-x LMS and multiple error LMS algorithms". In: *1996 IEEE International Conference on Acoustics, Speech, and Signal Processing Conference Proceedings* (). DOI: 10.1109/icassp.1996.544227.

[22] S.M. Kuo and D.R. Morgan. "Active noise control: a tutorial review". In: *Proceedings of the IEEE* 87.6 (1999), 943–975. DOI: 10.1109/5.763310.

[23] R.M. Schmidt. "Ultra-precision engineering in lithographic exposure equipment for the semiconductor industry". In: *Philosophical Transactions of the Royal Society A: Mathematical, Physical and Engineering Sciences* 370.1973 (2012), 3950–3972. DOI: 10.1098/rsta.2011.0054.

[24] C.G. Gordon. "Generic vibration criteria for vibration-sensitive equipment". In: *Optomechanical Engineering and Vibration Control* 3786 (1999), pp. 22–33.

[25] J. Giaime et al. "A passive vibration isolation stack for LIGO: design, modeling, and testing". In: *Review of scientific instruments* 67.1 (1996), pp. 208–214.

[26] D.C. Karnopp and A.K. Trikha. "Comparative Study of Optimization Techniques for Shock and Vibration Isolation". In: *Journal of Engineering for Industry* 91.1 (1969), 1128–1132.

[27] M.A. Beijen, D. Tjepkema, and J. Van Dijk. "Two-sensor control in active vibration isolation using hard mounts". In: *Control Engineering Practice* 26 (2014), 82–90. DOI: 10.1016/j.conengprac.2013.12.015.

[28] M.G. Beker et al. "State observers and Kalman filtering for high performance vibration isolation systems". In: *Review of Scientific Instruments* 85.3 (2014), p. 034501. DOI: 10.1063/1.4866659.

[29] F. Kerber et al. "Control concepts for an active vibration isolation system". In: *Mechanical Systems and Signal Processing* 21.8 (2007), 3042–3059. DOI: 10.1016/j.ymssp.2007.04.003.

[30] Y.P. Wang and A. Sinha. "Adaptive sliding mode control algorithm for a multi-degree-of-freedom microgravity isolation system". In: *Proceedings of the 1997 IEEE International Conference on Control Applications* (). DOI: 10.1109/cca.1997.627758.

[31] W.B.J. Hakvoort, G.J. Boerrigter, and M.A. Beijen. "Active vibration isolation by model reference adaptive control". In: *IFAC-PapersOnLine* 53.2 (2020), pp. 9144–9149.

[32] S.T. Spanjer and W.B.J. Hakvoort. "Optimal Active Vibration Isolation System with Multiple Noise Sources". In: *Preprint* (2021).

[33] M.A. Beijen et al. "Self-tuning MIMO disturbance feedforward control for active hard-mounted vibration isolators". In: *Control Engineering Practice* 72 (2018), 90–103. DOI: 10.1016/j.conengprac.2017.11.008.

[34] G.W. van der Poel. "An exploration of active hard mount vibration isolation for precision equipment". PhD thesis. Enschede, The Netherlands: University of Twente, 2010.

[35] V.E. Debrunner and D. Zhou. "Hybrid filtered error LMS algorithm: another alternative to filtered-x LMS". In: *IEEE Transactions on Circuits and Systems I: Regular Papers* 53.3 (2006), 653–661. DOI: 10.1109/tcsi.2005.859574.

[36] J. Van Dijk and R. Aarts. "Analytical one parameter method for PID motion controller settings". In: *IFAC Proceedings Volumes* 45.3 (2012), 223–228. DOI: 10.3182/20120328-3-it-3014.00038.

[37] L. Ljung. *System identification: theory for the user*. Prentice-Hall, 2009.

[38] S. Zhao and K.K. Tan. "Adaptive feedforward compensation of force ripples in linear motors". In: *Control Engineering Practice* 13.9 (2005), 1081–1092. DOI: 10.1016/j.conengprac.2004.11.004.

[39] D. Tjepkema. "Active hard mount vibration isolation for precision equipment". PhD thesis. Enschede, The Netherlands: University of Twente, 2012.

[40] A. Abu Hanieh. "Active Isolation and Damping of Vibrations via Stewart Platform". PhD thesis. Brussel, België: Université Libre de Bruxelles, 2003.

[41] R.M. Schmidt, G. Schitter, and A. Rankers. *The Design of High Performance Mechatronics: High-tech Functionality by Multidisciplinary System Integration*. Ios Press, 2020.

[42] S.M. Kuo and J. Tsai. "Residual noise shaping technique for active noise control systems". In: *The Journal of the Acoustical Society of America* 95.3 (1994), 1665–1668. DOI: 10.1121/1.408555.

[43] M.A. Beijen, and W.B.J. Hakvoort. "Filtered-error RLS for self-tuning disturbance feedforward control with application to a multi-axis vibration isolator". In: *Preprint* (2021).

[44] J. Zeng and R.A. De Callafon. "Recursive least squares generalized FIR filter estimation for active noise cancellation". In: *IFAC Proceedings Volumes* 37.12 (2004), 327–332. DOI: 10.1016/s1474-6670(17)31489-1.

[45] L.van de Ridder. "Vibration isolation for coriolis mass-flow meters". PhD thesis. Enschede, The Netherlands: University of Twente, 2015.

3. Design and verification of an active stage

This chapter presents the design and verification of an active stage with a moving part and sensitive equipment. The active stage is designed such that it can be mounted on top of a Stewart Gough vibration isolation system [13]. Both combined represent a benchmark system that can be used for control experiments wherein the goal is to accurately track a reference with the moving part and actively minimize internal deformation between the sensitive equipment and the moving part.

The active stage is constructed modular in which both a flexure-based and bearing can be used as guidance of the moving part. Moreover, the active stage framework is designed with intentional frame compliance that introduces an internal mode.

3.1. Introduction

High-tech machines with moving parts(s) and sensitive equipment are used in numerous applications [46]. In most, important characteristics are the accuracy of guidance of the moving part(s), dynamic behavior of the framework in which the guidance is fastened, and accuracy of the sensitive equipment in the framework that examines the moving part(s) by means of measurements or other processes.

The design principles of high-precision machines are often based on obtaining maximal stiffness and minimal mass in combination with symmetry and a kinematic design [47, 48]. The constraints are in practice material properties, geometrical shape, and dimensions. Another property is the damping of the parasitic modes. Usually, little focus is put on this property in the design of machines. The reason is that most damping components exhibit unwanted or complex phenomena, like non-linear characteristics and hysteresis [6].

The guidance of moving part(s) in an active stage is in most applications realised with bearings that have a medium of rollers, air, or magnetics [3]. Although a medium of air or magnetics shows promising results in terms of compliance and deterministic behavior, it is quite complex and in most cases expensive to implement. In the case of roller bearings, play and friction are present that cause hysteresis. An alternative is the use of flexure-based guidance [4, 5]. These create freedom of movement from elastic elements rather than kinematic joints [49]. Although most flexure-based guidance types have a limited stroke and support stiffness. They behave much more deterministic compared to roller bearings and in most cases are more simple to implement in practice than a bearing with a medium of air or magnetics.

It is favorable, for this and future research, to have control strategies validated for both types of guidance. Therefore, in this research, it is chosen to design an active stage in which both a flexure-based as bearing can be used as guidance. For this, a translational single Degree Of Freedom (DOF) is designed for the guidance of the moving part that needs accurate movements.

Another essential point, the framework of precision machines is fundamentally limited with a finite stiffness which inevitably introduces an internal mode. It is important that the active stage also has an internal mode such that controllers can be experimentally verified with the same conditions that are present in real applications. In order to mimic this behaviour, intentional frame compliance is designed. Herein, a sensor is fastened that measures the internal deformation. The sensor acts as sensitive equipment that measures the distance to the shuttle.

3.2. Chapter outline

The proceeding of this chapter is organized as follows. Section 3.3 gives a system description with requirements for the design of the active stage. The active stage has to be implementable on a Stewart Gough vibration isolation system. This system is already used in a number of studies and proven to be a suitable active vibration isolator [13, 12, 31]. The suspension consists out of an exact constrained design. This is realised with six judiciously placed isolator legs that each constraint one degree of freedom. Each leg consists out of an actuator that can provide a force in the axial direction, and a flexure that is only stiff in the axial direction and compliant in all other directions.

In Section 3.4 the conceptual design and construction of the active stage is given. Focus is put on the optimisation of the flexure-based configuration. It explains the design tradeoffs made for practical implementation and control aspects. The flexure-based configuration is constructed out of folded leaf springs and force is provided in one direction by means of two Voice Coil Motors (VCMs). Furthermore, the bearing configuration is explained and the design for the intentional compliance mode is given. Next to that, the system concept is validated with simulations performed in FEM software and SPACAR a flexible multibody dynamics software package in MATLAB. In Section 3.5 the realised active stage is presented, verified and characterised. Herein, the accuracy of guidance straightness, dynamics in the driving direction, parasitic modes, hysteresis, and achievable position error are investigated. Conclusions and recommendations are given in Section 3.6 and 3.7 .

3.3. System description

In this research, a single translational DOF active stage is considered. It requires an active stage that can be mounted on top of the Stewart Gough vibration isolation system. The associated workspace is therefore limited to $(0.12 \times 0.12 \times 0.1)$ m. A schematic overview of the vibration isolation system and the active stage is shown in figure 4.2. The vibration isolation system has a mass of around 5 kg and is equipped with six VCMs that can generate a force around 15 N in the x_i-direction. The aim is to mimic a benchmark system that is representative of a high-tech system. In such a system, it is common to have a ratio of $25-30$ between the mass of the vibration isolation system and the active stage moving part, the so-called shuttle.

3.3.1. Requirements

The active stage requires a modular design that is capable of guiding a shuttle in a straight line with means of a roller bearing or a flexure-based configuration. For the shuttle, a stroke of ± 5 mm and mass of ≤ 0.2 kg is specified. The reference that needs to be tracked with the shuttle is a third-order profile that analytical describes the jerk, acceleration, velocity, and position as shown in figure 3.1. In this the maximal acceleration is 50 m/s^2, velocity 0.5 m/s, and position 5 mm.

The use of actuators is restricted to VCMs [50] that are in stock at the laboratory of the University of Twente. The choice for a position encoder requires a balanced trade-off between accuracy and costs, as the active stage is only intended for scientific research.

The VCMs and position encoder are used to actuate and track the shuttle. In order to have equal conditions as in real applications, an internal mode around 350 − 400 Hz is needed. Moreover, the internal deformation between the framework and shuttle has to be measurable with a sensor. For this, a capacitive sensor [51] is used.

3.4. Design of the active stage

This section describes the active stage design. First, is discussed the conceptual design of the flexure-based configuration. Second, numerical optimization is performed for the flexure-based configuration. Herein is searched for minimal elastic storage in driving direction and high first parasitic mode. Third, the flexure-based configuration reinforcements are adapted with sandwich-constructed reinforcements that increase the frequency of the first parasitic mode. Fourth, the shuttle is adapted such that the actuators that provide force in the driving direction and incremental encoder that reads out the position can be implemented. Furthermore, a cut-out chamber is constructed in the shuttle for the guidance of the shuttle with a bearing. Also, a suspension is designed as a fastener for the sensor that measures perpendicular to the shuttle driving direction. Fifth, the constructed active stage is presented with the implemented shuttle, guidance, and sensor suspension assembly. Finally, simulation results are performed and analysed with the focus on frequencies at which parasitic modes are present.

3.4.1. Flexure-based configuration

Flexure-based configurations are in most applications exactly kinematic constrained. Different from bearings is that mobility is created from flexible elements and not kinematic joints. In the case of a straight guided shuttle, only a single DOF is needed. For clarity, a DOF is a motion in a direction that is free or relatively compliant in comparison to other stiff directions [52]. This means that a rigid body in three-dimensional space, that has six DOFs, needs to constrain five DOFs (y, z, Rx, Ry, and Rz) to create a guided shuttle as shown in the schematic *A* of figure 3.2.

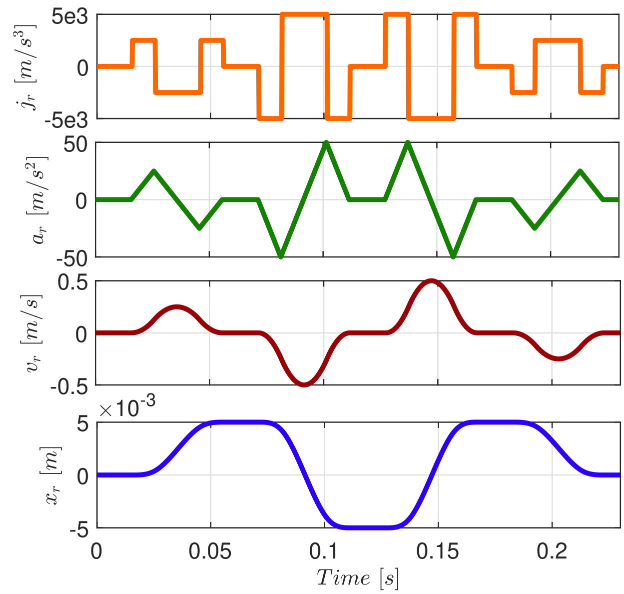

Figure 3.1: Third-order reference profile with components: jerk j_r, acceleration a_r, velocity v_r and displacement x_r

There exists a wide variety of flexure-based mechanisms in which the complete mechanism can be examined in a 2D perspective [52]. Although these mechanisms can be constructed simple, most exhibit a rather arc-like curve. Besides that, most are not symmetrical and are therefore susceptible to temperature changes. These disadvantageous properties can be circumvented with the use of more complex configurations. For this intermediate bodies and slaving mechanisms are proposed that can be seen as sub-assemblies [53]. Each sub-assembly 'releases' or confines certain degrees of freedom. However, this makes a design complex, and also in most mechanisms, it has a negative influence on the support stiffness or stroke. Therefore, in this research, a flexure-based mechanism in a 3D perspective is further examined. The reason is that with a rather simple design exact linear guidance can be realised, and approximately equal performance in terms of elastic storage and parasitic modes, compared to arc-like curve 2D perspective mechanisms [4].

In most applications, guidance in 3D perspective is a combination of flexure parts that each confine a single degree of freedom. For this, commonly are used wire or folded leaf springs [54]. With this, an exact constrained design can be realized by adding three such springs at the front and two at the back end of the shuttle. However, a wire spring configuration is not preferable. The reason is that it is asymmetric which is unwanted, and any shuttle movement in the (x) direction results in an inevitable rotation (Rx) [55]. Besides that, wire springs are highly fragile and require extreme care for assembly.

The folded leaf spring configuration as shown in schematic *B* of figure 3.2 is also asymmetric. However, this can be solved by adding another folded leaf spring, at the cost of a single over-constraint as shown in schematic *C* of figure 3.2. Examples of configurations like these are found

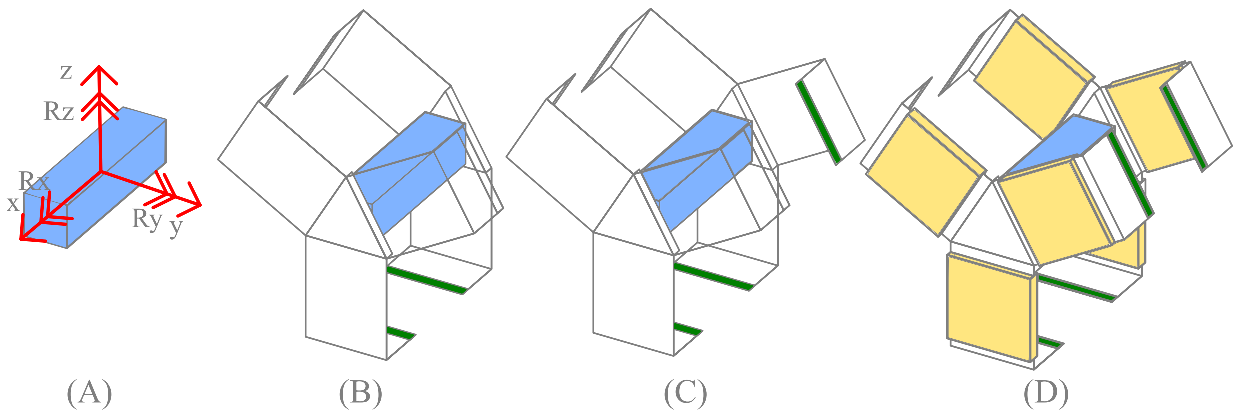

Figure 3.2: Folded leaf spring configurations with shuttle (blue), reinforcement (yellow) and fixed planes (green). (*A*) Shuttle, (*B*) exact constrained asymmetric design, (*C*) symmetric design and (*D*) symmetric design with reinforcements.

in a scientific instrument [56], calibration of a measuring device [53, 57] and focusing guidance for optics [58].

With such a configuration, roughly two choices can be made: the first is that the over-constrained is accepted. This at the risk of high stresses if large geometrical tolerances in the parts or misalignment in the assembly are present. The other option is to redesign the shuttle with a low torsional stiffness such that the design is (again) exactly constrained. The latter is not preferred, because on the shuttle top plane a measurement block is needed that is used as a reference for the capacitive sensor. This would require a mechanism in front or the back of the measurement block for which is no "easy" design solution due to space limitations of screws needed to fasten the folded leaf springs and to implement a bearing. Therefore in this research, it is chosen to use a configuration with six folded leaf springs without a low torsional stiffness of the shuttle.

A common inclusion in flexure-based configuration is the use of reinforcements. For the folded leaf spring configuration only at the long-side reinforcements are added as shown in schematic *D* of figure 3.2. It adds another six constraints and increases the risk of high stresses. However, it lowers the risk of buckling and it can increase the first parasitic mode [4].

3.4.2. Numerical optimization folded leaf springs

In order to achieve optimal dimensions for the folded leaf springs, an optimization algorithm is performed with the use of a Sequential Quadratic Programming (SQP) method [59]. In this optimization, the performance is assessed over the entire stroke with the flexible multibody software SPACAR [60, 61]. In SPACAR all leaf springs are modeled as 3D linear beams with the inclusion of geometrical non-linearities. The optimization is repeated multiple times with different initial parameters to ensure that a global minimum is found. Furthermore, the number of beam elements is set such that in the case of more beam elements, results only differ around a percent.

The objective of the numerical optimization is to obtain a high ratio between the first parasitic and nominal resonance frequency. The reason is that, with mass given, a low resonance frequency is directly linked to a minimal strain energy storage. As a result, smaller VCMs can be chosen. Besides that, with a high first parasitic frequency, greater bandwidth for a controller is possible.

In the numerical optimization algorithm, the requirement of a low resonance frequency is incorporated in the inequality constraint for a maximum actuator force. In an iterative manner, this inequality constraint is decreased to inspect the influence on the first parasitic frequency. In order to prevent high stresses, an inequality constraint is used to restrict the maximal stress ($\leq$ 600 MPa) in the folded leaf springs, and a constraint is added for the required stroke (= $\pm$5 mm). The variables in the algorithm are:

- Length shuttle $40 \leq l_s \leq 70$ mm
- Width shuttle $20 \leq w_s \leq 50$ mm
- Height shuttle $20 \leq h_s \leq 50$ mm
- Thickness springs $0.1 \leq t_f \leq 5$ mm
- Length folded part $1 \leq l_f \leq 30$ mm
- Length folded leaf spring $10 \leq l_l \leq 70$ mm
- Width springs $20 \leq w_f \leq 100$ mm
- Factor (length reinforcement l_r w.r.t. length folded leaf spring l_l) $0 \leq p \leq 0.9$

After iterative performing the algorithm, an actuator force of 14 N showed to be most suitable. Which is in agreement with the maximum force the vibration isolation system can provide in this direction ($\leq$ 15 N). With this the ratio of resonance and first parasitic frequency is $\omega_{par,1}/\omega_1 \approx 45$. The result is, with a shuttle weight of $m_a = 0.2$ kg, first parasitic frequency around 450 Hz, a resonance frequency in driving direction of 10.2 Hz, and maximum stress of 350 MPa. An overview of the optimized variables is shown in table 3.1.

Table 3.1
Optimized variables folded leaf spring configuration.

Description	Symbol	Value
Length shuttle	l_s	70 mm
Width shuttle	w_s	20 mm
Height shuttle	h_s	20 mm
Thickness leaf spring	t_f	0.1 mm
Length folded part	l_f	17 mm
Length folded leaf spring	l_l	47.86 mm
Width leaf spring	w_f	40 mm
Reinforcement factor	p	0.85

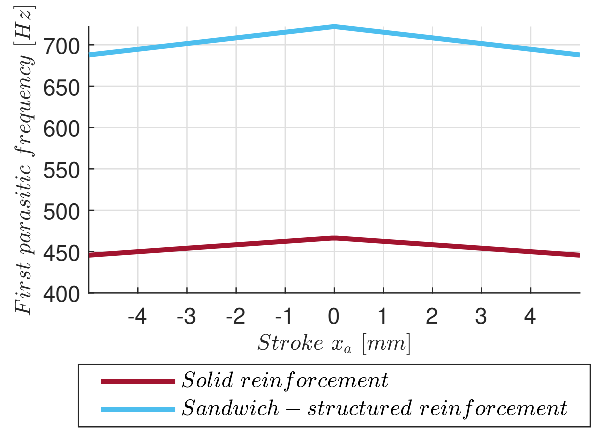

Figure 3.3: Comparison of the first parasitic mode for a solid and sandwich-constructed reinforcement as a function of the stroke.

3.4.3. Sandwich-constructed reinforcement

It is observed from simulations in SPACAR that the first parasitic frequency is due to a torsional mode of the reinforcement. Therefore, it is advantageous to adjust the reinforcement such that the weight decreases and stiffness increases. This can be realised with a sandwich-constructed reinforcement as shown in figure 3.4. The folded leaf spring and core are constructed with cut-out chambers to decrease the weight. In order to cope with a decrease in stiffness due to the cut-out chambers, both the cores are covered with facesheets.

In view of the parasitic modes, the reinforcement parts dimensions are chosen with consideration of the following trade-off. The core thickness significantly changes the reinforcement assembly bending stiffness and moment of inertia. A thick core is advantageous for a higher frequency in which the bending mode is present and disadvantageous for the frequency in which the torsional mode is present. Hence the thickness is chosen such that the frequency of both modes differs around 20 Hz. The result is that the ratio of first parasitic and resonance frequency increases to 70. The improvement compared to the solid reinforcement is shown in figure 3.3.

Another factor with the design of folded leaf springs and related reinforcements is the need for high clamping pressure to lower hysteresis. So far little research is conducted on the amount of clamping pressure needed to compensate tangential forces that are caused by a deflection of flexures. In this design, an educated guess is made for the construction of the reinforcements and clamping blocks. This resulted in a theoretical clamping pressure of 120 MPa approximately 1/3 of the maximum stress that occurs with deflection of the folded leaf springs. For this, the area of contact between the core and folded leaf spring is made minimal and for each reinforcement assembly, nine screws are used to fixate all reinforcement parts.

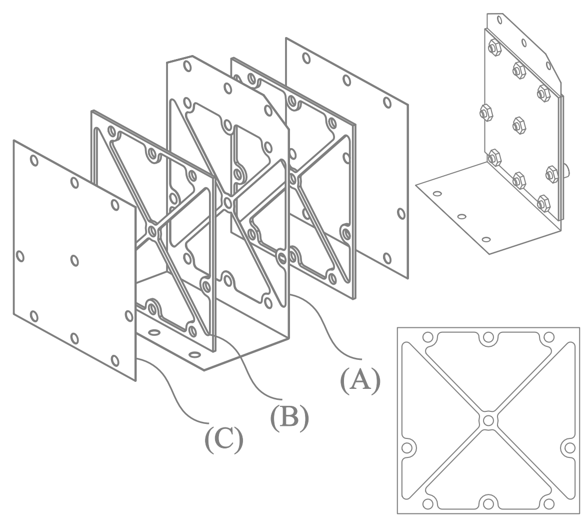

Figure 3.4: Folded leaf spring with sandwich-constructed reinforcement. (*A*) folded leaf spring, (*B*) core and (*C*) facesheet.

3.4.4. Bearing, actuators and sensors

The crossed-roller bearing [62] is chosen according to the required reference characteristics and weight of the bearing. For implementation, a cut-out chamber is made in the shuttle such that the risk of moments on the bearing due to the VCM is minimal. The related design is shown in figure 3.5. The shuttle is equipped with two VCMs that are fastened to the shuttle with brackets. Due to the lack of space in the front and back end of the shuttle, and the wish for symmetry, it is chosen for two VCMs that are in parallel. These VCMs can generate the force needed to track the given reference and to deflect the folded leaf springs.

In order to measure the position of the shuttle, an optical encoder scale [63] is glued at the bottom of the shuttle. At the front and back end of the shuttle, tapping holes are placed. These tapping holes are used for fastening the triangular brackets that each clamp three folded leaf springs. In the center of both triangular brackets, a dowel hole is placed. With this, the triangular brackets can be aligned with respect to the shuttle. The respective triangular brackets and folded leaf springs are shown in figure 3.8.

On top of the shuttle, a measurement block is mounted as a reference for the capacitive sensor. The capacitive sensor is fastened inside a suspension that consists out of a mounting block with a suspension of two leaf springs in parallel as shown in figure 3.6. The dimensions of the leaf springs and

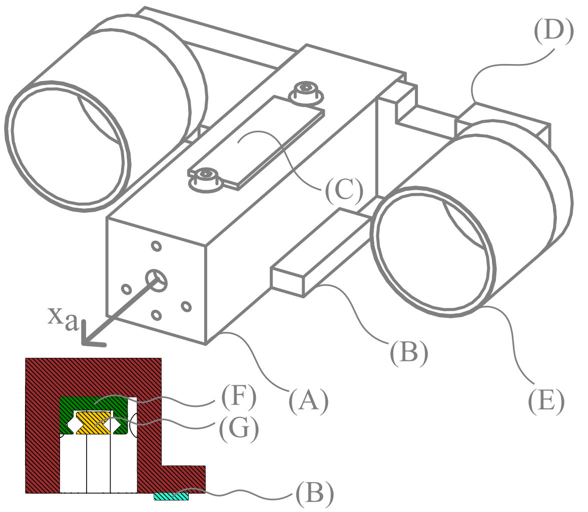

Figure 3.5: Bearing configuration. (*A*) Shuttle, (*B*) linear scale, (*C*) measurement block, (*D*) actuator bracket, (*E*) coil, (*F*) bearing upper slide and (*G*) bearing duplex.

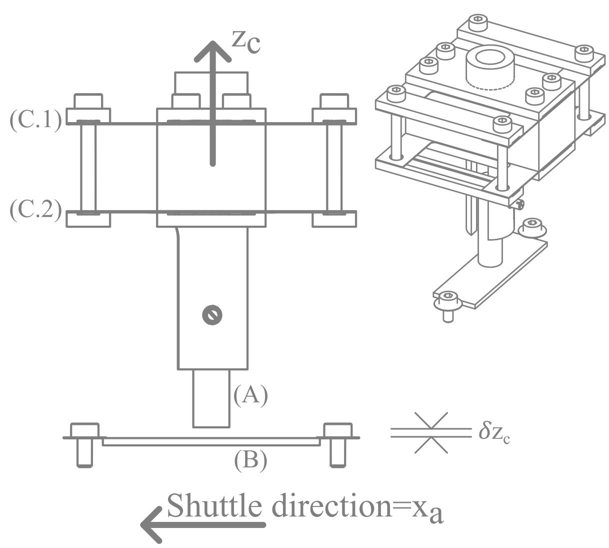

Figure 3.6: Capacitive sensor assembly. (*A*) capacitive sensor, (*B*) measurement block and (*C*) intentional frame compliance.

their location to each other are chosen such that an internal mode is present at 350 Hz in the z_c-direction. Through the mounting block, a rod is placed perpendicular to the shuttle. At the bottom of the rod, a tapped hole is placed to fasten the capacitive sensor by means of a set screw. In the rod, a slit is designed such that the cable of the capacitive sensor can be wired. The capacitive sensor measures the relative distance to the reference block mounted on top of the shuttle. For setting up the correct distance from the sensor to the shuttle the rod can be corrected in height by means of another set screw.

3.4.5. Detailed design of the active stage

This section explains the complete active stage according to the constructed framework and both guidance configurations as shown in figure 3.7. An exploded view of the complete active stage with the folded leaf spring configuration is shown in figure 3.8. The framework consists out of two plates with a cut-out section in the middle. These plates are interconnected with eight rods. At the left and right lower sides mounting blocks are located that enable fixation between the active stage and vibration isolation system. Furthermore, tapped holes are provided for clamping of the folded leaf springs and for fastening the capacitive sensor assembly as shown in figure 3.6. All clamping blocks are designed with a recess too lower hysteresis [64]. The area and type of fasteners are chosen such that clamping pressure is maximal (same method as with the sandwich-constructed reinforcements).

Also, tapped holes are placed in the left plate for mounting two magnets. These magnets are the stators of the VCM used for the actuation of the shuttle as shown in figure 3.5. The shuttle and related parts are placed in between the two plates. Above the shuttle, the capacitive sensor assembly (figure 3.6) is located.

The framework is designed such that parasitic modes are expected at frequencies $\geq$ 600 Hz and the effect on the guidance resonance frequency is minimal. This is important because the framework stiffness is in series with the folded leaf spring stiffness. Moreover, a lower stiffness makes it more difficult to minimize internal deformations, since a vibration isolation system underneath the active stage does not measure vibrations in the active stage framework. Another requirement is that the active stage framework has a minimum effect on the dynamics of the vibration isolation system. This means that the center of mass, of the vibration isolation system in which the framework of the active stage is part, does not change significantly. For ease of production, it is aimed for a minimal number of production steps and low complexity of each part. Further limitations were build-dimensions, weight, and implementation of the shuttle and related parts inside the framework.

The analog incremental encoder that measures the position of the linear scale is attached to the framework by means of brackets. These brackets are relatively thick such that the collocation in view of the controller is guaranteed for frequencies $\leq$ 600 Hz. The same is done for the brackets of the coils attached to the shuttle.

3.4.6. Modal analysis active stage

Recall the requirement for frequencies of parasitic modes higher than 600 Hz. To verify this requirement, modal analysis is performed with aid of SolidWorks Simulation (FEM software). Also, the resonance mode in the driving direction and intentional frame compliance in which the capacitive sensor is suspended is verified. All analysed modes not shown in this chapter can be found in Appendix C.

In order to lower the computational complexity in simulations, the active stage is divided into two assemblies: framework and shuttle with guide. Furthermore, all nuts and screws are replaced with rods with approximately equal weight and inertia (omitted in the figures). In the case of the framework both the mounting blocks that are intended for

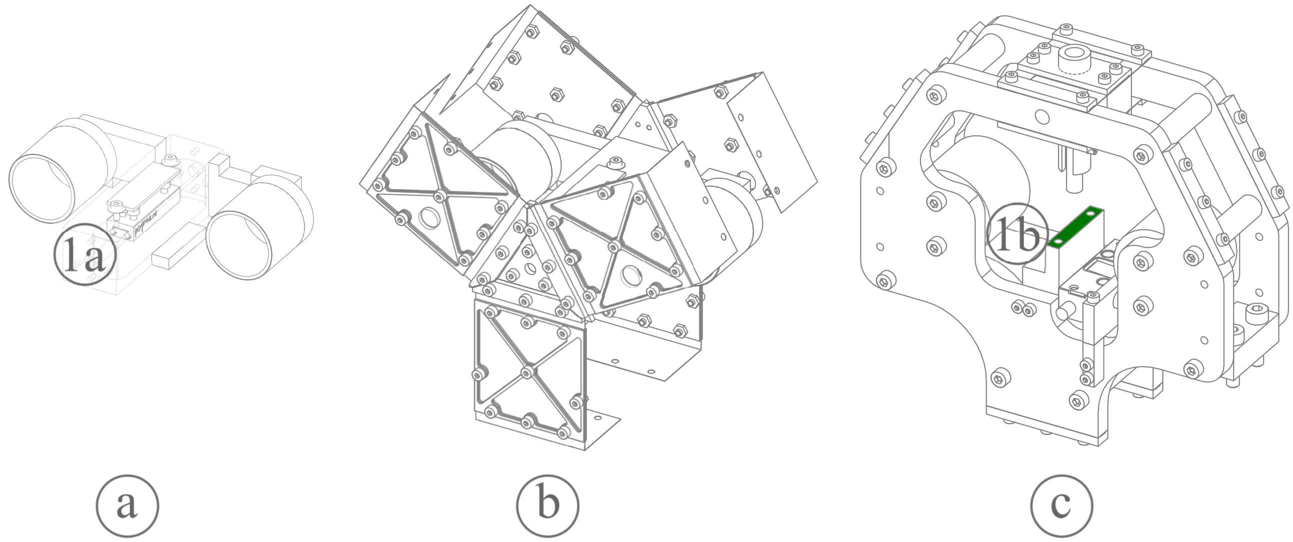

Figure 3.7: Configurations active stage with a roller bearing, b folded leaf springs, c framework. On surface 1b is fixed the bearing surface 1a. In a the shuttle is made transparent such that the bearing can be seen.

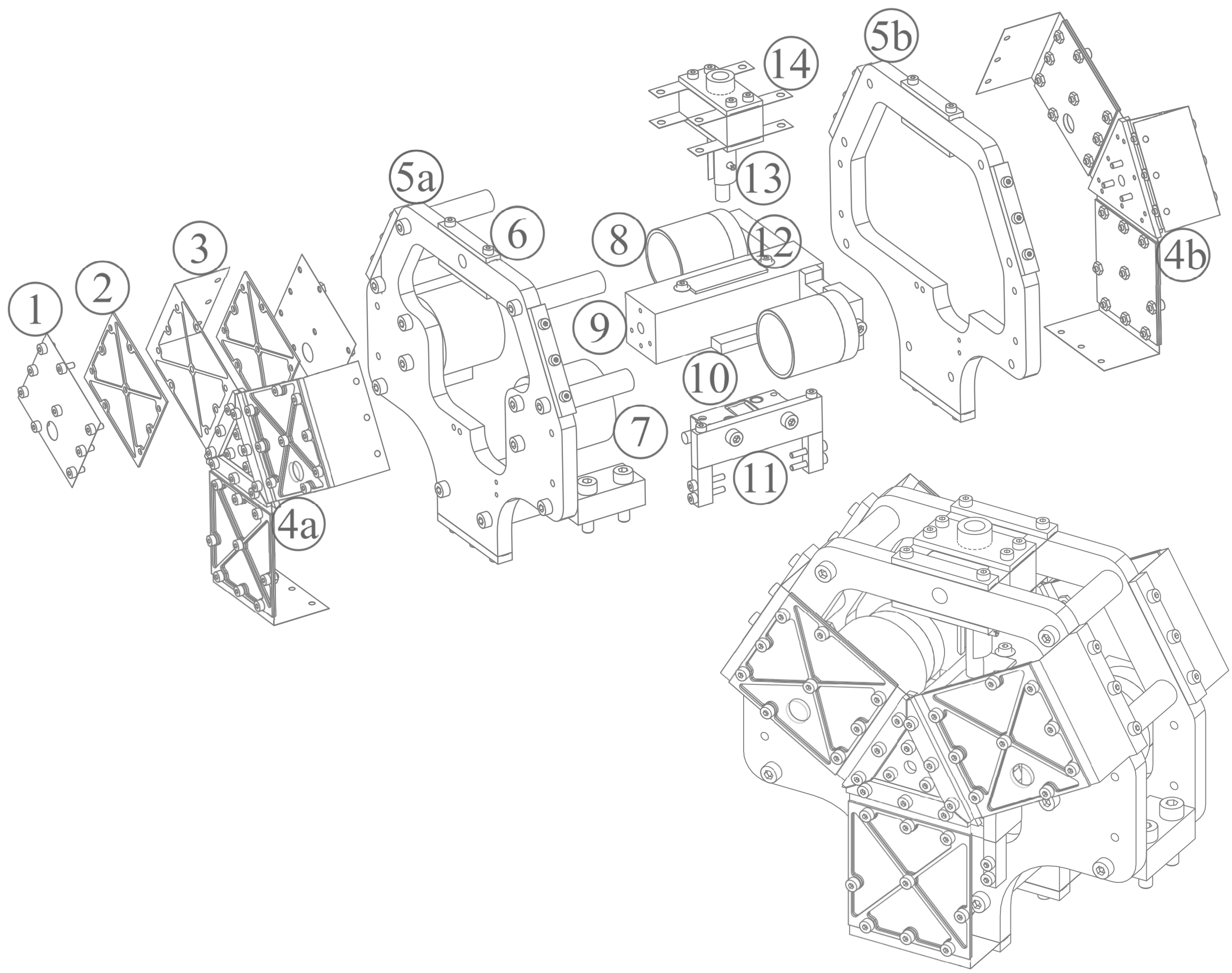

Figure 3.8: Exploded view active stage with 1 facesheet, 2 core, 3 folded leaf spring, 4 shuttle guide, 5 framework, 6 spring clamp, 7 magnet, 8 voice coil, 9 shuttle, 10 linear scale, 11 optical encoder, 12 measurement block, 13 capacitive sensor, 14 intentional frame compliance.

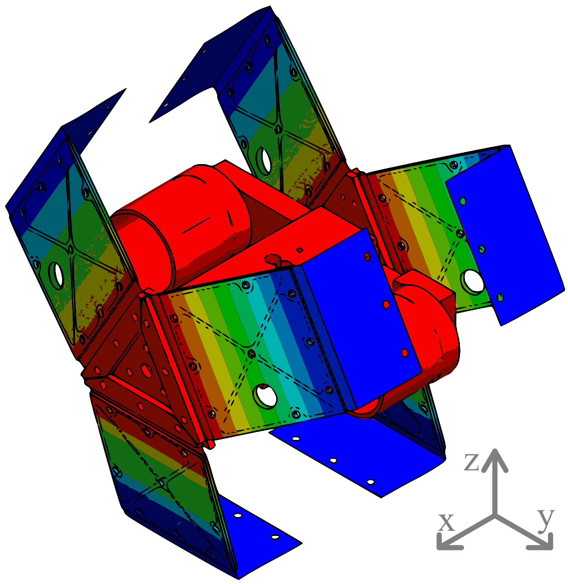

Figure 3.9: Resonance mode in the driving direction at 10.2 Hz with deformation scale 0.0010.

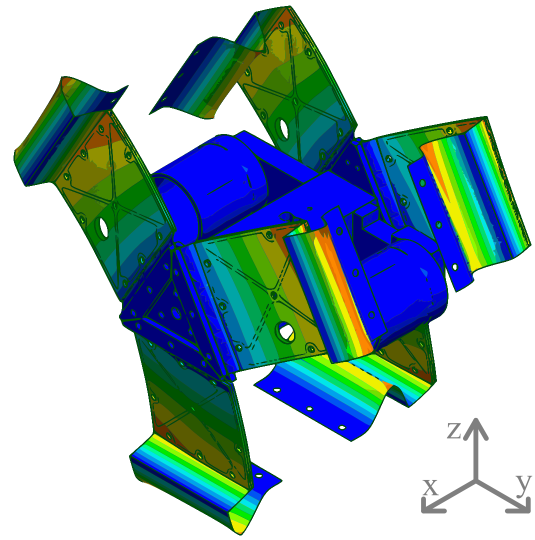

Figure 3.11: Internal tilting modes of the sandwich-constructed reinforcements at 740 Hz with deformation scale 0.0010.

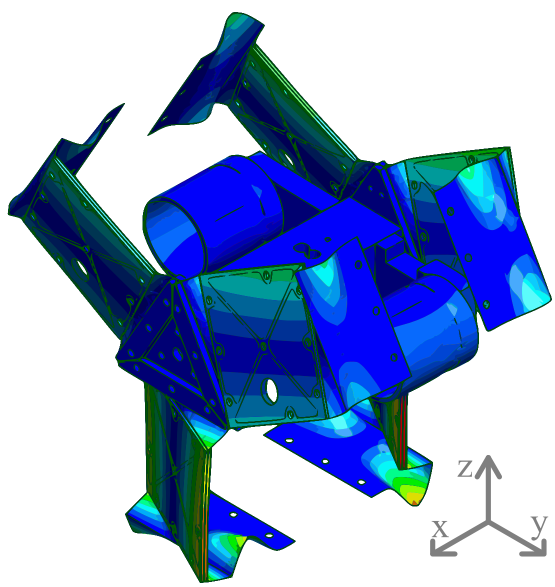

Figure 3.10: Internal torsional modes of the sandwich-constructed reinforcements at 720 Hz with deformation scale 0.0010.

connecting the active stage to the vibration isolation system are assumed fixed. For the other simulation the folded leaf springs ends, which are normally clamped by blocks on the active stage framework, are fixed. The folded leaf springs and facesheets are modelled as beam elements and all other parts with parabolic tetrahedral solid elements.

In the case of the shuttle and the guidance, it is observed that the first mode relates to the resonance frequency in the DOF at 10.2 Hz as shown in figure 3.9. The second mode is in the z_c-direction at 350 Hz and it is caused by the intentional frame compliance. In practice, it is expected that this mode is a fraction lower due to the capacitive sensor wire that adds some weight.

Hereafter several internal torsional modes are present between $720-740$ Hz that are mainly caused by the moment of inertia of the sandwich-constructed reinforcement and thin folded leaf springs. In between $740-780$ Hz internal tilting modes are present due to finite bending stiffness of the sandwich-constructed reinforcement and non-reinforced short-side of the folded leaf springs. The presence of both types of internal modes in almost the same frequency region confirms that the core thickness is chosen correctly. The internal modes with the largest mass participation are shown in figure 3.10 and 3.11 (amount of mass participation usually indicates the contribution to the response of the overall system).

The shuttle with guide shows modes at 840, 870, 880, 1470, 1485 Hz, wherein primarily the shuttle translates and rotates around its center of mass. These relate to a torsional mode around the z-axis, translational mode along the z-axis, translational mode along the y-axis, and torsional mode around the x-axis. Note however that in practice the modes are expected to be a fraction lower. The reason is that in practice not all parts are ideally interconnected and the shuttle its guide is in series with the framework.

The framework exhibits a tilting mode around the y-axis at 835 Hz. The cause of this mode is mainly due to the thickness of the plates, the distance between each other, the outer diameter of the rods, and the moment of inertia around the y-axis (due to the magnets and intentional frame compliance assembly). Another observation is that bending and torsional modes are present at 1330 and 1380 Hz. These result from a number of factors. First, both plates require a large cut-out chamber to fit in the shuttle and associated component which results in a lower torsional stiffness around the z-axis and bending stiffness in the xy-plane. Second, (again) the distance between the two plates is a limiting factor. Third, the middle of both plates are not fixated which results in a relatively high non-supported mass and this increases the susceptibility for a bending mode in the xy-plane. Finally, both magnets have a relatively high moment of inertia and are mounted near the cut-out chamber where support stiffness is low.

The incremental encoder which is mounted on a bracket that is interconnected with the framework plates shows a tilting mode around the x-axis at 1655 Hz. The linear scale which uses the incremental encoder as reference is mounted on an extruded boss of the shuttle. This extruded boss shows a tilting mode around the z-axis at 2000 Hz. However, due to the modes in which the shuttle translates or rotates around its center of mass in combination with the modes of the framework, it is expected that collocation between the VCMs and incremental encoder is lost in a lower frequency region.

In the case of the capacitive sensor, it is expected that the translational compliance of the framework along the z-axis can be accurately monitored up to 835 Hz. Everything after this frequency is a combination of framework deformation in other directions and shuttle guide deformations.

3.5. Active stage realisation, verification and characterisation

This section presents and characterises the realised active stage. First, some considerations with fabrication and assembling of the active stage are explained. Second, the straightness of the bearing and folded leaf springs guidance are compared. This straightness is important in order to minimize the error made by the capacitive sensor that measures perpendicular on the shuttle its driving direction. Third, the resonance frequency in driving direction is identified as well as the related stiffness over the entire stroke. This identifies the properties of the designed folded leaf springs and indicates what kind of controller can be used to actuate the shuttle. Fourth, the parasitic modes are analysed, which is used to compare the bearing and folded leaf spring configuration. For this, the identified path from the force of the VCMs to the position measured with the incremental encoder is used. Besides that, it is experimentally determined what the influence is of reaction forces due to the VCMs and shuttle movements on the measurements of the capacitive sensor. Fifth, the hysteresis and achievable position error of the folded leaf spring configuration is experimentally determined. Hysteresis can degrade the performance of the system. Therefore, it is useful to investigate this, such that with designing a controller this knowledge can eventually be incorporated.

3.5.1. Fabrication and assembly

The geometrical tolerances of all parts, except for the bearing, are around 0.1 mm. Therefore, it is expected that the folded leaf spring configuration show straightness in the micrometer range. The folded leaf spring is bend to 90 deg bend with a tolerance of ± 0.1 ° (figure 3.12). With simulations, it is assumed that there is no inner and outer radius present. However, in practice, an inner radius of approximately 0.05 mm and an outer radius of approximately 0.2 mm is measured. It is assumed that this has minimal effect on the stiffness properties. Furthermore, the edges of the core and clamps that are in contact with the folded leaf springs, have a chamfer/fillet of approximately 0.01 mm. As a result, the clamping pressure is not equally distributed and an increase in hysteresis is expected.

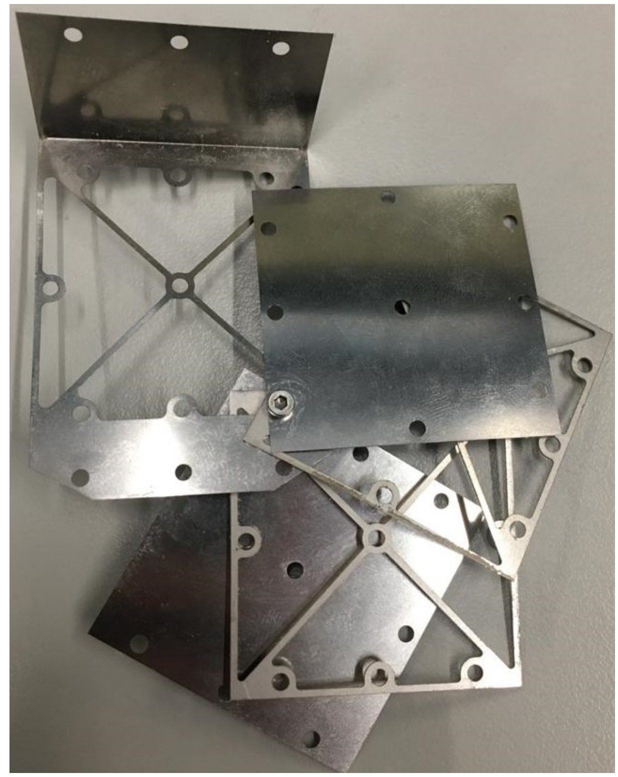

Figure 3.12: Realised folded leaf spring and sandwich-constructed reinforcement.

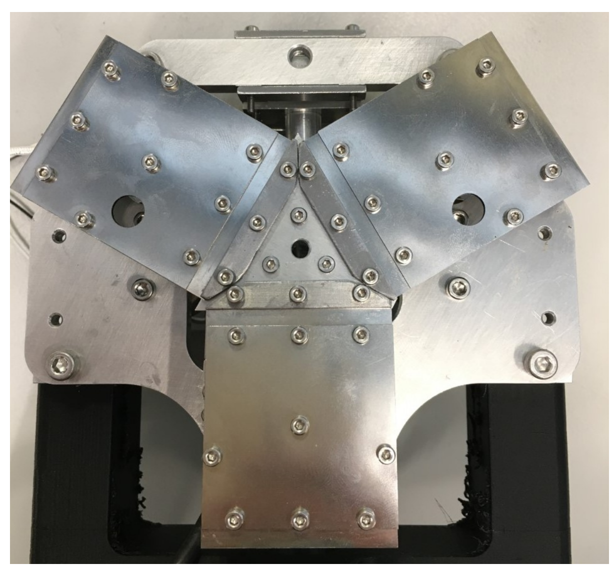

Figure 3.13: Front view of the folded leaf spring configuration.

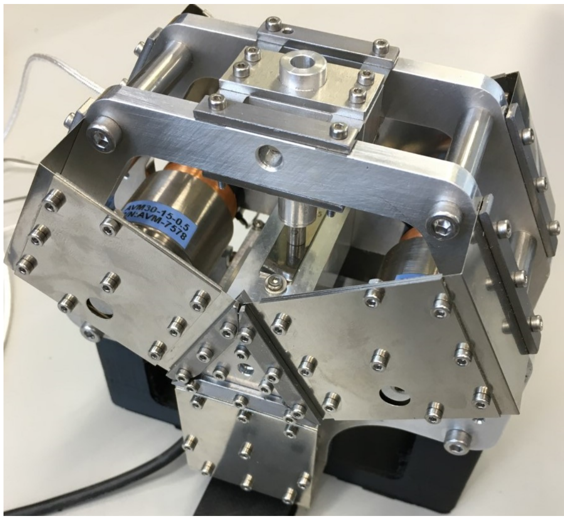

Figure 3.14: Isometric view of the folded leaf spring configuration.

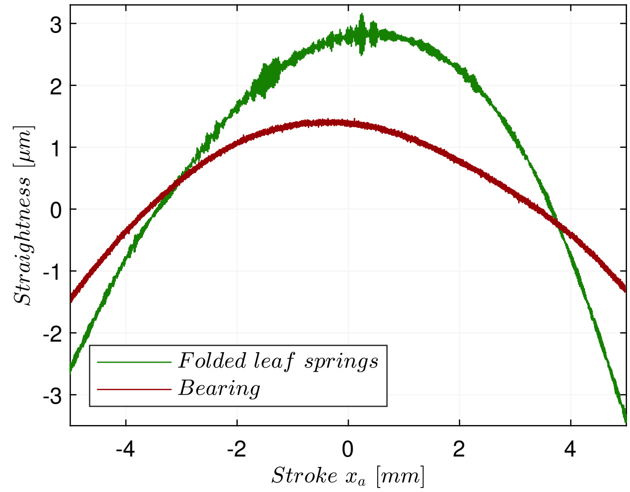

Figure 3.15: Measured straightness of the bearing and folded leaf spring configuration.

Figure 3.13 shows the front-view of the folded leaf spring configuration. The distance between the clamping blocks that fixate the folded leaf spring to the triangular brackets and reinforcement is aligned with gauge blocks. In the center of the triangular bracket, the dowel hole is used to align the folded leaf springs with the shuttle. In two reinforcement assemblies, holes are made that are used to align and fixate the magnet and coil to each other (figure 3.13). After fixation of the shuttle with the folded leaf springs guide, a gauge block is used to align the optical encoder scale with the incremental encoder, which is located underneath the shuttle. The distance between the capacitive sensor and measurement block that is located on top of the shuttle (figure 3.14) is set with a feeler gauge. The measurement block itself is fixated with two screws. The set screw torque of the screws is set minimal such that the measurement block does not show any increase in curvature.

3.5.2. Straightness guidance types

The folded leaf springs and bearing are compared on the aspect of straightness. In figure 3.15 the measured straightness of both configurations are shown. These measurements are made with the capacitive sensor that is located above the shuttle. It can be seen that the straightness of the bearing is around 3 μm which is in agreement with the specifications of the respective bearing. For the folded leaf springs a straightness around 6.5 μm is measured. It shows, that even with geometrical tolerances of ±0.1 mm for the flexure construction almost equal performance is obtained compared to the bearing with geometrical tolerances of ±0.01 mm.

An observation from this straightness measurement is that any shuttle movement generates forces to the framework in both the driving x-direction and also z-direction. More specifically, any shuttle movement generates a force equal to the mass and respective acceleration with a component in the driving x-direction and z-direction. In the case of a vibration isolation system located underneath the active stage, it means that also forces other than in the driving direction need to be countered.

Furthermore in this research, a topic of interest is the internal deformation that is measured with the capacitive sensor. To guarantee that the internal deformation and not the straightness of the guidance is measured, this straightness measurement are used to correct the data.

3.5.3. Dynamics driving direction

In order to verify the stiffness of the folded leaf springs in the driving direction, a comparison is made between the simulated stiffness in SPACAR and the fitted stiffness (figure 3.16) obtained from an experiment. For this, the active stage is rotated 90 degrees and subsequently, weights are added to the shuttle as shown in figure 3.17. The additional weight is step-wise increased to (5, 10, 20, 30, 40, 50, 100, 150) g. The method is repeated a total of 10 times in which the active stage is flipped after 5 times.

The mass of the shuttle, associated components, and additional weights are known and can be related to the shuttle's position measured with the incremental encoder. Hence, the data obtained from the experiment can be used to derive the stiffness with respect to the shuttle position. Due to gravity, the folded leaf springs deflect to around 2 mm if the active stage is rotated. In order to also determine the stiffness at a smaller deflection, the transfer path from force VCMs to the shuttle's position is used (figure 3.18). Herewith the stiffness around a zero deflection can be derived, with a known mass, from the resonance frequency. These datasets combined are used for a cubic fit to derive a relation between the shuttle displacement and stiffness (figure 3.17). It can be seen that the measured stiffness is around 180 N/m lower than the simulated stiffness. It is assumed that this is primarily due to misalignment and geometrical tolerances. Furthermore, the measured stiffness shows corresponding non-linear characteristics with the simulated stiffness.

For control purposes, the model is linearised around the zero deflection of the folded leaf springs. In doing so, the

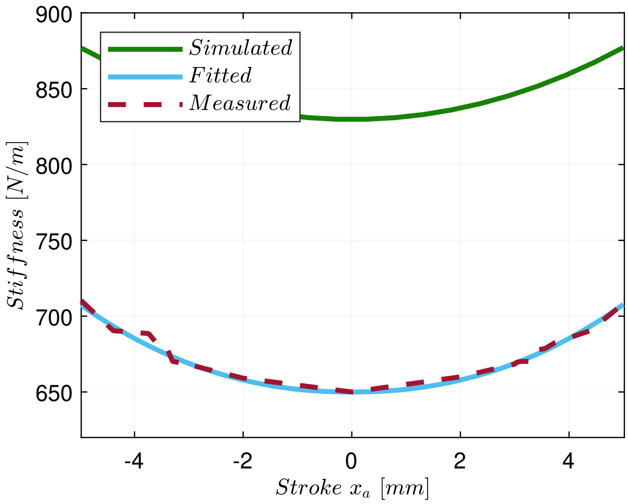

Figure 3.16: Simulated, fitted, and measured stiffness of the folded leaf spring configuration in the DOF direction.

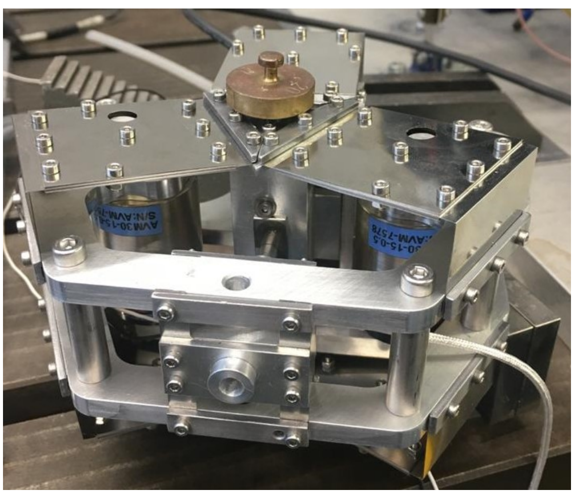

Figure 3.17: Experimental setup with a 90 degrees rotated active stage and an additional weight placed on the shuttle.

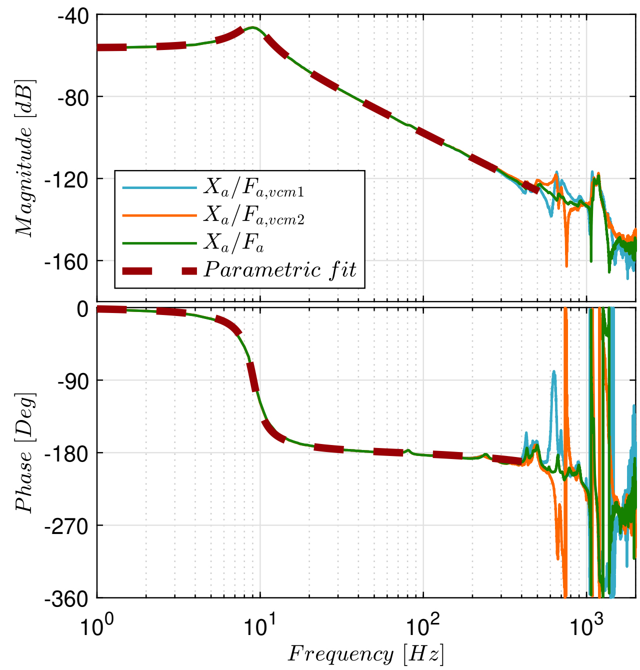

Figure 3.18: Transfer paths: (blue) corrected transfer of VCM 1, (orange) corrected transfer of VCM 2, (green) merged transfer path and (dashed-red) parametric fit.

transfer path is identified between the force of the VCMs and measurement of the incremental encoder position as shown in figure 3.18. For this, the VCMs are measured separately and afterwards corrected such that the transfer path of both are aligned in the frequency domain. The correction is needed, because the motor constants of the VCMs are not equal. After correction, both VCMs control outputs are merged to create a single transfer path. This transfer is used to make the parametric fit for control purposes.

3.5.4. Collocation and parasitic modes

The accuracy of shuttle movements is partly dependent on the guidance and the framework that fixates the guidance, since parasitic modes in the guide and framework result in increased susceptibility of vibrations, thus position errors. Therefore in this section, the parasitic modes of the active stage are examined. For this, the phase data of the green line in figure 3.18 and transfer between the VCMs and incremental encoder for both configurations as shown in figure 3.19 are examined in more detail.

Another topic of interest in this section is the collocation between VCMs and the incremental encoder which is dependent on the parasitic modes. The collocation partly determines the maximal achievable bandwidth of a controller and is useful to identify such that this can be accounted for when designing a controller.

From the figures, it can be seen that both configurations have a collocated actuator-encoder-pair up to 900 Hz. Hereafter the phase angle is no longer in between 0 ° and −180 ° and collocation is lost. The loss of collocation is caused by the flexibilities of the framework and the shuttle with VCM brackets. This can be assumed because these modes are also present in the bearing configuration transfer path. In other words, if the folded leaf springs and sandwich-constructed reinforcement were causing a loss of collocation, the bearing configuration would not measure these modes.

In the case of the folded leaf spring configuration, parasitic modes are present in between 420 − 920 Hz. These can be related to the internal torsional and internal tilting modes of the sandwich-constructed reinforcement and folded leaf springs (figure 3.10 and 3.11). The internal modes are lower than simulations. However, the system response is little influenced by these modes and it is not expected that these are performance limiters for accurate shuttle movements. It is assumed that this mismatch is due to assembly misalignments, geometric tolerances, and sandwich-constructed reinforcement weights a fraction higher.

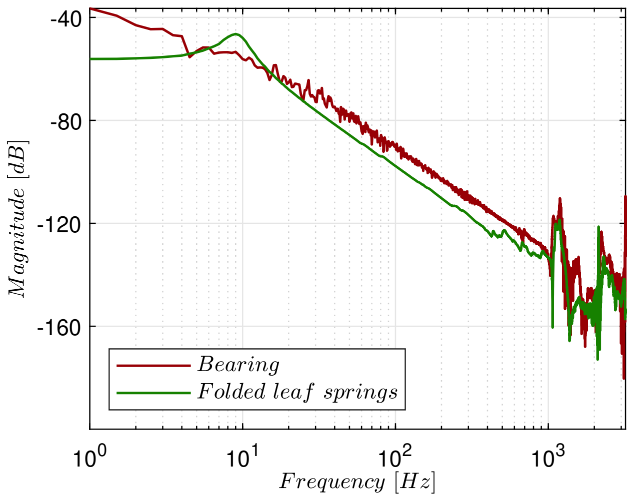

Figure 3.19: Transfer paths between VCMs and incremental encoder: (green) folded leaf spring configuration and (red) bearing configuration.

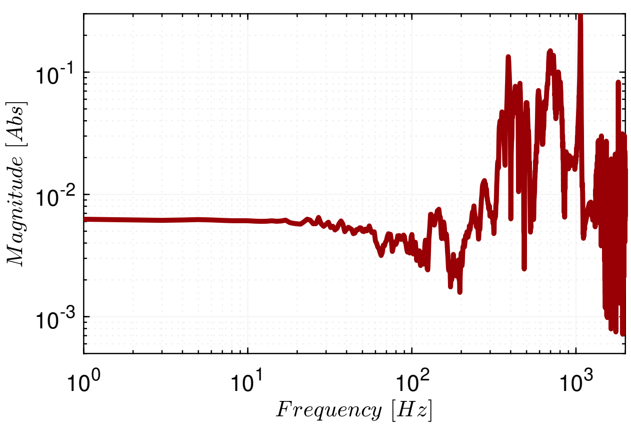

Figure 3.20: Transfer path between the incremental encoder and capacitive sensor.

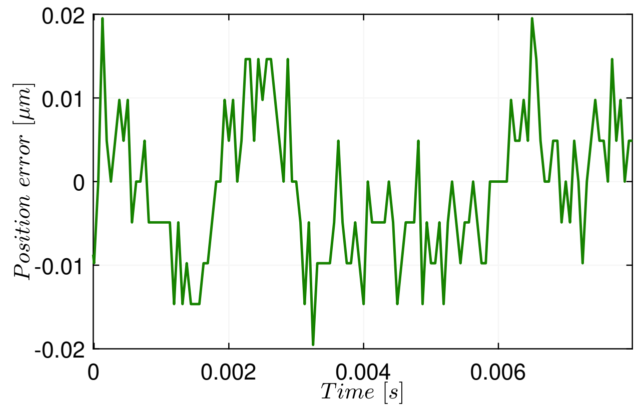

Figure 3.21: Measured incremental encoder position error at the outer stroke (folded leaf springs deflected in outer-state).

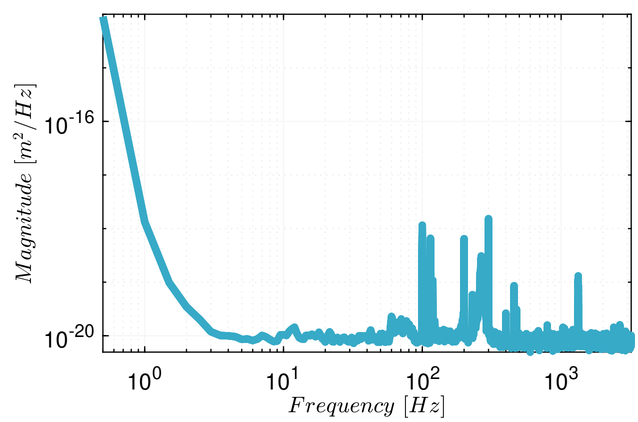

Figure 3.22: Power spectral density of incremental encoder noise.

3.5.5. Coupling shuttle movement and internal deformation

It is observed that shuttle movements and reaction forces of the VCMs affect the capacitive sensor measurement through vibrations of the active stage framework. These vibrations are a result of parasitic modes in the active stage framework and shuttle with guidance. It is expected that the influence of this transfer path is difficult to attenuate with a vibration isolation system located underneath the active stage, as the vibration isolation system uses sensors that are located on the isolation base and not the active stage framework. Figure 3.20 shows that the susceptibility of vibrations increases significantly around the intentional frame compliance mode (350 Hz). The transfer (coupling) in front of <100 Hz is mainly due to the misalignment of the shuttle with respect to the capacitive sensor and straightness of the shuttle's guidance.

3.5.6. Hysteresis

The hysteresis of the folded leaf spring configuration is determined with an open-loop controller in which the VCMs are excited with an impulse. The difference between the initial and final position measure determines the hysteresis. The result is a hysteresis of approximately 30 μm. It is assumed that this is mainly caused by the clamping blocks and stacked sandwich-constructed reinforcements. The clamping pressure is not equally distributed due to geometrical tolerances, surface irregularities, and chamfer/fillet of the respective components. As a result, the clamping pressure is not able to compensate for all tangential forces present when the folded leaf springs are deflected.

3.5.7. Position error

In order to get an indication of the achievable closed-loop position error for the shuttle, it is required to identify the noise sources, since it is known that noise degrades the performance and limits the maximum achievable accuracy of a system.

For this, the shuttle is actuated with a step to the outer deflected state. The resulting steady-state error is 0.01 μm RMS as shown in figure 3.21. The actuator driver and corresponding hardware can be identified as the source of this residual error since this error is only present when the actuator driver is active. To further validate this, the noise of the incremental encoder is measured by firmly locking the shuttle in its zero position and subsequently measuring the modulated output. The result is shown in figure 3.22. It can be seen that the noise of the incremental encoder is approximately an order lower than the measured steady-state error. Therefore, it can be concluded that the main limitation is the actuator driver and corresponding hardware. However, note that the effect of the noise on the tracking error can be partly suppressed with feedback control.

3.6. Conclusions

A modular active stage with two types of guidance for a shuttle by means of a roller bearing or folded leaf springs is designed. Perpendicular to the driving direction of the shuttle a capacitive sensor is mounted inside the framework which has intentional frame compliance. This compliance is realised with two parallel leaf springs that introduce an internal mode. The active stage is designed such that it is implementable on a Stewart Gough vibration isolation system. Both combined represent a benchmark system that can be used for exploring control strategies wherein the goal is to accurately track a reference with the shuttle and minimize internal deformations with the vibration isolation system.

The active stage guidance allows the shuttle to translate with a stroke of ± 5 mm. For both types of guidance, straightness around $3 - 6$ µm is realised.

The folded leaf spring configuration is optimized for low stiffness in the DOF and a maximal frequency in which the first parasitic mode is present. For this, a novel sandwich-constructed reinforcement is optimally tuned taking into account both the modes in which the shuttle moves and local internal modes of the guidance. This resulted in a first parasitic mode around 720 Hz and a resonance frequency in the driving direction of 10.2 Hz. From experiments, a resonance frequency at 9.5 Hz is identified, which indicates good agreement. It is assumed that the offset in stiffness, that relates to the resonance frequency, primarily is caused by assembly misalignments and geometrical tolerances.

Furthermore is identified that collocation for the VCMs and incremental encoder is guaranteed up to 900 Hz for both configurations. Although internal local modes of the folded leaf spring configuration are lower than simulations, the transfer between VCMs and incremental encoder is little influenced.

With the realised active stage, the following individual conclusions can be made:

- Hysteresis is present which is primarily caused by the construction method of clamping blocks, a stacked reinforcement, and too low clamping pressure. However, with feedback control, it is expected that these effects can be reduced.

- Actuator driver and associated hardware noise are limiting factors for accurate shuttle movements.

3.7. Recommendations

Hereafter a list of suggestions for further improvement of the active stage construction and to gain more knowledge for designing controllers:

- Redesign the folded leaf springs and sandwich constructed reinforcement with integrated clamping blocks, and combine the folded leaf spring with the core into a single part by means of EDM or die sinking. As a consequence, the influence of hysteresis reduces.

- The symmetry of the folded leaf springs guidance is at the cost of an over-constrain. An option is to redesign the shuttle or one triangular bracket, that fastens the three folded leaf springs to the shuttle, such that it confines five degrees except for one rotational degree of freedom around the axial direction (torsion) of the shuttle.

- The shuttle movement and the reaction forces of actuators cause vibrations in the active stage framework. It is expected that these vibrations are difficult to attenuate with a vibration isolation system. If this is a limiting factor a solution is to stiffen the framework with braces or more rods between the two plates and a larger outer diameter of the rods.

- Examine with experiments the parasitic modes that are present at a full deflection of the folded leaf springs to better understand the guidance characteristics. Furthermore, conduct an experimental modal analysis such that the dynamics of the shuttle, folded leaf springs and active stage framework can be linked to the parasitic modes examined with simulations. This knowledge can be used to improve the active stage construction and to design robustly stable controllers.

- The active stage is mostly validated for the folded leaf springs configuration. Although experiments show promising results it is recommended to conduct more experiments with the bearing configuration to compare results and gain more knowledge about the pros and cons of both types of guidance.

- The measurement block, that is used as a reference for the capacitive sensor, shows a small curvature due to the two screws at both short sides. It is therefore recommended to add another two screws at the long sides.

- It is shown that a folded leaf spring configuration with sandwich reinforced construction has a position error accuracy of 0.01 µm RMS, which is limited by the noise of the actuator driver. A solution is to select another type of actuator driver or choosing an actuator with a different motor constant.

4. Characterisation of a vibration isolation system with an active stage

This chapter gives a description, analysis, and characterisation of the realised active stage mounted on top of a Stewart Gough vibration isolation system [13]. Both combined represent a benchmark system which is used for the validation of vibration isolation control strategies.

The functions of the benchmark system are: mimicking an industrial floor spectrum, active vibration isolation of internal deformations, straight-line reference tracker, and measuring internal deformation.

The structure of this chapter is as follows. A description of the benchmark system is given in section 4.1. In Section 4.2, the transfer paths of importance are identified and analysed to characterise the benchmark system. Conclusions are given in Section 4.3

4.1. System description

The complete system is shown in figure 4.1 and visualized in a schematic 2D section view, as shown in figure 4.2. A broken-out section view of the bridge is chosen for proper visualisation. The floor assembly resembles an industrial floor that can be excited using piezoelectric actuators. It consists of a rigid rectangular floor plate with on top a total of three bridges that are positioned at equal distances to each other. With the aid of leaf springs and wire flexures, the floor plate is suspended to the "fixed world". In total three piezos with each in series with a leaf spring, can excite the floor plate in three independent directions of respective z_f, θ_{yf} and θ_{xf}. All floor plate vibrations are measured with six accelerometers and mapped to a global coordinate system (red-arrows) with means of a transformation matrix. In each bridge, two isolator legs are positioned and mirrored to each other with one end fixed to the bridge and the other end to the isolated base, creating a Stewart Gough vibration isolation system. Furthermore, accelerometers measure the respective vibrations of the floor for control purposes. The isolated base is suspended from the floor assembly with the Gough-Stewart representation. The isolated base consists out of a rigid axisymmetric block. For an exact constrained design, a total of six judicious isolator legs are fastened between the floor plate and isolated base. Each isolator leg consists out of a wire spring and VCM in series. The wire spring is stiff in the axial direction and compliant in all other directions. The magnet of the VCM is fixed to the isolated base and the coil is guided by circular leaf springs. Furthermore, vibrations of the isolated base are measured with a total of six accelerometers. The accelerometers each are located on an isolator leg and are oriented in the direction of its respective isolator leg. Again all accelerometer signals are mapped to a global coordinate system (red-arrows) with means of a transformation matrix. The vibration isolation system can excite all six independent directions of the isolated base in a three-dimensional space (x_i, y_i, z_i, θ_{xi}, θ_{yi} and θ_{zi}).

The active stage framework is built out of two plates that are connected to each-other by means of rods. For control purposes this is considered to be rigid. The active stage framework is rigidly connected to the isolated base. In between the two plates a so-called shuttle is located that represents the body that needs to accurately track a certain reference. With a total of six folded leaf springs the shuttle is guided and fastened to the active stage framework. This enables the shuttle to have a motion of ±5 mm in the x_a-direction. On the bottom of the shuttle a linear scale is placed and on the active stage framework an incremental encoder to measure the relative position of the shuttle. At both sides of the shuttle a VCM is positioned to provide a certain force for achieving the specified motion. Herein the magnet is fastened to the active stage framework. The coil is fastened to the shuttle with the use of brackets.

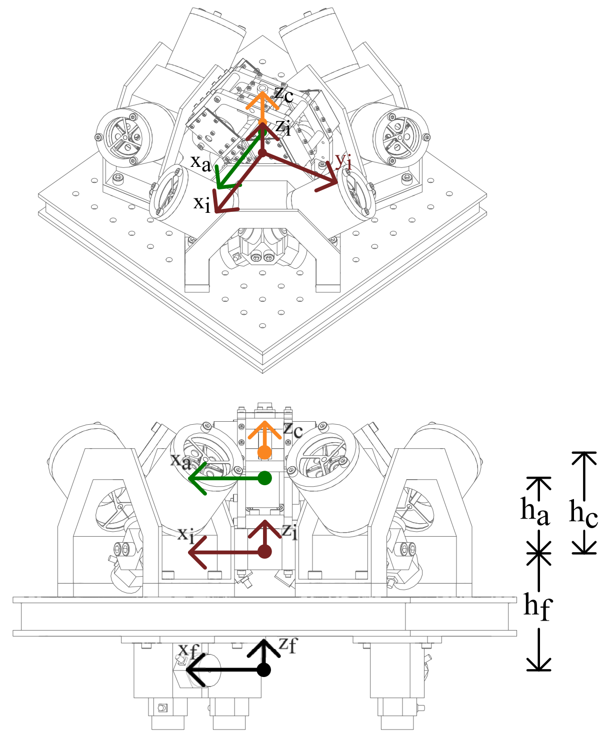

Figure 4.1: Isometric view and xz-plane of the benchmark system (without piezos that induce floor vibrations).

At the top of the active stage and in between the two plates a capacitive sensor is located. The capacitive sensor is oriented such that it is able to measure the distance to the top side of the shuttle with respect to the sensor itself. The capacitive sensor is fastened with two leaf springs in parallel. These leaf springs are relatively compliant in the z_c-direction and stiff in all other directions. With this, an intentional frame compliance is created.

4.2. System characterisation

In this section, all transfer paths are identified and analysed with a 2D conceptual model in the Laplace domain and

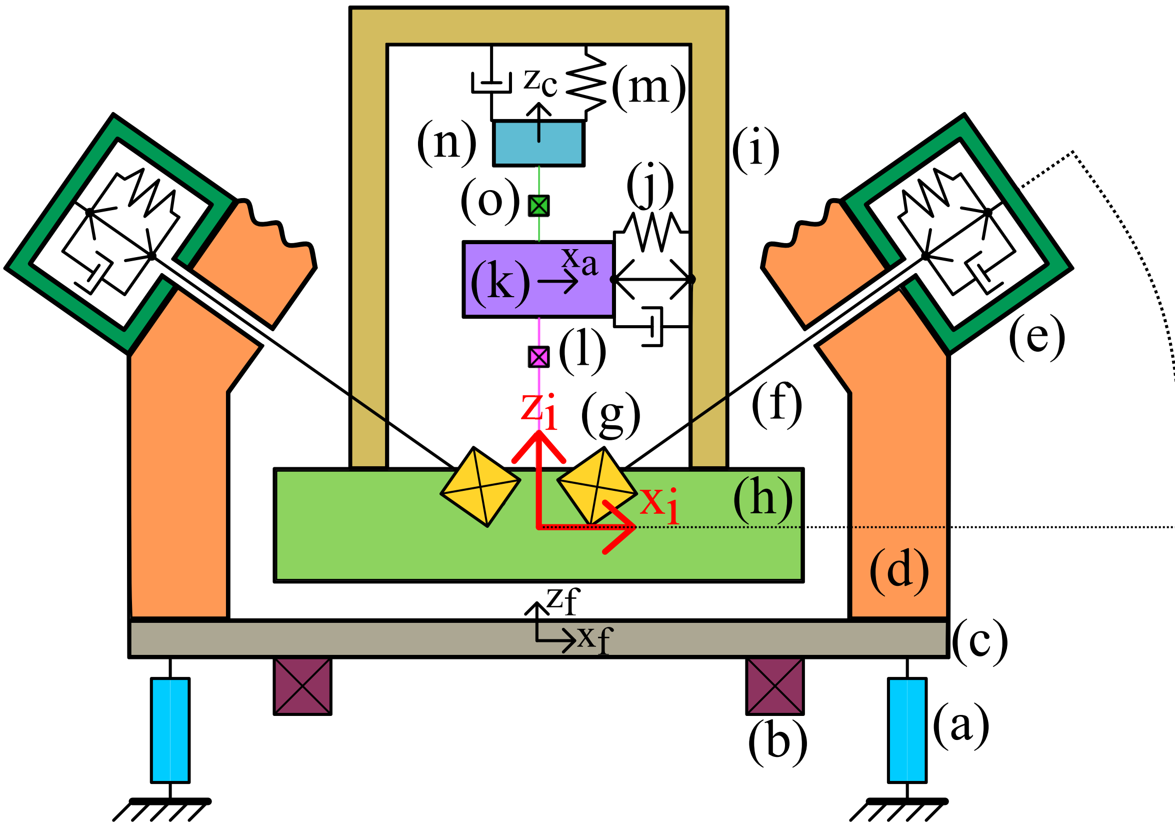

Figure 4.2: Schematic section view of the benchmark system: (a) piezo for floor excitation, (b) accelerometer floor, (c) floor base frame, (d) floor frame, (e) active vibration isolation system with VCMs and circular leaf springs, (f) wire springs, (g) accelerometer isolation system, (h) isolated base, (i) active stage framework, (j) active stage with VCMs and guidance by means of folded leaf springs, (k) shuttle, (l) incremental encoder, (m) intentional frame compliance, (n) capacitive sensor assembly and (o) capacitive sensor. The global coordinate system is denoted with red-arrows, DOF of the active stage with $x_a(t)$ and parasitic deformation with $z_c(t)$.

measurements of the benchmark system in the frequency domain. This is useful for the design of control strategies, as it gives more insight into the influence of each disturbance and actuator force on measured vibrations and displacements.

The 2D model is a simplified version of reality. It is modelled as a series of rigid bodies with mass, spring, damper and force components. It gives an insight into the dominant transfer paths and interaction between the sub-assemblies. However, it does not include parasitic modes of the framework and other components individually, except for the intentional frame compliance. Comparison of the model with measurement results should show the higher-order dynamics by parasitic modes and non-ideal dynamics that result in cross-coupling.

The conceptual overview of the complete system in 2D is shown in Figure 4.3. It represents the structure and spring, damper and actuator components in a section view. The system is made out of four main sub-assemblies: floor assembly, vibration isolation system, active stage and capacitive sensor assembly. The floor assembly is considered to be rheonomic and represent an industrial floor with vibrations. The isolated base (m_i, I_y) is suspended from the floor assembly with springs (k_x, k_z, $k_{\theta y}$) and dampers (c_x, c_z, $c_{\theta y}$). Those terms function as passive isolators of disturbances. The terms F_x, F_y and M_y are intended for providing forces and a moment to attenuate vibrations. On top of the isolated base an active stage is located. The parameters (m_a, I_{ya}) represents the shuttle that needs to track a reference. The shuttle is guided with the folded leaf springs. In the conceptual representation it is assumed that the guidance is rigid in all directions except for the x_a-direction. The compliant characteristics are represented by stiffness k_a and damping c_a. The term F_a is intended for providing a force to achieve a specified stroke of the shuttle. Above the active stage framework a capacitive sensor assembly (m_c, I_{yc}) is positioned. The assembly resembles high-sensitive equipment that measures perpendicular to the top plane of the shuttle with aid of a capacitive sensor. In order to simulate a finite stiffness of the framework the sensor assembly is fastened with stiffness k_c and damping c_c, such that an intentional frame compliance is present in the rigid body dynamics. The sensor assembly is considered to be relatively compliant in the z_c-direction and stiff in all other directions.

In the proceeding sub-sections, all important transfer paths are measured and compared with the paths derived from the 2D model. The transfer paths are experimentally

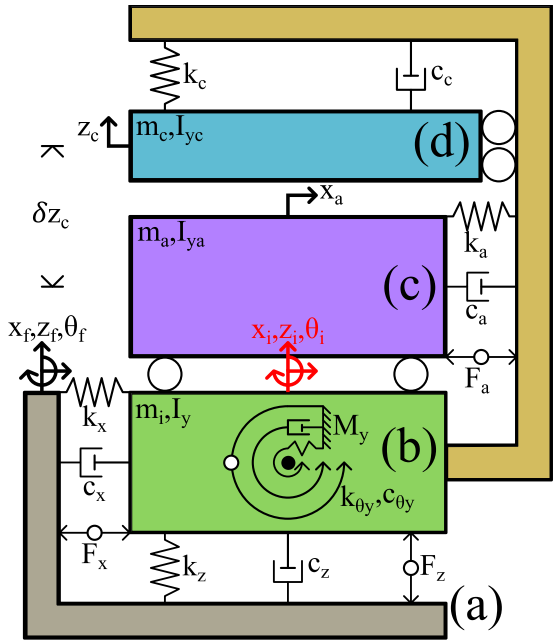

Figure 4.3: Conceptual 2D-representation of the active stage with the vibration isolation system: (a) floor assembly, (b) isolated base, (c) active stage, (d) intentional frame compliance. All rigid body dynamics parameters are denoted with: force F or moment M, mass m, inertia I, damping c, stiffness k and height h.

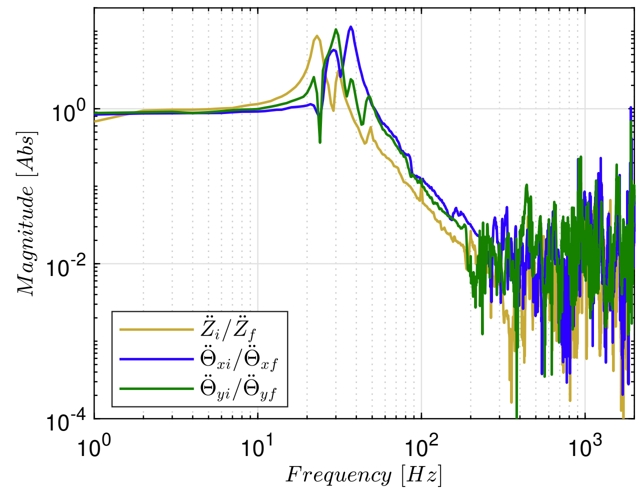

Figure 4.4: Dominant primary paths in the global coordinate system.

obtained by exciting the actuators with a Pseudo-Random Binary Signal (PRBS) signal. The PRBS signal variance for the active stage VCMs is 5 V and 0.4 A for the vibration isolation system VCMs. In the case of the piezos the voltage variance is set to the specified voltage range of the amplifier. The input-output signals are processed with a time length of 100 s at a sample rate of 6.4 kHz. Further processing is done with aid of window-function-based Welch's method [65] in which the signal is split up into overlapping segments of 2 s.

4.2.1. Primary paths

The isolated base is subject to indirect disturbances of the rheonomic floor through the primary path called $\boldsymbol{P_i}(s)$. For a 2D representation, this gives three paths characterized with passive components. The isolated base in the x_i-direction and θi-rotation are dependent on the passive components of both the floor assembly and active stage. Due to the active stage, the transfer is rather complex for the x_i-direction as well as θi-rotation. The reason is that a transfer from the isolated base through the shuttle with guidance dynamics on the isolated base exists, which creates a feedback loop. In the case of the z_i-direction these feedback loops are not present and the transfer path simplifies to

$$P_{iz}(s) = \frac{\ddot{Z}_i(s)}{\ddot{Z}_f(s)} = \frac{N_i(s)}{D(s)}\left(c_z s + k_z\right), \tag{4.1}$$

with nominator

$$N_i(s) = \left(m_c s^2 + c_c s + k_c\right), \tag{4.2}$$

and denominator

$$D(s) = ((m_i + m_a)s^2 + (c_z + c_c)s + (k_z + k_c)) \\ (m_c s^2 + c_c s + k_c) - (c_c s + k_c)^2. \tag{4.3}$$

Note that the transfer path is expressed in acceleration components. The equation (4.1) and associated nominator and denominator reveals that both the dynamics of the vibration isolation system and intentional frame compliance with the capacitive sensor assembly defines the complete transfer path.

In practice, the floor can only be excited in the direction z_f and rotations θ_{xf}, θ_{yf}, and coupling is present between the degrees of freedom. The result is that a total of nine paths exist in which there are three dominant couplings. These dominant coupling measurements are shown in figure 4.4. Compared to equation (4.1) the bounce mode of the isolated base and respective suspension in the z_i can be clearly seen. However, the (anti-)resonance frequency and coupling of the isolated base to the active stage and intentional frame compliance with capacitive sensor assembly are not identified. This is mainly due to the identification technique and the maximum amount of power that can be put into the piezos which causes fluctuations after frequencies higher than 200 Hz.

In front of the resonance peak of all three transfer paths both the floor and isolated base move or rotate as two bodies in phase and with equal amplitude. From the (anti-)resonance frequency peaks it can be seen that all degrees of freedoms are coupled. After the resonance peak, the functionality of the passive isolators is visible, since the influence of floor vibrations on the isolated base drastically decreases. Furthermore, it is observed that the suspension of the vibration isolation system cannot be considered rigid, because reaction forces of the vibration isolation system VCMs influence the floor dynamics. Therefore, the assumption of a rheonomic floor is not completely true.

4.2.2. Secondary paths

The vibration isolation system is controlled with $F_x(s)$, $F_y(s)$ and $M_y(s)$ through the secondary path called $\boldsymbol{S_i(s)}$. The z_i-direction is used as an example (due to the rather simple representation of dynamics), and can be written as

$$S_{iz}(s) = \frac{\ddot{Z}_i(s)}{F_z(s)} = \frac{N_i(s)}{D(s)} s^2. \tag{4.4}$$

Equivalent dynamics are involved in this path compared to the primary path. The difference is that in this situation actuator force is considered and not the floor vibrations, that equals $F_{fz}(s) = (c_z s + k_z) Z_f(s)$. It shows that the force of actuator and disturbance equals when

$$F_z(s) = (c_z s + k_z) s^{-2} \ddot{Z}_f(s). \tag{4.5}$$

In practice, the isolated base can be excited in all degrees of freedom. It results in a total of 36 paths, that are dominant in six paths. The measured dominant paths are shown in figure 4.5. The resonance frequency of the first and second degree of freedom is related to a coupled quadruple of shear and bending modes of the isolated base, at 21 Hz and 22 Hz. The third resonance frequency is in the z_i-direction and relates to a bounce mode at 23 Hz. The last resonance frequency at 40 Hz relates to a torsional mode.

The negative slopes after the resonance frequencies are caused by the voltage-controlled VCMs in which actuator dynamics introduce another pole. The choice of voltage-controlled actuators is due advantageous low-noise characteristics [12]. The only drawback is that this actuator pole is varying slightly over time.

The fluctuations after 600 Hz are a result of parasitic modes of the VCM guidances and wire springs.

In the case of a controller in local coordinates, it is also useful to visualize the secondary paths in local coordinates. These measurements are shown in figure 4.6 and can be interpreted as follows. The location and height of the resonance peak are defined by the electrical properties of the VCM and guidance stiffness and damping. Besides that, partly by the mass of the isolated base and associated components. It can be seen that each guidance does not have equal dynamics. This is one of the reasons that the vibration isolation system in global directions is not completely decoupled.

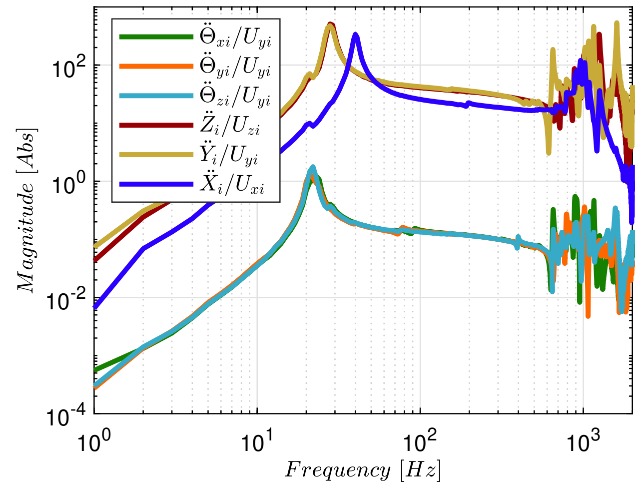

Figure 4.5: Dominant secondary paths in the global coordinate system.

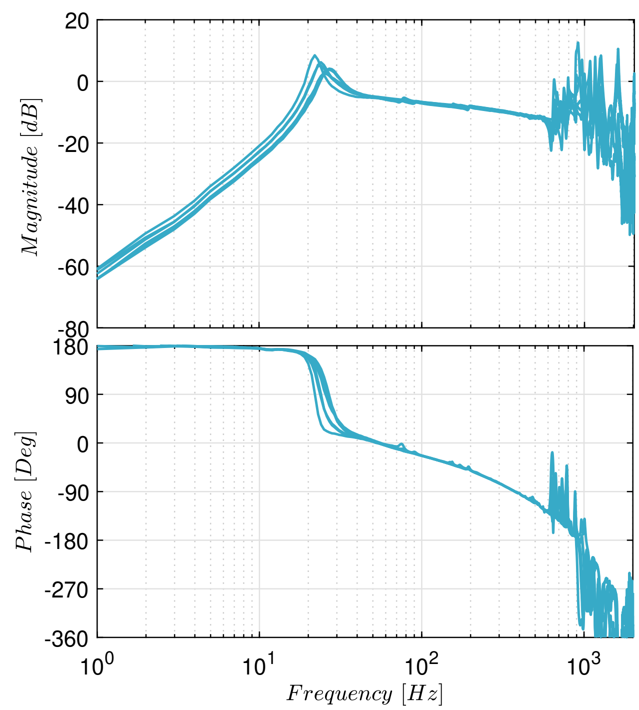

Figure 4.6: Dominant secondary paths in local coordinate systems of each isolator leg. With the voltage of the VCM as input and accelerometer as output.

4.2.3. Tertiary paths

The active stage exerts forces on the isolated base when a reference is tracked with the shuttle or when indirectly other disturbances cause a motion of the shuttle. According to newton's law, the force of the active stage on the isolated base in the x_i-direction equals

$$F_{active,stage} = m_a \ddot{x}_a, \tag{4.6}$$

and for θ_{yi}-rotation

$$M_{active,stage} = h_a m_a \ddot{x}_a. \tag{4.7}$$

These forces act through a so-called tertiary path $\boldsymbol{T_i}(s)$ on the isolated base. The derivation based on the conceptual design in those coordinates, gives

$$\begin{aligned} T_{ix}(s) &= \frac{\ddot{X}_i(s)}{X_a(s)} \approx \frac{m_a s^4}{(m_i + m_c)s^2 + c_x s + k_x}, \\ T_{i\theta y}(s) &= \frac{\ddot{\Theta}_{yi}(s)}{X_a(s)} \approx \frac{h_a m_a s^4}{I_{tot} s^2 + c_{\theta y} s + k_{\theta y}}, \\ I_{tot} &= I_y + I_{ya} + I_{yc} + h_c^2 m_c. \end{aligned} \tag{4.8}$$

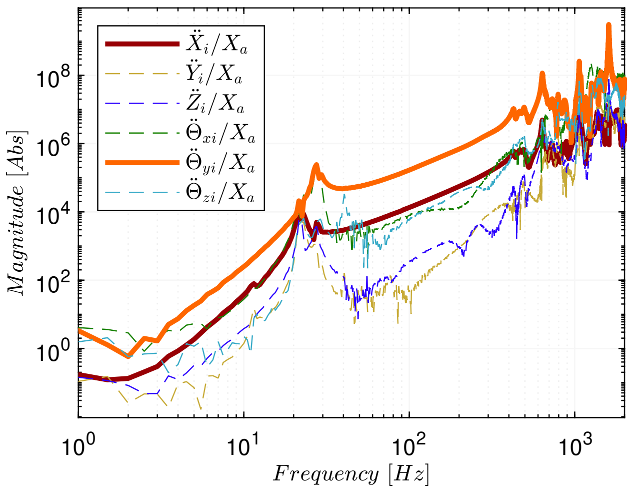

Figure 4.7: Dominant tertiary paths in the global coordinate system.

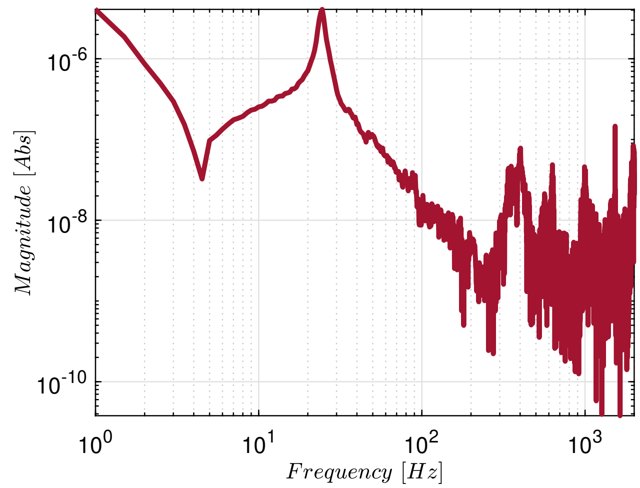

Figure 4.8: Indirect jitter path from floor vibrations z_f on the internal deformation δz_c.

Note that the transfer path is expressed in position and acceleration components. Moreover, the equations are a simplified version of the real linear dynamics because translation and rotation of the isolated base are indirectly coupled to each other and make the transfer path rather complex. The explanation for this is given in the primary path section.

It can be derived that the secondary and tertiary path equals in the x_i-direction when

$$F_x(s) = -m_a s^2 X_a(s), \tag{4.9}$$

and for θ_{yi}-rotation, when

$$M_y(s) = -h_a m_a s^2 X_a(s). \tag{4.10}$$

This force and moment are related to the two dominant paths. However, in practice, a total of six transfer paths exist, which is mainly caused by coupled dynamics in the vibration isolation system suspension and non-ideal shuttle guidance. The latter is due to the straightness of the guidance that causes also forces and moments other than in the x_i-direction and θ_{yi}-rotation.

The measured six dominant transfer paths are shown in figure 4.7. It can be seen that x_a movement mainly influences the x_i-direction and θ_{yi}-rotation of the isolated base. All other directions and rotations do show a rather uncoupled system.

4.2.4. Jitter paths

The floor vibrations cause internal deformation in the active stage framework. These indirect disturbances of the floor are transmitted through the vibration isolation system and measured with the capacitive sensor. This capacitive sensor measures the difference between the z_c-displacement of the capacitive sensor assembly and z_i-displacement of the isolated base. The path that defines the transfer from floor vibrations to internal deformation is given by the so-called indirect jitter path,

$$T_{ij}(s) = \frac{\delta Z_c(s)}{Z_f(s)} = \frac{N_c(s) - N_i(s)}{D(s)}\left(c_z s + k_z\right), \tag{4.11}$$

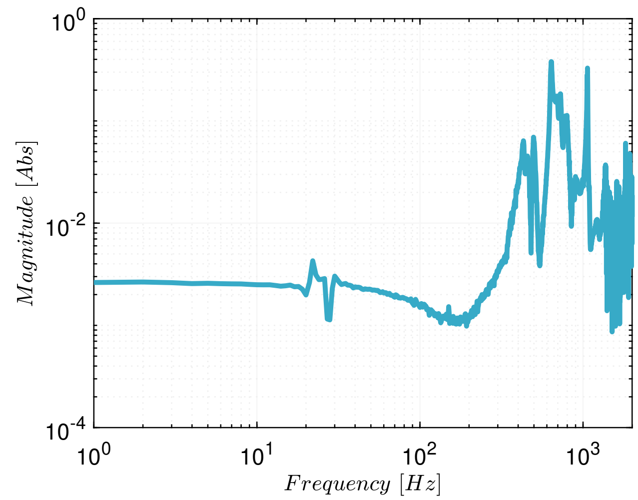

Figure 4.9: Direct jitter path from shuttle displacment x_a on the internal deformation δz_c.

with

$$\begin{aligned} N_c(s) &= (m_i + m_a)s^2 + (c_z + c_c)s + (k_z + k_c), \\ N_i(s) &= \left(m_c s^2 + c_c s + k_c\right). \end{aligned} \tag{4.12}$$

The transfer is mainly dependent on the dynamics of the vibration isolation system and capacitive sensor assembly. From this expression can be stated that vibrations attenuated on the isolated base reduce the internal deformation. Since floor vibrations need to be transmitted through the isolated base before they can cause any internal deformation. The most dominant transfer path is experimentally identified and shown in figure 4.8. As expected below the resonance frequency an anti-resonance is present due to the coupling of the isolated base and capacitive sensor assembly. The resonance frequencies are related to the bounce mode of the vibration isolation system suspension at approximately 23 Hz and capacitive sensor assembly suspension at approximately 370 Hz.

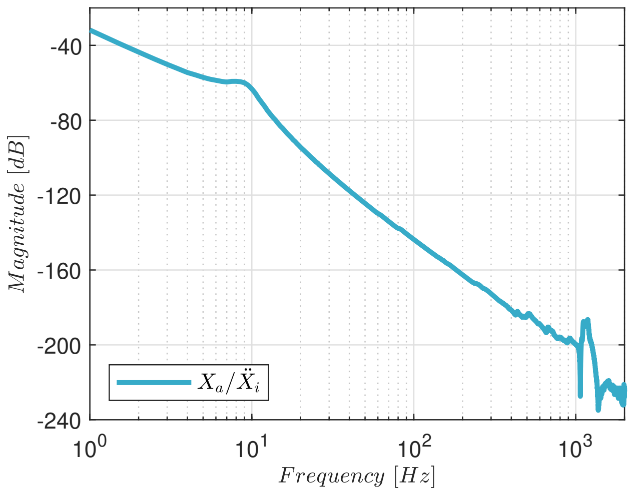

Figure 4.10: Primary path of the active stage.

Another cause of internal deformation is due to shuttle movements. Any shuttle movement causes direct vibrations in the vibration isolation system and as a result indirect to the capacitive sensor assembly. Besides that, active stage movements causes vibrations in the active stage framework due to the finite stiffness. Hence, also vibrations are transmitted on the capacitive sensor assembly through the active stage framework vibrations.

The path that defines the transfer from shuttle movement is given by the so-called direct jitter path and shown in figure 4.9. At 22 Hz the bounce mode and 27 Hz coupled bending-shear mode of the vibration isolation system can be seen. Furthermore, from 350 Hz the internal mode of the capacitive sensor assembly causes increased sensitivity to internal deformations due to shuttle movements.

In the low-frequency region, a non-zero transfer is measured. For the experimental results, this is corrected such that only an internal deformation is measured, as it is the goal to measure internal deformation and not the guidance characteristics. The non-zero transfer in the low-frequency region is a result of folded leaf springs that guides the shuttle in an arc-like line and the shuttle driving direction not exactly aligned perpendicular to the capacitive sensor.

4.2.5. Active stage primary paths

The shuttle is subject vibrations of the isolated base that are transmitted through the primary paths $\boldsymbol{P_a(s)}$ of the active stage. These transfer paths can be written as

$$\begin{aligned} P_{ax}(s) &= \frac{X_a(s)}{\ddot{X}_i(s)} = \frac{c_a s + k_a}{s^2(m_a s^2 + c_a s + k_a)}, \\ P_{a\theta i}(s) &= \frac{X_a(s)}{\ddot{\Theta}_{yi}(s)} = \frac{h_a(c_a s + k_a)}{s^2(m_a s^2 + c_a s + k_a)}. \end{aligned} \tag{4.13}$$

Both transfer paths are completely described by the dynamics of the shuttle and its guidance. The susceptibility for vibrations of the isolated base decreases significantly after the resonance frequency of the active stage DOF. In the case of

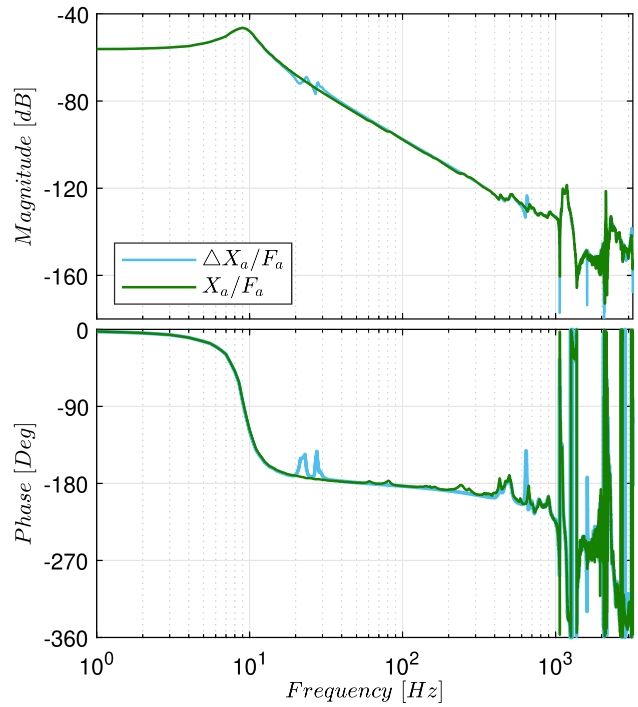

Figure 4.11: Secondary paths of the active stage. Visualized for the case of a passive and active vibration isolation system.

the conceptual design, only vibrations of the isolated base in the x_i-direction and around θ_{yi}-axis influences the shuttle displacements. However, in practice a total of six transfer paths are present with two dominant paths that also are derived for the conceptual design. The transfer relating to vibrations of the isolated base in the x_i-direction is shown in figure 4.10. This transfer path is reconstructed from the identified secondary path of the active stage as shown in figure 4.11.

4.2.6. Active stage secondary path

The shuttle tracks a reference with a force $F_a(s)$ generated by a controller. In practice the relative position $\triangle X_a(s)$ is used as control input. This is the difference between the shuttle x_a-displacement and isolated base x_i-displacement. The transfer that defines $F_a(s)$ to $\triangle X_a(s)$ is given by

$$\begin{aligned} S_{\triangle a}(s) &= \frac{X_a(s) - X_i(s)}{F_a(s)} = \\ \frac{\triangle X_a(s)}{F_a(s)} &\approx \frac{w_2^2(s^2 + w_3^2)(s^2 + w_{ar}^2)}{m_a w_{ar}^2 (s^2 + w_1^2)(s^2 + w_2^2)(s^2 + w_3^2)} \\ \omega_1 &= \sqrt{\frac{k_a}{m_a}},\ \omega_2 = \sqrt{\frac{k_i}{m_i + m_c}},\ \omega_3 = \sqrt{\frac{k_\theta}{I_{tot}}}, \\ \omega_{ar} &= \sqrt{\frac{k_i}{m_i + m_a}}. \end{aligned} \tag{4.14}$$

In this ω_1 is the resonance frequency of the shuttle guidance in the DOF direction. The influence of the vibration isolation system is reflected with the resonance frequencies ω_2, ω_3, and anti-resonance frequency ω_{ar}. These latter terms can be interpreted as follows; ω_2 is the suspension frequency in the x_i-direction, ω_3 in θ_{yi}-rotation and ω_{ar} is the mode in which the shuttle and isolated base move in phase with equal amplitude.

In case of an active vibration isolation system in which the suspension frequencies are damped properly and $m_a << (m_i + m_c)$. The transfer simplifies to

$$S_a(s) = \frac{X_a(s)}{F_a(s)} = \frac{1}{m_a s^2 + c_a s + k_a}. \tag{4.15}$$

Both experimental obtained transfer paths are shown in figure 4.11.

4.3. Conclusions

Modelling and identification are performed to characterize all dominant transfer paths. For this, a linear dynamic model in combination with experimental data are used. The experimental results show that the rigid body modelling is valid up to about 500 Hz.

It is found that the indirect and direct disturbances influence the vibrations of the isolated base, internal deformations of the active stage, and dynamics of the shuttle guidance. Furthermore, it can be stated that indirect disturbances due to the floor vibrations and direct disturbances that are transmitted by means of the indirect jitter path, can be attenuated with a controller that attenuates the vibrations of the isolated base. However, the direct disturbances that are transmitted through the direct jitter path can only be properly attenuated up to frequencies about 500 Hz because at higher frequencies the active stage framework cannot be considered rigid. Hence, the active stage framework can vibrate even if the vibration of the isolated base are attenuated completely.

For control purposes of the active stage, it is shown that the active stage path can be simplified if the vibration isolation system suspension modes are actively damped and certain mass ratios are present. As a result, a rather simple model-based feedforward controller can be implemented.

5. Conclusions and recommendations

In this research, a multi-objective control strategy is designed with feedback and adaptive feedforward controllers. A theoretical framework is set up for relating the control designs to the performance objectives that are, minimizing the tracking error and internal deformation. It has been derived and verified that the internal deformation primarily depends on the vibrations of the isolated base up to frequencies around 500 Hz. The feasibility of the controllers is demonstrated on a flexure-based active stage mounted on top of a Stewart Gough vibration isolation system. The vibration isolation system is adopted from earlier research and the active stage is designed, realised and verified in this research. The main conclusions and recommendations for future research are listed in this chapter.

5.1. Conclusions

Vibration isolation system controllers

A promising feedforward controller is designed in which measured floor vibrations and components of the reference profile are used as control inputs to minimize the internal deformation and tracking error. The feedforward controller is implemented as a self-tuning generalized FIR filter in which optimal parameters are estimated with a FeLMS algorithm that includes deviations of the parameters from their nominal values and optimises for noise characteristics of the sensors and actuators. The algorithm estimates a total of 66 parameters that relate to the primary and tertiary paths of the system's dynamics. The parameters all converge to values that correspond to the physics derived in the theoretical framework.

In the case of indirect disturbances, it is found that performance limiters are the weak integrators, bandpass of the noise shaping filter, accuracy of the secondary path estimate, finite stiffness of the floor, and discrete implementation of the controller.

A drawback of the proposed feedforward controller is that it uses components of the reference profile as control input which slightly differ from moving part states that are the source of the direct disturbance. More specifically, the vibration isolation system feedforward assumes that the direct disturbance generated by the moving part is equal to the jerk and acceleration reference components with the respective physical parameters. However, in practice, the moving part states differ from the reference profile components due to a tracking error.

To further attenuate vibrations of the isolated base causing internal deformation and that are not cancelled by the feedforward controller, a high-gain feedback controller is used with virtual mass, skyhook damping, and skyhook stiffness. For this, the input-output relations of the isolated base are written in terms of power spectral densities, and subsequently, the feedback controller parameters are tuned such the vibrations of the isolated base are minimal in a frequency range of $1 - 300$ Hz.

Experiments show that with the feedforward and feedback controller operational, the internal deformation reduces with a ratio of five and tracking error with a ratio of three compared to the passive vibration isolation system.

Active stage controllers

Accurate reference tracking is achieved with PID control and adaptive feedforward control. The PID control parameters are set with a technique that only requires choosing the cross-over frequency of the open-loop. This cross-over frequency is determined by first writing the input-output relations of the tracking error in terms of the sensitivity and complementary sensitivity with the corresponding reference components, disturbances, and noises. Subsequently, a cross-over frequency of 200 Hz is chosen such that the influence of all components on the error is approximately balanced. The feedforward control parameters are estimated with a Kalman filter. It is observed with experiments that the algorithm exhibit stable behavior and all three parameters convergence in around 10 s.

The combined control strategies show a maximum tracking error around 1 µm if the moving part is accelerated with $50\ \mathrm{m/s^2}$. After each reference step the moving part settles in 0.048 s.

5.2. Recommendations

Stability of vibration isolation system feedforward controller

The floor has a finite stiffness which induces another transfer path from the vibration isolation system actuators through the floor assembly on the isolated base. It is observed that this transfer path causes an unstable indirect disturbance feedforward controller. A topic of further research is to include this effect in the theoretical framework.

Another observation is that the FeLMS algorithm with the generalized FIR filter and noise shaping filter is not robustly stable. To improve this, future research should set up a systematic approach for a robustly stable algorithm with applications for active vibration isolation systems, which considers the weak integrator parameters, noise shaping filter, secondary path estimate and finite stiffness of the floor.

Improvements direct disturbance control input

The mismatch in the acceleration and jerk state of the moving part compared to the reference profile components used as direct disturbance control input for the feedforward controller in the vibration isolation system, limits the effectiveness of the proposed control strategy. For this several techniques are available that could lower the mismatch. First, improve the model-based feedforward controller of the active stage with the inclusion of higher-order dynamics and hysteresis. Second, equip the shuttle with for example an acceleration sensor and use this measurement for both active stage feedback control and an additional feedback controller for the vibration isolation system. Third, make use of internal model control that generates the difference between the actual and measured states. These differences can both be used to correct the control inputs of the active stage feedforward control and direct disturbance feedforward control of the vibration isolation system.

Improvement feedforward controller active stage

The active stage feedforward controller is designed according to a linearised model. This is based on the zero deflection configuration of the folded leaf springs. However, it is known from simulations and experiments that the stiffness is non-linear. This behaviour can be included in the adaptive feedforward controller such that tracking error is improved.

Higher-order reference

The chosen reference is a third-order profile with aggressive setpoints. In view of both the active stage and vibration isolation system, a more suitable solution is to use a higher-order profile. It lowers the energy content of the tracking error and the indirect disturbances that causing the isolated base to vibrate.

Redesign vibration isolation system

The parasitic modes of the vibration isolation system limit the bandwidth of the feedback and achievable performance of the feedforward controller. It is therefore recommended to reinforce the wire springs and optimize the circular leaf springs for the guidance of the actuators.

A. Extended results

This appendix provides additional information on the implemented control strategies and the obtained results of the paper in Chapter 2.

A.1. Proportional Integral Derivative (PID) control

The active stage feedback controller in is tuned such that with a parameter uncertainty of 10 % stability is guaranteed. This results in a gain margin of 10 and phase margin of 10° and open-loop shown in figure A.1.

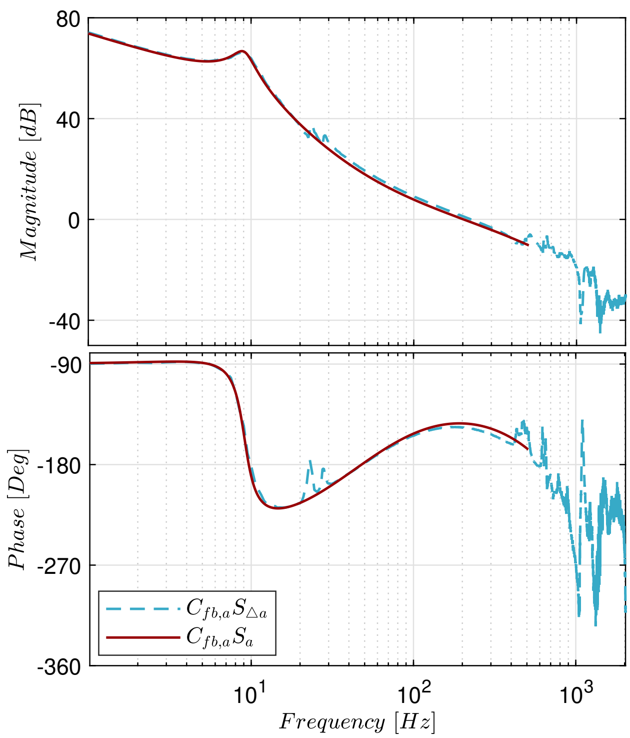

Figure A.1: Open-loop active stage with manually tuned feedback controller $C_{fb,a}$. Visualized for the case of a passive and active isolation system.

A.2. Power spectral density minimisation

The vibration isolation system feedback controller is tuned with minimisation of the local accelerometer power spectral density. For this, the local secondary paths are identified. Due to the coupling of all isolator legs, each local secondary path is identified step-wise with a low-gain feedback controller on all other isolator legs (figure A.2). In order to apply a high-gain feedback controller for each secondary path, notch filters are added to cope for parasitic modes that causes instability. The notch filters are listed in table A.1 and are written as

$$N_f = \frac{s^2 + 2\zeta_n\omega_n s + \omega_n^2}{s^2 + 2\zeta_d\omega_n s + \omega_n^2}. \tag{A.1}$$

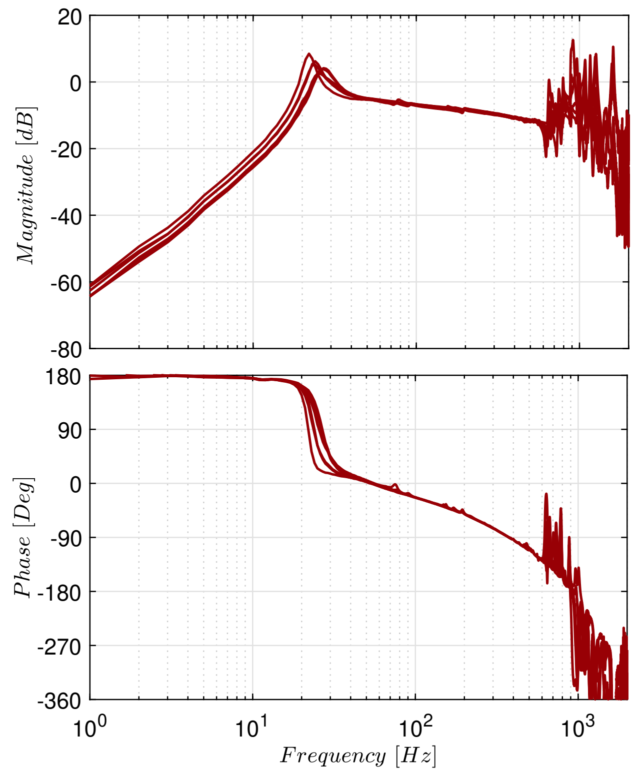

Figure A.2: Identified secondary paths in local-coordinates

Table A.1
Frequencies of the notch filters for the local vibration isolation system feedback controller. With $\zeta_n = 1e-3$ and $\zeta_d = 1e-1$.

Isolator leg	Frequencies ω_n
1	1609Hz
2	895Hz
3	650,976,1261 and 1579Hz
4	941Hz
5	971Hz
6	1262Hz

The stability is examined with the open-loop shown in figure A.3. It can be seen and it is also observed that the feedback controller is not robust stable. With a gain margin around 5 an parameter uncertainty of 5 % results in an unstable system due to parasitic modes.

A.3. Filtered-error LMS (FeLMS) control

The weights obtained from the parameter Filtered-error LMS algorithm that relate to the reference jerk and acceleration component in local coordinate system are shown in figure A.4 and A.5. The weights that relates to the floor acceleration, velocity and position can be found in earlier research [43].

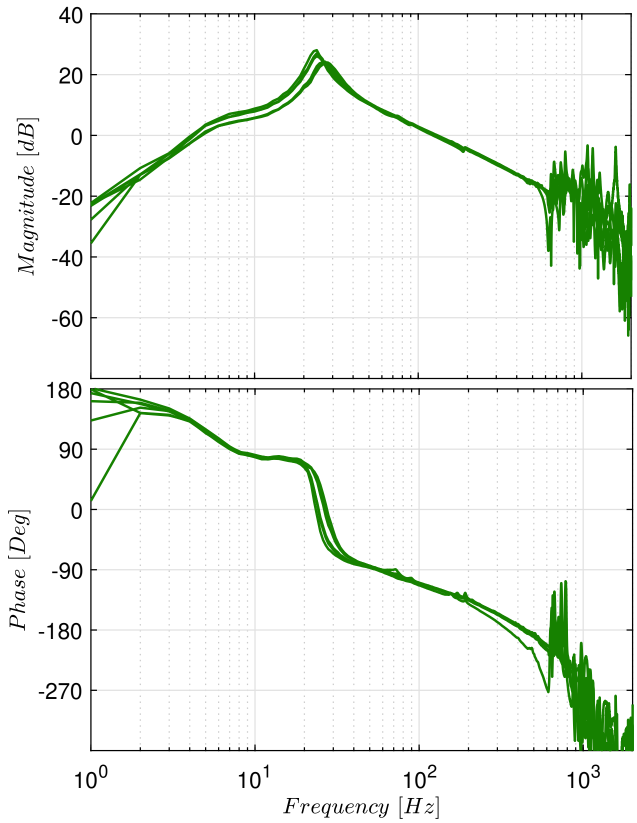

Figure A.3: Open-loop isolation system in local-coordinates with manually tuned feedback controller $\boldsymbol{C_{fb,i}}$.

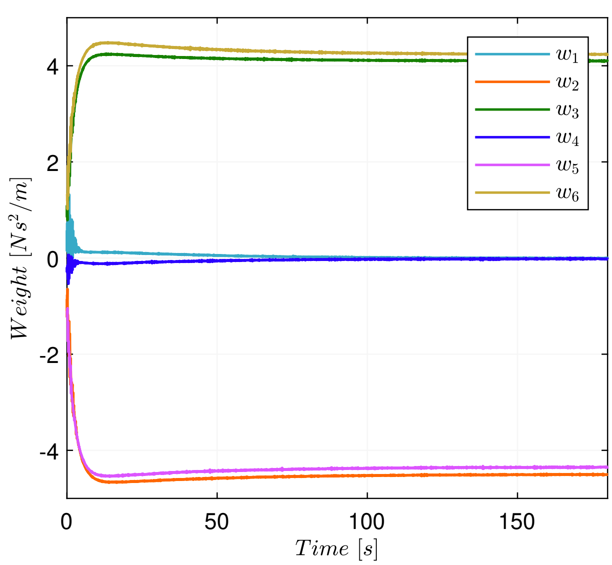

Figure A.4: Estimated weights in local coordinate system related to the reference acceleration component.

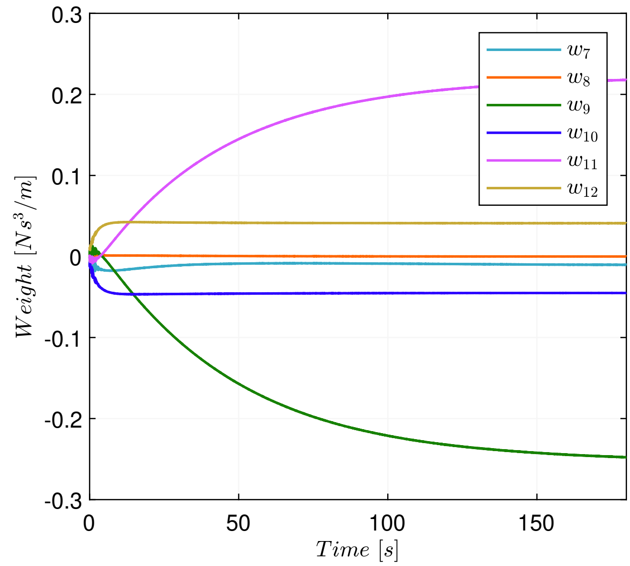

Figure A.5: Estimated weights in local coordinate system related to the reference jerk component.

A.4. Tracking error

A zoomed-in version of the tracking error with both control strategies active is shown in figure A.6.

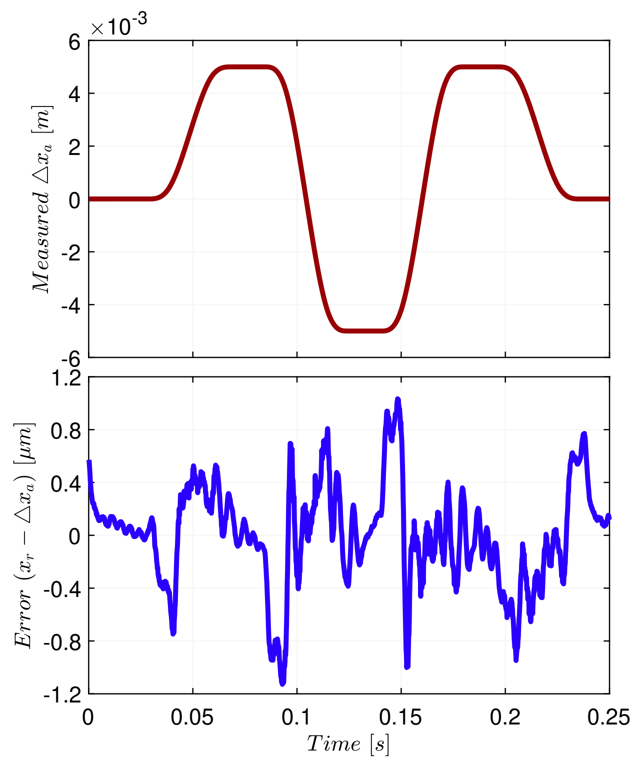

Figure A.6: Measured incremental encoder position and related tracking error with both control strategies active.

A.5. Capacitive sensor measurements

The shuttle and its guidance are not correctly aligned with the capacitive sensor. The related raw-data of the incremental encoder and capacitive sensor measurements are shown in figure A.7

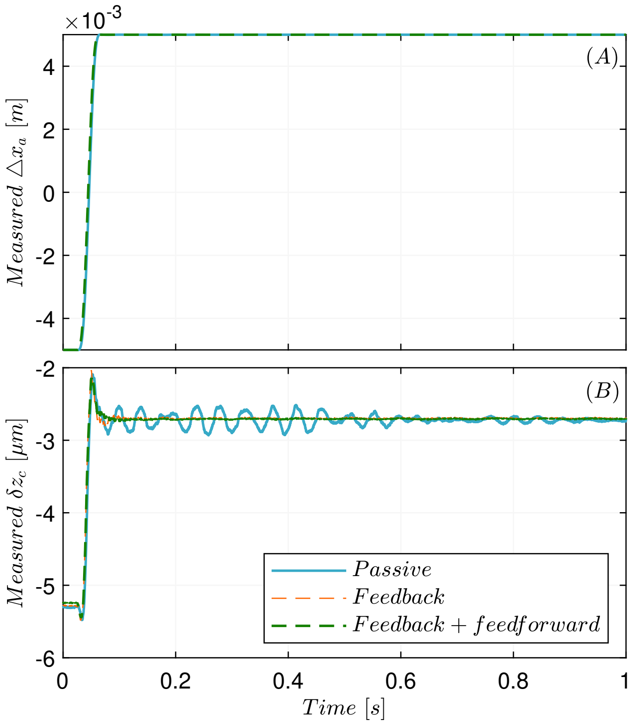

Figure A.7: Measured (A) incremental encoder position $\triangle x_a$ and (B) capacitive sensor position δz_c. Visualized for the passive, feedback $C_{fb,i}$ and feedback + feedforward $C_{ff,i}$ configuration.

B. Block diagram manipulation

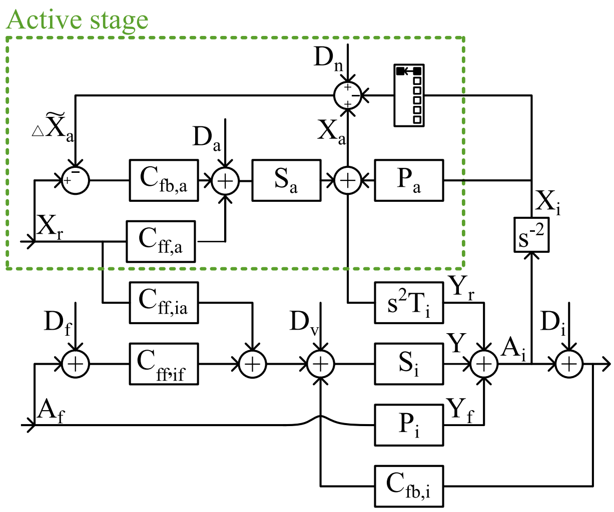

Figure B.1: Step 1. Write down controllers and paths with associated signals.

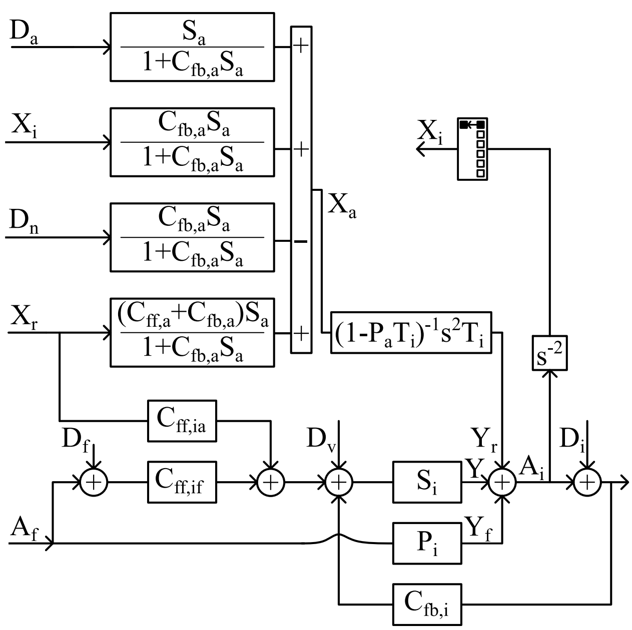

Figure B.2: Step 2. Manipulate the active stage blocks and rewrite them as individual sources.

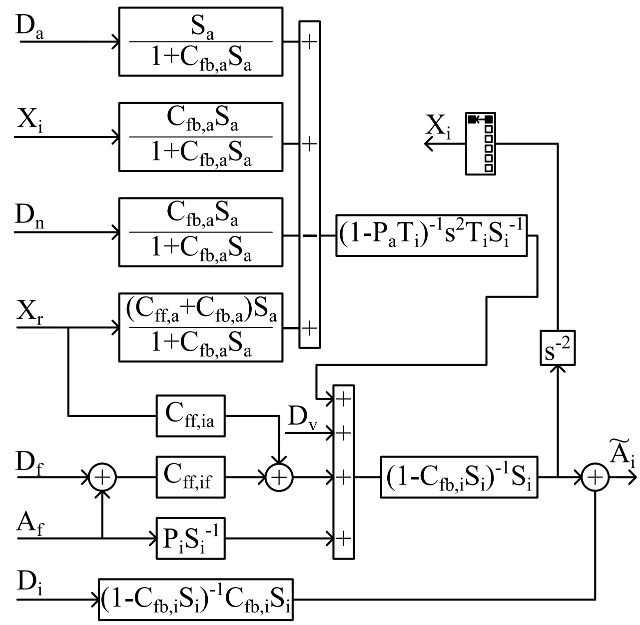

Figure B.3: Step 3. Manipulate the vibration isolation system feedback controller.

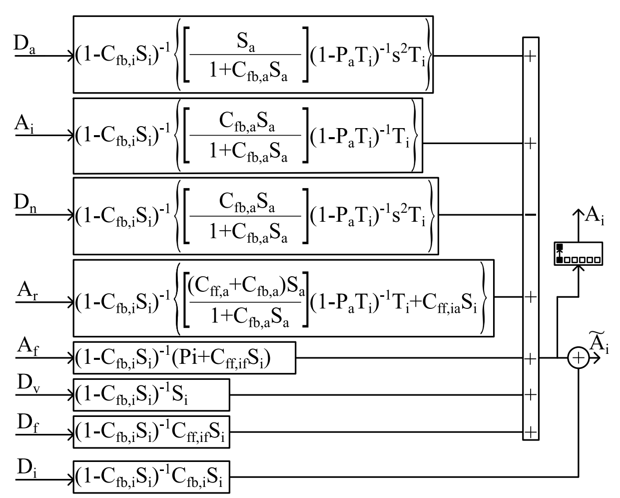

Figure B.4: Step 4. Write all disturbances and noises as individual sources, and replace x_r for a_r and rewrite the blocks. Note that a_i is a feedback signal which can be simplified to the return difference.

C. Modal analysis of the active stage

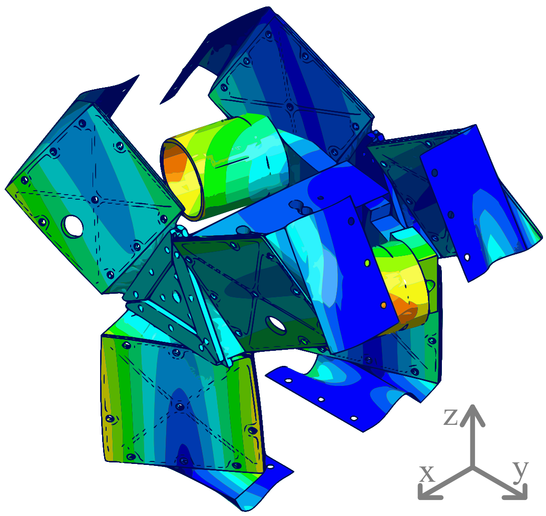

Figure C.1: Torsional mode around the z-axis at 840 Hz.

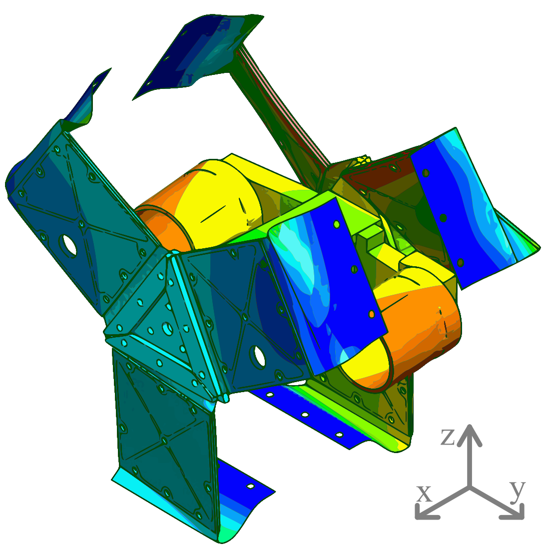

Figure C.2: Translational mode along the z-axis at 870 Hz.

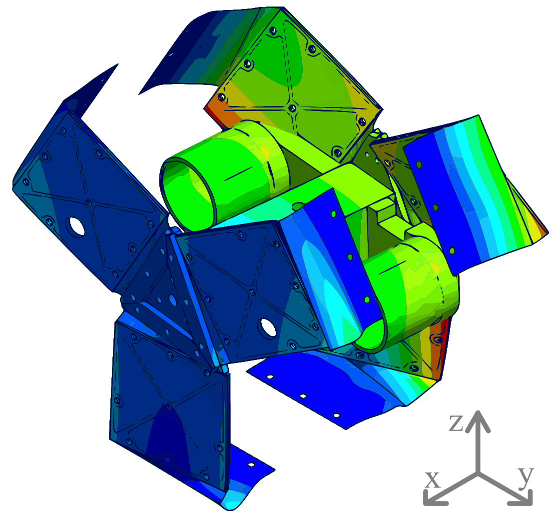

Figure C.3: Translational mode along the y-axis at 880 Hz.

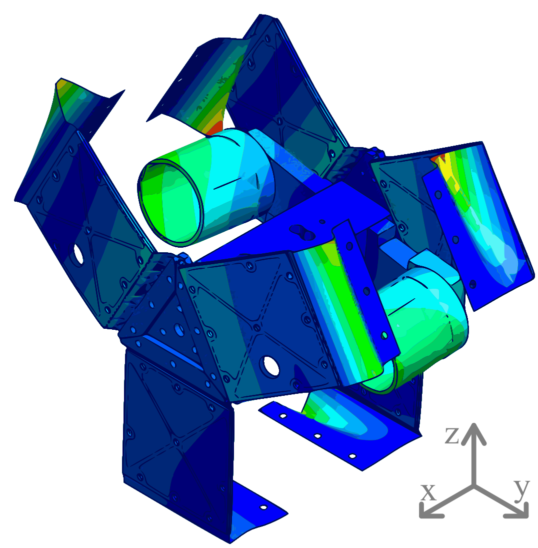

Figure C.4: Torsional mode around the x-axis at 1470 Hz.

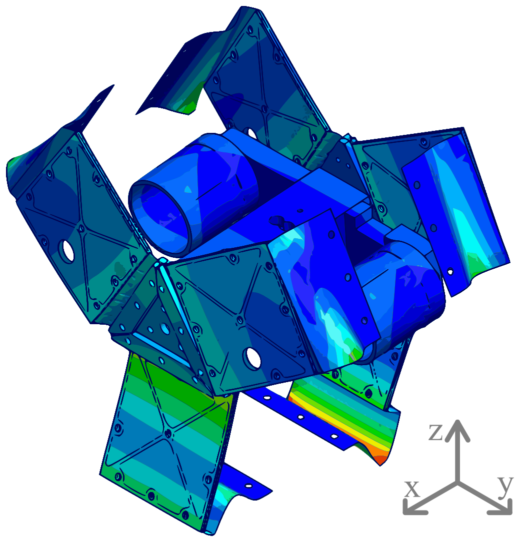

Figure C.5: Torsional mode around the y-axis at 1485 Hz.

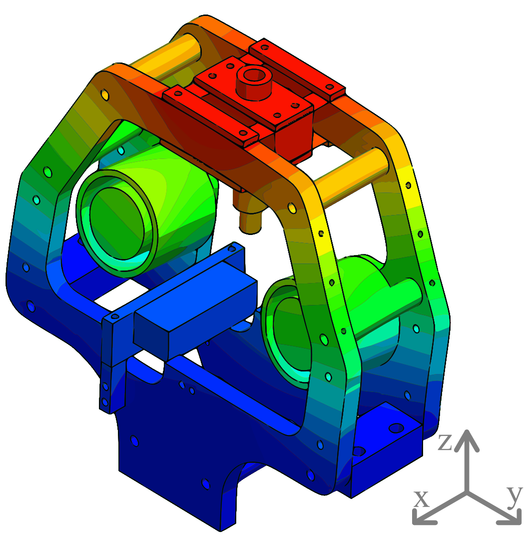

Figure C.6: Tilting around the y-axis at 835 Hz.

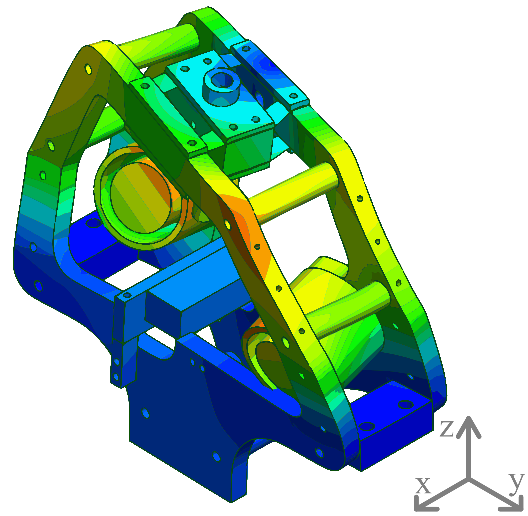

Figure C.7: Torsional mode around the z-axis at 1330 Hz.

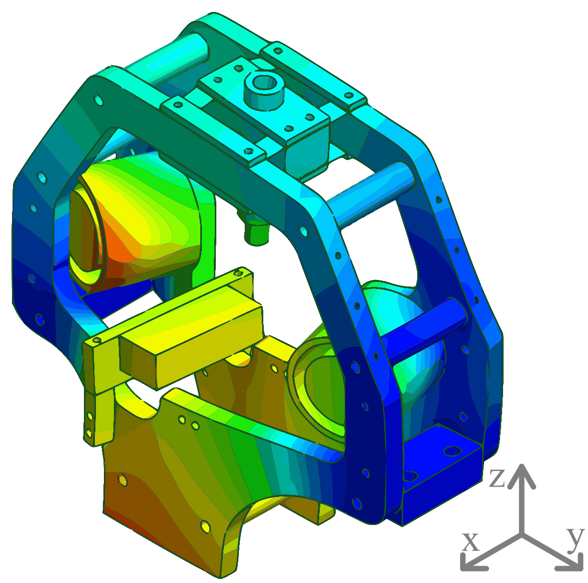

Figure C.8: Bending mode in the xy-plane at 1379 Hz.

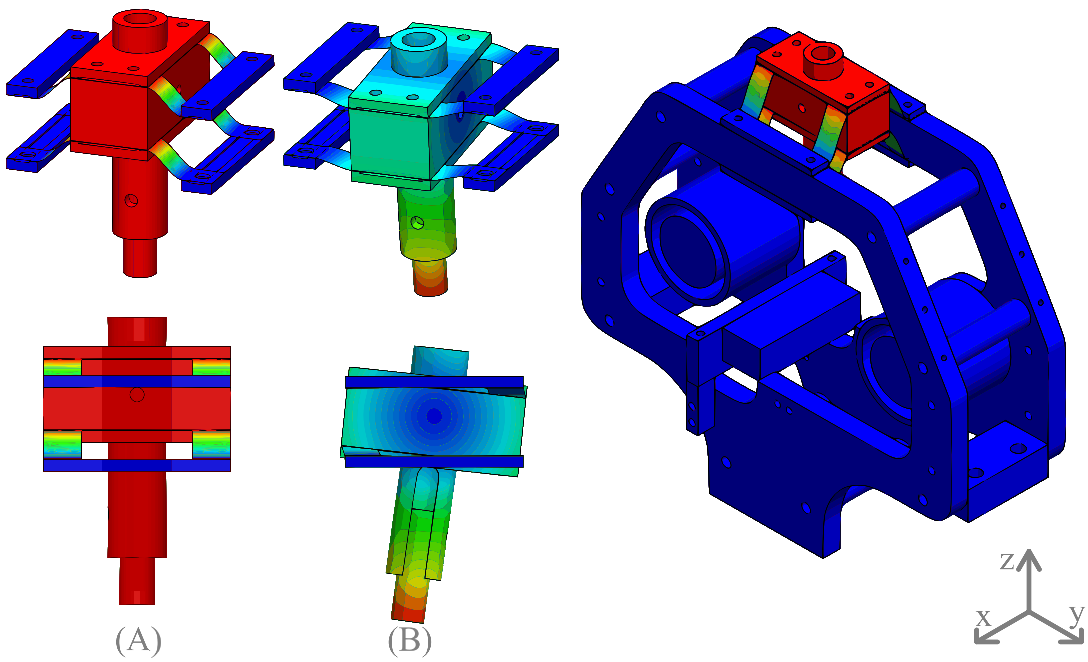

Figure C.9: (A) Intentional frame compliance mode along the z-axis at 350 Hz and (B) tilting mode around the x-axis at 1550 Hz.

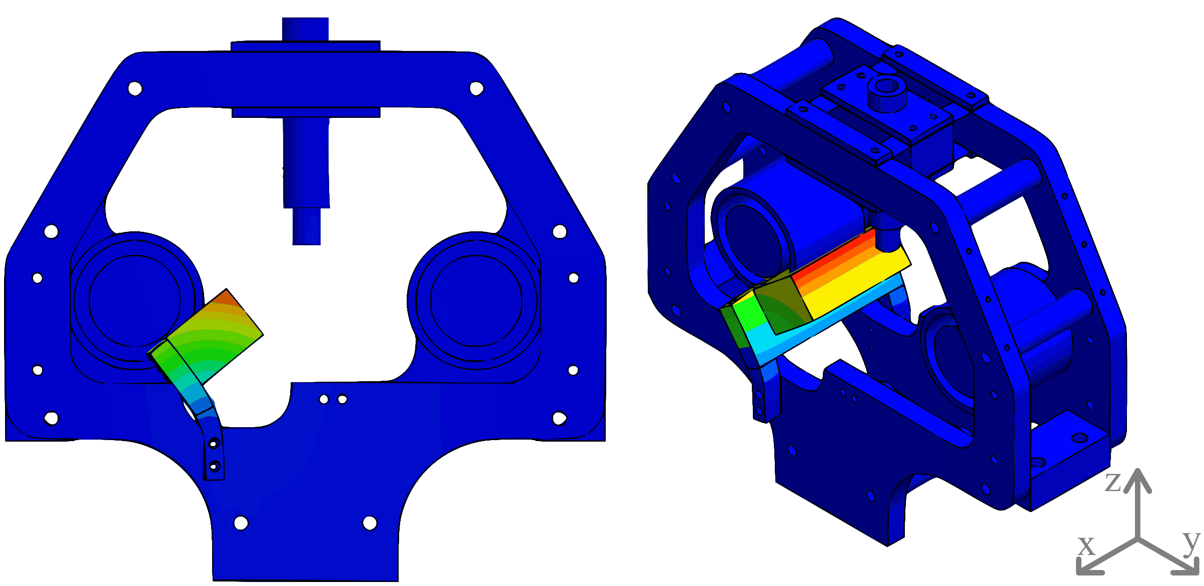

Figure C.10: Tilting mode in the yz-plane at 1655 Hz visualized by means of a front-view and isometric-view.

Bibliography

[1] H. Butler. "Position control in lithographic equipment [applications of control]". In: *IEEE Control Systems Magazine* 31.5 (2011), pp. 28–47.

[2] "Semiconductor Machines: active isolation system for process stability and throughput enhancement". In: (2019). URL: https://www.etel.ch/fileadmin/PDF/White_papers/ETEL_QuiET_an_active_isolation_system_for_process_stability.pdf.

[3] D. Laro. "Mechatronic design of an electromagnetically levitated linear positioning system using Novel multi-DoF actuators". PhD thesis. Delft, The Netherlands: Delft University of Technology, 2009.

[4] H.M.J.R Soemers. *Design principles: for precision mechanisms*. Enschede, The Netherlands: University of Twente, 2017.

[5] J. van Eijk. "ON THE DESIGN OF PLATE-SPRING MECHANISMS". PhD thesis. Delft, The Netherlands: Delft University of Technology, 1985.

[6] J. Holterman. "Vibration control of high-precision machines with active structural elements". PhD thesis. Enschede, The Netherlands: University of Twente, 2002.

[7] Aström K.J. and Murray M.J. *Feedback systems: an introduction for scientists and engineers*. Princeton University Press, 2021.

[8] M. Boerlage et al. "Model-based feedforward for motion systems". In: *Proceedings of 2003 IEEE Conference on Control Applications, 2003. CCA 2003.* (). DOI: 10.1109/cca.2003.1223174.

[9] P. Lambrechts, M. Boerlage, and M. Steinbuch. "Trajectory planning and feedforward design for electromechanical motion systems". In: *Control Engineering Practice* 13.2 (2005), pp. 145–157.

[10] J. Giaime et al. "A passive vibration isolation stack for LIGO: design, modeling, and testing". In: *Review of scientific instruments* 67.1 (1996), pp. 208–214.

[11] D.C. Karnopp and A.K. Trikha. "Comparative Study of Optimization Techniques for Shock and Vibration Isolation". In: *Journal of Engineering for Industry* 91.1 (1969), 1128–1132.

[12] G.W. van der Poel. "An exploration of active hard mount vibration isolation for precision equipment". PhD thesis. Enschede, The Netherlands: University of Twente, 2010.

[13] D. Tjepkema. "Active hard mount vibration isolation for precision equipment". PhD thesis. Enschede, The Netherlands: University of Twente, 2012.

[14] W.B.J. Hakvoort, G.J. Boerrigter, and M.A. Beijen. "Active vibration isolation by model reference adaptive control". In: *IFAC-PapersOnLine* 53.2 (2020), pp. 9144–9149.

[15] M.A. Beijen et al. "Self-tuning MIMO disturbance feedforward control for active hard-mounted vibration isolators". In: *Control Engineering Practice* 72 (2018), 90–103. DOI: 10.1016/j.conengprac.2017.11.008.

[16] S.S. Haykin. *Adaptive filter theory*. Prentice Hall, 1996.

[17] M.S. Kuo and D.R. Morgan. *Active noise control systems: algorithms and DSP implementations*. J. Wiley, 1996.

[18] P.R. Fraanje. "Robust and fast schemes in broadband active noise and vibration control". PhD thesis. Enschede, The Netherlands: University of Twente, 2004.

[19] R.A. De Callafon, J. Zeng, and C.E. Kinney. "Active noise control in a forced-air cooling system". In: *Control Engineering Practice* 18.9 (2010), pp. 1045–1052.

[20] S.J. Elliott. *Signal processing for active control*. Elsevier, 2000.

[46] D. de Roover. "Motion Control of a Wafer Stage: a Design Approach for Speeding up IC Production". PhD thesis. Delft, The Netherlands: Delft University of Technology, 1997.

[47] M.P. Koster. *Constructieprincipes voor het Nauwkeurig Bewegen en Positioneren*. Enschede, The Netherlands: University of Twente, 2000.

[48] A.H. Slocum. *Precision Machine Design*. Prentice Hall, 1992.

[49] D. Blanding. *Exact Constraint: Machine Design Using Kinematic Principles*. New York: ASME Press., 1996.

[50] *Akribis Systems Korea. Website: Voice coil motors*. URL: http://www.akribis-sys.co.kr/.

[51] *Lion Precision. Website: Capacitive Vibration and Position Sensors*. 2021. URL: https://www.lionprecision.com/products/capacitive-sensors-1.

[52] D.M. Brouwer. "Design principles for six degrees-of-freedom MEMS-based precision manipulators". PhD thesis. Enschede, The Netherlands: University of Twente, 2007.

[53] B. Braam. *ARCADE, A linear guide with nanometer accuracy*. Tech. rep. 2006. URL: https://www.dspe.nl/publication/arcade-a-linear-guide-with-nanometer-accuracy/.

[54] R.G.K.M. Aarts, J.P. Meijaard, and J.B. Jonker. "Flexible multibody modelling for exact constraint design of compliant mechanisms". In: *Multibody system dynamics* 27.1 (2012), pp. 119–133.

[55] R Koster. *THE OPTIMUM FLEXURE LINEAR GUIDANCE*. Tech. rep. 2013. URL: https://www.dspe.nl/wp-content/uploads/2013/01/Mikroniek-Issue-1-2013.pdf.

[56] F. Villar, J. David, and G. Genevès. "75 mm stroke flexure stage for the LNE watt balance experiment". In: *Precision engineering* 35.4 (2011), pp. 693–703.

[57] P. Verhoeff et al. "Development of an in-orbit refocusing mechanism for the Meteosat second-generation weather satellites". In: *Search the world's largest collection of optics and photonics applied research.* (1998).

[58] R Henselmans. "Non-contact Measurement Machine for Freeform Optics". PhD thesis. Eindhoven, The Netherlands: Eindhoven University of Technology, 2009.

[59] R.H. Byrd, J.C. Gilbert, and J. Nocedal. *A trust region method based on interior point techniques for nonlinear programming*.

[60] J.B. Jonker and J.P. Meijaard. "SPACAR — Computer Program for Dynamic Analysis of Flexible Spatial Mechanisms and Manipulators". In: *Multibody Systems Handbook* (1990), pp. 123–143.

[61] *SPACAR Wiki*. URL: https://www.spacar.nl/wiki/doku.php.

[62] *PM. Website: Crossed-roller miniature slides PMMR*. URL: https://www.pm.nl/en/articles/miniature-slide-pmmr-crossed-roller-type.

[63] *Renishaw. Website: TONiC™ incremental encoder system with RGSZ20 linear scale*. URL: https://www.renishaw.com/en/tonic-incremental-encoder-system-with-rgsz20-linear-scale--10187.

[64] P. Witkof. "Hysteresis in Flexure Elements". Master's Thesis. Enschede, The Netherlands: University of Twente.

[65] P. Welch. "The use of fast Fourier transform for the estimation of power spectra: a method based on time averaging over short, modified periodograms". In: *IEEE Transactions on audio and electroacoustics* 15.2 (1967), pp. 70–73.